Politecnico di Torino

Department of Structural, Geotechnical and Building Engineering

Master of Science in Building Engineering

Strain-based method for assessing the influence of aleatory uncertainties on shear and bending failure modes of RC beams

Advisors:

Paolo Castaldo

Diego Gino

Elena Miceli

Candidate:

Stefano Bozza

December 2024

Abstract

Structural performance is increasingly impacted by factors such as material deterioration, rising traffic loads or structural adjustments, which necessitate advanced analytical methods to make accurate assessments. The introduced methodology, based on Global Resistance Factor (GRF), examines the application of reliability-based non-linear finite element analysis (NLFEA) for improving the evaluation and design of reinforced concrete structures failing in shear.

A database of 20 reinforced concrete beams, selected from literature, has been created. The beams, characterized by a regular geometry and standard transverse reinforcement, exhibit brittle behavior due to a shear failure mechanism. Adopting non-linear constitutive equations and broadly validated assumptions, these models were able to accurately capture the experimental behavior, providing a reliable framework for understanding the structural performance of the beams under specific loading conditions.

Mechanical uncertainties have been addressed through an extensive probabilistic analysis of the structural behavior, utilizing a non-linear model featuring average (experimental) values. Following the methodology introduced by the Strain-based Method, the statistical properties of the corresponding probabilistic distribution are associated with the peak strains in the reinforcement involved in the failure mechanism.

This approach allows the statistical parameters of the Global Structural Resistance to be expressed as a function of the strains in the reinforcing steel, providing a direct and time-effective way to estimate the Global Safety Factor and consequently the design value of the Global Structural Resistance, ensuring compliance with target reliability

levels for both new and existing reinforced concrete structures.

Key words: Non linear finite element analysis, Shear failure, Reinforced concrete beams, ATENA, Strain-based method.

Acknowledgements

Ringrazio la mia famiglia per aver reso possibile l'impossibile.

Ringrazio la mia ragazza e i miei amici per esserci sempre stati.

Ringrazio Paolo Castaldo per aver creduto in me e trasmesso la passione per la materia.

Ringrazio Diego Gino per essere stato un ottimo maestro.

A Nonno Renato,

che faceva dell'Ingegneria una pratica quotidiana

Abbreviations

3PBT	Three-Points Bending Test
4PBT	Four-Points Bending Test
CDF	Cumulative Density Function
CoV	Coefficient of Variation
ECoV	Estimation of Coefficient of Variation
FEA	Finite Element Analysis
FEM	Finite Element Modeling
FORM	First order reliability method sensitivity factor
GRF	Global Resistance Format
GRM	Global Resistance Method
GSF	Global Safety Factor
LC	Load Case
LHS	Latin Hypercube Sampling
LVDT	Linear Variable Displacement Transducer
NLFEA	Non-linear Finite Element Analysis
NLNA	Non-linear Numerical Analysis
PFM	Partial Factor Method
PM	Probabilistic Method
RC	Reinforced Concrete

Contents

Abstract **i**

Abbreviations **v**

1 Introduction **1**

1.1 Local vs Global approach 2

1.2 Global Resistance Format (GRF) 4

1.2.1 Safety-Formats for NLFEA within GRF 7

1.3 Strain-based method 11

2 Shear failure mechanisms **13**

2.1 Shear failure modes 13

2.2 Shear capacity influencing factors for reinforced concrete beams 15

3 Experimental Program **18**

3.1 Bending test 18

3.2 Database 20

3.2.1 C.G Karayannis, C.E. Chalioris (2013) [7] 21

3.2.2 L. Jin et al (2023) [18] 23

3.2.3 M. Hamrat et al (2018) [20] 26

3.2.4 C. Lee et al (2010) [12] 28

3.2.5 M. Tahir et al (2019) [21] 30

3.2.6 R. Guo et al (2020) [25] 32

3.2.7 C. Cucchiara et al (2003) [11] . . . 34
3.2.8 C. Lee et al (2015) [13] . . . 36
3.2.9 H.Ma et al (2023) [16] . . . 38

4 FEA theory and ATENA 2D application 40
4.1 Theory of Finite Element Analysis . . . 40
4.1.1 Non-linear Finite Element Analysis . . . 42
4.2 ATENA 2D . . . 44
4.2.1 Pre-processing . . . 44
4.2.2 Analysis . . . 55
4.2.3 Post-processing . . . 55

5 RC Beams modeling based on inverse analysis of experimental data 58
5.1 Inverse analysis procedure . . . 58
5.2 Geometry, boundary conditions and loads . . . 62
5.3 NLNAs results . . . 63

6 Probabilistic analysis 69
6.1 Probabilistic Analysis Framework . . . 69
6.2 Relevant random variables . . . 70
6.3 LHS . . . 71
6.4 Statistical test . . . 73
6.5 Probabilistic analysis of the global structural resistance . . . 73

7 Application of the Strain-based method to RC beams failing in shear 80
7.1 Results of the Probabilistic Analysis . . . 80
7.2 Assessment of the Global Safety Factors . . . 83
7.3 Sensitivity analysis of the global structural response . . . 86
7.4 Proposal for a more accurate estimation of the global safety factor considering different failure modes on its own . . . 88
7.5 Different approaches to assess the global safety factors . . . 90

7.6 Comparison with other safety formats within GRF 93

8 Conclusions **95**

A1 Appendix **101**

A1.1 Load-deformation curves 102

A1.2 Mechanical and geometrical properties 104

List of Figures

1.1 Comparison between local approach and global approach 3
1.2 Calibration philosophy for the novel Strain-based method 12

2.1 Elastic beam 14
2.2 Shear failure modes 15
2.3 Bazant's size effect law 16
2.4 Cracking pattern 17

3.1 Geometry and failure mode of ST80/ST120 22
3.2 Geometry and failure modes of S-series beams 25
3.3 Geometry and failure modes of A/B-series beams 27
3.4 Geometry and failure modes of S06/S10 29
3.5 Geometry and failure mode of S890 31
3.6 Geometry and failure mode of F0S0 33
3.7 Geometry and failure mode of A0/B0 series beams 35
3.8 Geometry and failure mode of B-series beams 37
3.9 Geometry and failure mode of RCTB-series beams 39

4.1 Plane stress state components 45
4.2 ATENA concrete constitutive model 46
4.3 Fixed/rotated crack model 47
4.4 ATENA reinforcement constitutive model 49

5.1 Inverse analysis methodology 61

5.2 Comparison between experimental results and NLNAs outcomes (1) . . 64
5.3 Comparison between experimental results and NLNAs outcomes (2) . . 65
5.4 Comparison between experimental results and NLNAs outcomes (3) . . 66
5.5 Comparison between experimental results and NLNAs outcomes (4) . . 67
5.6 Realization of the model uncertainty 68

6.1 LHS 72
6.2 Probabilistic load-displacement curves (1) 75
6.3 Probabilistic load-displacement curves (2) 76
6.4 Empirical and lognormal CDFs of RC members(1) 77
6.5 Empirical and lognormal CDFs of RC members(2) 78
6.6 Empirical and lognormal CDFs of RC members(3) 79

7.1 Trend of variation of the mean-to-mean deviation 81
7.2 Trend of variation of the CoV of the global resistance 82
7.3 Assessment of the Design global structural resistance 84
7.4 Global resistance safety factors (1) 85
7.5 Sensitivity analysis: aleatory and epistemic uncertainties 87
7.6 Global resistance safety factors (2) 87
7.7 CoV of the global resistance in presence of multiple fits 88
7.8 Global resistance safety factors (3) 89
7.9 Double fit Sensitivity analysis: aleatory and epistemic uncertainties . . . 90
7.10 Different approaches to estimate the Global safety factor 92
7.11 Comparison between safety formats within GRF 94

A1.1 Load-deformation curves of experimental benchmark (1) 102
A1.2 Load-deformation curves of experimental benchmark (2) 103
A1.3 Mechanical and geometrical properties distribution (1) 104
A1.4 Mechanical and geometrical properties distribution (2) 105

List of Tables

3.1 Experimental program database 20

3.2 Reinforcement mechanical properties of ST-80/120 21

3.3 Reinforcement mechanical properties of S-series beams 23

3.4 Reinforcement mechanical properties of A/B series beams 26

3.5 Reinforcement mechanical properties of S890 30

3.6 Reinforcement mechanical properties of F0S0 32

3.7 Reinforcement mechanical properties of A0/B0 series beams 35

3.8 Reinforcement mechanical properties of B series beams 36

3.9 Reinforcement mechanical properties of RCTB series beams 38

5.1 Newton Raphson solver modeling assumptions 59

6.1 Outputs of 30 LHS samples 70

6.2 Relevant random variables 71

7.1 Coefficient of Variation accounting epistemic uncertainties 86

A1.1 Database: geometrical and mechanical properties (1) 106

A1.2 Database: geometrical and mechanical properties (2) 107

A1.3 Database: modeling parameters (1) 108

A1.4 Database: modeling parameters (2) 109

Nomenclature

A_{s_l}	Area of the tension steel reinforcement	m^2
$A_{s'_l}$	Area of the compression steel reinforcement	m^2
a_{exp}	Experimental geometrical properties	$-$
a_n	Nominal values associated to geometrical properties	$-$
D	Material stiffness matrix	$-$
E	Elastic Modulus	GPa
E_s	Steel Elastic Modulus	GPa
E_c	Concrete Elastic Modulus	GPa
b	Width of the cross section	m
d	Effective depth of the cross section	m
e	Strain vector	$-$
f_t	Tensile strenght	MPa
f_c	Mean cylinder compressive strenght	MPa
f_{c_u}	Mean cube compressive strenght	MPa
f_{exp}	Experimental material properties	$-$
f_m	Mean values associated to material properties	$-$
k	Stiffness	MPa
R	Global Structural Resistance	$-$
R_d	Design value of the Global Structural Resistance	$-$
R_{exp}	Experimental outcomes	$-$
s	Stress vector	$-$
s	Stirrups spacing	m
V_R	Coefficient of variation of Resistance	$-$
$V_{R,g}$	Coefficient of Variation related to the aleatory uncertainty of geometrical properties	$-$

$V_{R,m}$	Coefficient of Variation related to the aleatory uncertainty of material properties	$-$
V_c	Coefficient of variation of cylinder compressive concrete strength	$-$
V_y	Coefficient of variation of reinforcement strength	$-$
α	Thermal expansion coefficient	$1/K$
α_R	FORM factor	$-$
β	Shear retention factor	$-$
β_t	Target reliability index	$-$
δ	Bias factor	$-$
$\delta_{R,g}$	Bias factor related to geometric uncertainties	$-$
$\delta_{R,m}$	Mean-to-mean deviation	$-$
ϵ_c	Compressive strain at compressive strength	$-$
$\epsilon_{s,max}$	Maximum strain of reinforcement involved in failure mechanism	$-$
ϵ_x	Strain component along X-axis	$-$
ϵ_y	Yielding Strain of reinforcement	$-$
γ	Specific material weight	N/m^3
γ_R	Global safety factor related to aleatory uncertainties	$-$
γ_{R_d}	Global safety factor related to epistemic uncertainties	$-$
γ_{x_y}	Engineering shear strain	$-$
μ	Poisson's ratio	$-$
μ_m	Mean value of the global resistance achieved by the probabilistic analysis	$-$
ρ	Density	kg/m^3
ρ_l	Reinforcement content in tension zone	$-$

ρ'_l	Reinforcement content in compression zone	$-$
ρ_{s_w}	Reinforcement content in shear	$-$
σ_x	Normal stress component along X-axis	MPa
σ_y	Normal stress component along Y-axis	MPa
τ_{x_y}	Tangential stress in plane X-Y	MPa

1 | Introduction

In recent decades, the aging of infrastructure and the continuous increase in traffic frequency and intensity have raised significant concerns about the ability of structures to maintain adequate performance. These factors substantially contribute to the deterioration of engineering works, highlighting the need for more thorough analysis of their structural behavior [10]. Consequently, the development and application of advanced methodologies capable of accurately assessing the condition of existing structures has become essential.

Current standards and guidelines primarily focus on the design of new structures, often overlooking the evaluation of existing ones that may no longer comply with modern codes. However, these older structures may still possess hidden reserves of capacity, prompting the question of how to avoid unnecessary over-dimensioning during evaluations. In this context, advanced nonlinear finite element analysis (NLFEA), combined with structural reliability methods, offers a promising solution. Recent advancements in computational mechanics have made non-linear finite element analysis a feasible and widely accessible tool for structural assessment. This methodology provides a more detailed insight into the behavior of structures by accurately representing the response of materials under complex loads. At the same time, physical models are evolving to incorporate probabilistic dimensions, explicitly accounting for uncertainties related to material properties, actions, and modeling assumptions.

With the adoption of the next generation of international design codes, such as Eurocode 2.0, the use of these advanced techniques in structural verification is expected

to expand. In particular, there is a growing need for efficient and user-friendly methods that integrate structural reliability analysis with non-linear finite element analysis. This thesis aims to explore these innovative approaches, focusing on the integration of advanced non-linear structural analysis with reliability methods, to provide more reliable and precise tools for designing and assessing new/existing RC structures in an increasingly complex and uncertain environment.

1.1 Local vs Global approach

The distinction between the local and global approaches, shown in Figure 1.1, in structural safety verifications is rooted in how each method addresses uncertainties and evaluates structural performance. The local approach, which is widely adopted in design codes, is primarily based on a semi-probabilistic safety format. It focuses on cross-sectional verifications where the internal actions E_d are compared to the local resistances R_d, typically evaluated through linear elastic analyses.
This method uses partial safety factors to account for uncertainties in material properties and geometry but does not consider the redistribution of internal forces or the overall deformation capacity of the structure. As a result, it can be insufficient when the structure operates near its limit state, particularly in the assessment of existing reinforced concrete (RC) structures, where the global response plays a critical role [23].

On the other hand, the global approach takes a probabilistic safety format into account. It compares the design value of external actions F_d with the global structural resistance R_d, both estimated using non-linear finite element analysis (NLFEA).
This method includes both aleatory (inherent material and geometric) and epistemic (modeling) uncertainties by defining appropriate partial safety factors as a function of target reliability levels [10].
Unlike the local approach, the global method reflects the overall structural behavior, considering factors such as force redistribution, non-linear material properties, and

potential instabilities.

In summary, while the local approach is simpler and effective for routine design checks, it may not adequately capture the true behavior of structures under extreme conditions. In contrast, the global approach, grounded in probabilistic analysis, provides a more holistic assessment by considering the entire structure's response.

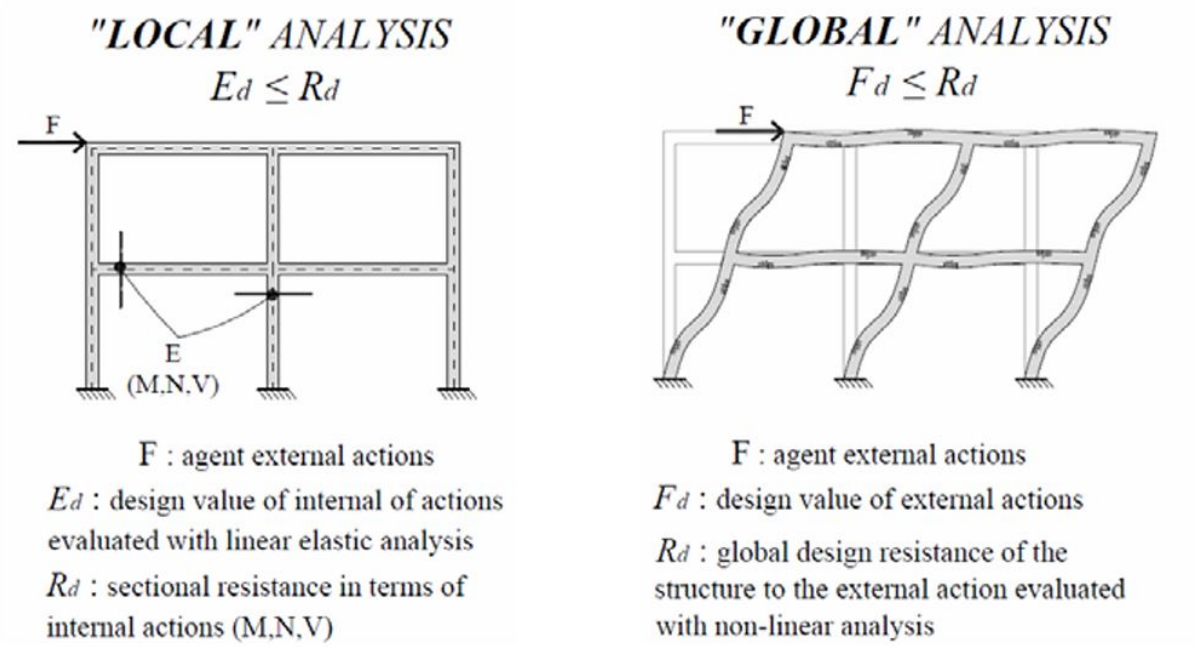

Figure 1.1: Comparison between local approach and global approach [29]

The adoption of non-linear finite element analyses (NLNAs) for safety evaluations offers significant benefits but comes with notable challenges, particularly in terms of computational complexity and cost. Three key stages need to be performed before completing the analysis. First, the characterization of input variables and model definition, which involves gathering information about the structure, defining representative values for mechanical and geometrical properties, and setting up the model based on appropriate assumptions, such as iterative methods and constitutive models.
Second, the structural analysis itself is conducted, often using specialized software like ATENA 2D, to simulate the response of structural elements under load.
Lastly, the post-processing phase requires careful interpretation of the results, distinguishing between real physical failures and numerical issues, such as convergence

problems. This step is particularly complex when failure modes are not well understood in advance. Additionally, NLNA outcomes are highly sensitive to material properties, and adjustments, such as applying a safety factor, may be necessary to refine the estimated structural resistance.

In light of the computational intensity of NLNAs, simplified methods are needed to facilitate their broader use among practitioners.

This study proposes a novel strain-based approach within the Global Resistance Format (GRF) to estimate the design value of the global structural resistance R_d more efficiently. The methodology focuses on assessing the impact of aleatory uncertainties, such as material and geometric variations, on the global resistance of 20 reinforced concrete beams failing in shear.

Similar studies on reinforced concrete structures, slender columns and beams failing in flexure are available in [5, 14, 24].

These RC beams are modeled using non-linear finite element models in ATENA 2D, accounting for both mechanical and geometric non linearities.

An extensive probabilistic analysis is then conducted using Latin Hypercube Sampling (LHS). For each of the 20 RC columns, 30 sampled models are generated, and the influence of uncertainties is analyzed as a function of the strain ratio $\epsilon_{s,max}/\epsilon_y$. The global resistance safety factor γ_R is calculated, according to a specific target reliability index.

A further analysis is considered by taking into account the Global safety factor related to epistemic uncertainties [37].

1.2 Global Resistance Format (GRF)

The Global Resistance Format (GRF) provides a framework for evaluating the design value of the global structural resistance R_d using non-linear numerical analysis (NLNA), factoring in both material and geometric uncertainties. In this approach, R_d is calculated using Eq. (1.1) by dividing the global structural resistance derived from

NLNA with representative material and geometric properties R_{NLNA} by two safety factors: the global resistance factor γ_R and the model uncertainty factor γ_{R_d}. The first factor accounts for aleatory uncertainties related to material and geometric properties and can be estimated using a log-normal distribution model of structural resistance. Meanwhile, the model uncertainty factor addresses epistemic uncertainties, capturing the assumptions made by the analyst when modeling.

It is important to mention that the calibration of the two safety factors is completely independent because of the different type of uncertainties addressed. This statement remains valid as long as the same Target reliability index β_t is considered.

A first evaluation will be done by considering a fixed value for γ_{R_d} [23], then latest results available [37] will be considered in case of shear and bending failure of RC beams.

$$R_d = \frac{R_{NLNA}(f_{rep}; a_{exp})}{\gamma_R \gamma_{Rd}} \tag{1.1}$$

where:

f_{rep}: Representative values of material properties

a_{exp}: Representative values of geometric properties

The ultimate safety verification is performed by comparing the design value of external actions F_d with the global structural resistance R_d (Eq. (1.2)), ensuring that the structure can withstand the applied loads under specified reliability targets.

$$F_d \leq R_d \tag{1.2}$$

The global resistance safety factor γ_R is essential for assessing structural reliability in non-linear analysis, particularly under the assumption of a log-normal probabilistic distribution for the global structural resistance. It can be expressed as follows:

$$\gamma_R = \frac{exp(\alpha_R \beta_t V_R)}{\delta_R} \geq 1 \tag{1.3}$$

where:

α_R: First order reliability method sensitivity (FORM) factor

β_t: Target reliability Index

V_R: CoV of the global structural resistance (log-normal distribution)

δ_R: Global bias factor

The FORM factor is assumed equal to 0.8 following the hyphotesis of dominant aleatory uncertainties [28], while further considerations on epistemic uncertainties will be introduced in Chapter 7.3.

The Target reliability index β_t takes different values between 2,8 and 4,3 depending on the condition and working life of the structure.

The term δ_R of Eq. (1.3) accounts for deviations in both material properties and geometrical dimensions, quantified by two components: $\delta_{R,m}$ representing mean-to-mean deviations and $\delta_{R,g}$ which addresses geometrical bias.

$$\delta_R = \delta_{R,m}\delta_{R,g} \tag{1.4}$$

These components, whose relation is shown in Eq. (1.4) quantify discrepancies between the results from non linear analyses performed with mean material properties and nominal geometrical values, compared to results from probabilistic simulations. For most failure modes, both of them can be set to 1 as demonstrated in Chapter 6.3, except for highly slender structures, where geometric deviations play a more significant role.

The coefficient of variation V_R in Eq.(1.3) reflects the variability of the global structural resistance, which is assumed to follow a log-normal distribution. This variability can be calculated using Eq.(1.5), as long as $V_R \leq 0.3$.

$$V_R = \sqrt{V_{R,m}^2 + V_{R,g}^2} \tag{1.5}$$

where $V_{R,m}$ represents the CoV associated with material properties and $V_{R,g}$ the one linked to geometric properties.

For non-slender RC structural elements, $V_{R,g}$ can reasonably be set at 0.05 based on existing studies [24], as it has minimal impact compared to the material uncertainty. However, the value of $V_{R,m}$ must either be explicitly determined through a probabilistic analysis as done fot this thesis or derived within a specific safety format of the Global Resistance Format (GRF). This approach ensures that the influence of both material and geometric uncertainties is appropriately captured in the overall assessment of structural reliability.

In cases where multiple failure modes are present an additional safety factor of 1.15 may be applied to further adjust Eq.(1.1).

1.2.1 Safety-Formats for NLFEA within GRF

In general, lower levels of approximation (LoA) involve using simplified and typically more conservative models, allowing for a quicker evaluation of structural safety. In contrast, the highest level of approximation allows for the use of advanced numerical methods [28].
Various techniques based on differing applications of probability theory can be utilized to determine the design structural resistance R_d. As accuracy increases, a more precise evaluation of uncertainties in the assessment process is possible.
Here below are provided, in order of LoA, different safety-formats following the general framework introduced by Global Resistance Format (GRF):

- **Probablistic Method (PM)**: The probabilistic method (PM) evaluates the global structural resistance by representing it as a probabilistic distribution derived from non-linear finite element analyses (NLFEAs).

  This method incorporates both aleatory and epistemic uncertainties as random variables, directly determining the design resistance based on the target reliability level. By using sampling techniques such as Monte Carlo or Latin Hypercube to generate input data, the results are fitted to a probabilistic model, allowing the statistical parameters (mean and dispersion) to be estimated. Assuming a log-

normal model, the design global resistance can be expressed as:

$$R_d = \frac{R\alpha_R\beta}{\gamma_{Rd}} \tag{1.6}$$

Unlike the Global Safety Format (GSF) method, which relies on a lognormal model and a first-order Taylor approximation based on mean material properties, the PM approach directly references the quantile of the global resistance distribution [23].

- **Global Resistance Methods (GRMs)**: In [28], three main methods are outlined for deriving the design resistance: the *Global Resistance Factor (GRF)*, the *Estimation of Coefficient of Variation of Resistance (ECOV)* and *Global Safety Format (GSF)*. All of them belong to the broader category of Global Resistance Methods (GRMs), which provide safety formats for evaluating design resistance using global resistance safety factors, as defined by the Global Resistance Format (GRF). These methods offer alternatives to the more computationally intensive probabilistic method (PM), with several techniques proposed in the literature to streamline the calculation process and reduce the computational effort required.

  - ***Global Resistance Factor (GRF)***:The Global Resistance Factor method calculates the design global resistance R_d using a global safety factor γ_{GL} set at 1.27 [23].

$$R_d = \frac{R_{NLFEA}(f_{cmd}, f_{ym})}{\gamma_{GL}} \tag{1.7}$$

    This safety factor accounts for both material and structural uncertainties, with γ_{Rd} assumed to be equal to 1 for simplicity. To estimate the representative global resistance, the mean yield strength of reinforcing steel f_{ym} is set as 1.1 times the characteristic yield f_{yk} strength. For concrete, a reduced value of characteristic compressive strenght is considered.

$$f_{cmd} = 0.85 f_{ck} \tag{1.8}$$

This approach harmonizes the partial safety factors for steel and concrete, leading to effective safety margins of approximately 1.15 for steel and 1.5 for concrete.

– ***Estimation of Coefficient of Variation (ECoV)***: The Estimation of Coefficient of Variation of Resistance (ECoV) method, simplifies the evaluation of design global resistance by assuming a log-normal distribution for the structural resistance.

The method involves performing two non-linear finite element analysis, one with mean material properties and the other with characteristic properties [38].

$$R_m = r(f_{ym}, f_{cm}, ...) \quad R_k = r(f_{yk}, f_{ck}, ...) \tag{1.9}$$

The design resistance R_d is evaluated as follows:

$$R_d = \frac{R_m}{\gamma_R \gamma_{Rd}} \tag{1.10}$$

while the Coefficient of Variation V_R of Eq. (1.3) is easily computed as:

$$V_R = \frac{1}{1.65} \ln(\frac{R_m}{R_k}) \tag{1.11}$$

– ***Global Safety Format (GSF)***: This safety format is similar to ECoV as concerns the calculation of the design global resistance, but it differs from the ECOV method in how it evaluates the coefficient of variation:

$$V_R = \frac{\sigma_R}{\mu_R} \tag{1.12}$$

assuming a log-normal distribution for the structural resistance. The mean μ_R and the standard deviation σ_R are estimated through a reduced Monte Carlo simulation or LHS to account for material randomness.

- **Partial Factor Method (PFM)**:This method estimates the design resistance R_d

using a single non-linear finite element analysis with design values of material properties f_d.

The design resistance is calculated as:

$$R_d = \frac{R_{NLFEA}(f_d)}{\gamma_{Rd}} \tag{1.13}$$

where $R(f_d)$ represents the global structural resistance based on the reduced design values of material strengths.

The PFM method provides a simplified approach but may lead to deviations in structural response, such as inaccurate failure modes, making it less reliable than more refined methods. It is particularly challenging for existing reinforced concrete structures, where deriving appropriate design values can be complex. However, it can be useful when no better alternatives are available.

According to [23] to understand whether the various Global Resistance Methods (GRMs) can be used to estimate the design ultimate load, two preliminary NLFEAs simulations of the structure should be performed considering first mean value for concrete properties and then design values.

If the failure mode remains consistent across both analyses all formats are equally valid, however, if the failure mechanisms differ, the Probabilistic Method (PM) is recommended as the only safety format capable of reliably estimating the design ultimate load within a reliability framework.

To extend the use of GRMs, which offer reduced computational effort, even when the failure mode changes, an additional failure mode-based safety factor γ_{FM} equal to 1.15 is proposed by [23] under the following assumptions:

α_r=0.8

β=3.8

Working life=50 years

1.3 Strain-based method

The strain-based methodology for estimating the global resistance safety factor γ_R represents a novel approach for conducting safety verifications of reinforced concrete structures through non-linear numerical analyses (NLNAs).
This methodology is contextualized within the framework of the Global Resistance Methods (GRM) and aims to evaluate the coefficient of variation (CoV) of the global resistance, specifically addressing the aleatory uncertainty associated with material properties.

The process, resumed in Figure 1.2 (a) begins with establishing an experimental benchmark that consists of 20 RC structural members, taken from literature that encompass a wide range of material properties and a brittle failure mode typical of shear collapses.
To minimize model uncertainties, a series of modeling assumptions were devised, leading to the development of 20 NLN models tailored for probabilistic analyses of global structural resistance. The probabilistic models consider aleatory uncertainties by differentiating between the statistical parameters of material properties, with particular attention given to the quality of concrete. According to established guidelines, the CoV of the concrete cylinder compressive strength (Vc) for new RC structural members is conservatively set at 0.15.
Even if this value can be highly sensitive to factors such as casting quality and construction technology, especially in existing structures, it was proven by [14] that its influence does not play a significant role in the estimation of global safety factor.

The probabilistic analyses utilized the Latin Hypercube Sampling (LHS) method, employing 30 samples for each of the 20 RC structural members and resulting in a comprehensive campaign consisting of 600 NLNAs, which, although computationally intensive, provided valuable insights into the probability distribution of the global structural resistance, yielding key statistical parameters, such as the mean value $\mu_{R,m}$ and

CoV $V_{R,m}$ for each structural component.

Moreover, these statistical parameters are correlated with the significant peak strain $\epsilon_{s,max}$ observed in the primary reinforcement during the failure mechanism.

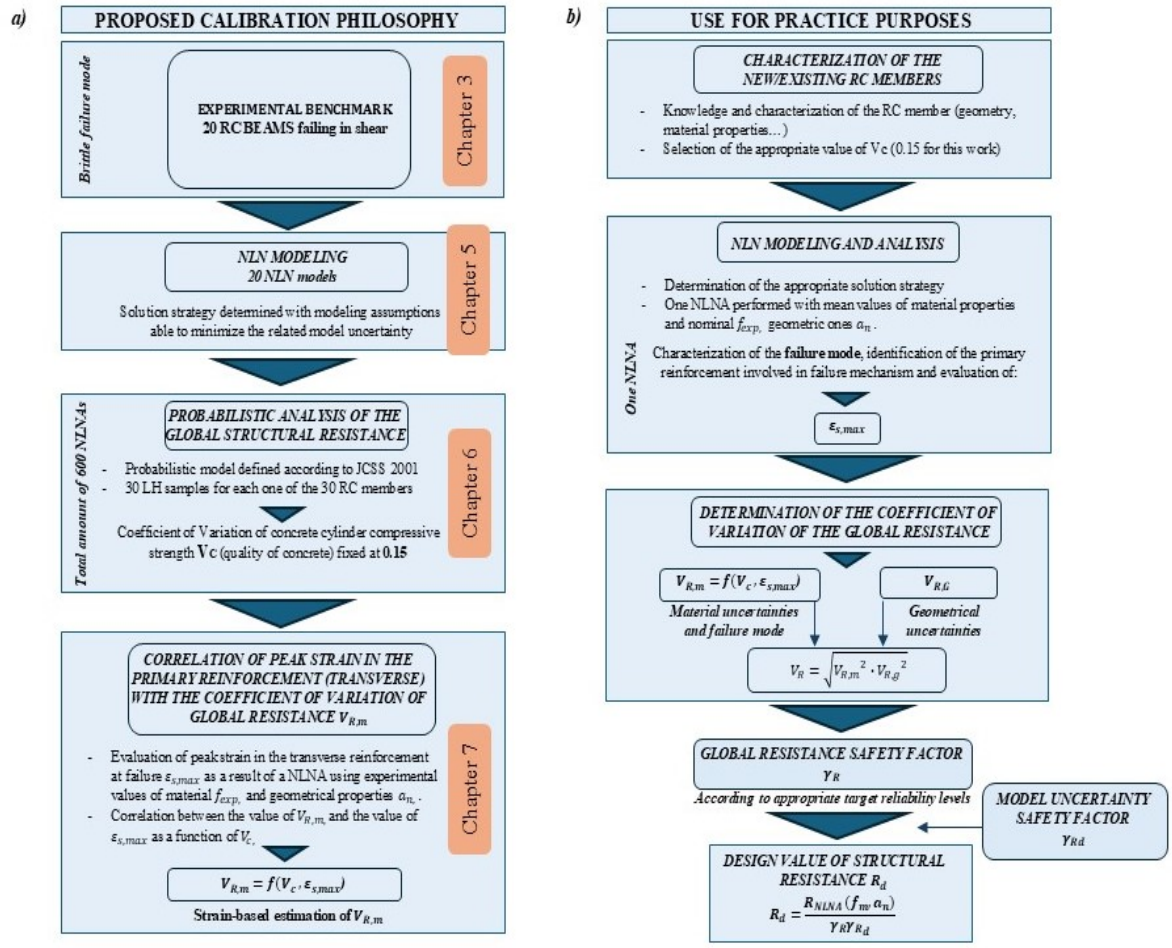

Figure 1.2: Calibration philosophy for the novel Strain-based method (a) and application of GRF for practice purpose (b).

Thanks to this novel methodology, by performing a single NLNA with mean material values and nominal geometrical values, the peak strain can be accurately assessed as well as the CoV of global structural resistance and γ_R as a consequence. Provided these values, and selecting an appropriate value for the model uncertainty safety factor $\gamma_{R,d}$ it is immediate to calculate the design global structural resistance R_d with Eq. (1.1).

2 | Shear failure mechanisms

2.1 Shear failure modes

The manner in which a concrete structure fails, along with the initiation and propagation of cracks, is ultimately determined by the stress distribution within the structure under loading conditions and the material's capacity to withstand high stresses in critical areas. Crack patterns observed after loading a structure can reveal when and where local points will exceed their strength limits.

A match between common crack patterns and specific failure modes has been documented in past years through many experiments (e.g. [19]).

In order to do so, it is crucial to record crack propagation throughout a material test to comprehend the failure mode being addressed when analyzing the experimental data later.

A simply supported concrete beam under transverse loading can experience two primary types of failure modes, which depend on the span-to-depth (a/d) ratio, the applied load, and the quantity and effectiveness of the reinforcement. These failure modes are: flexural failure and shear failure. Distributed shear stresses and normal stresses are induced by transverse loads, like a concentrated load at midspan, along any section of the beam, as shown in Figure 2.1.

It is known, from the elastic beam theory, that pure compression and tensile stresses are generated at the top and bottom edges of the beam, while a pure shear stress appears at mid-depth.

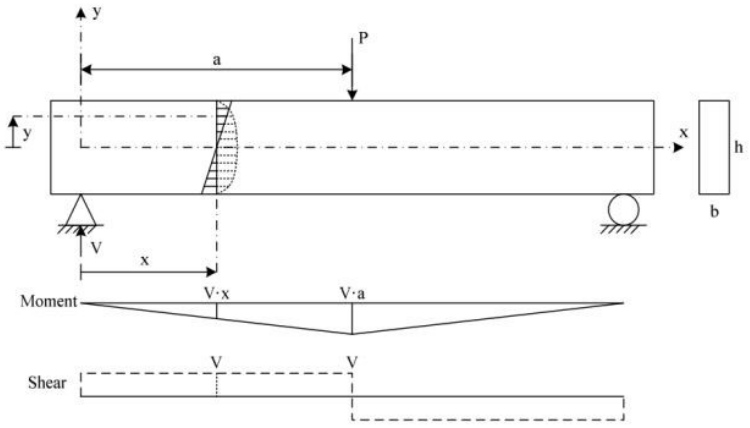

Figure 2.1: Moment and shear diagrams for a simply supported beam loaded at midspan [8].

Shear failure is sudden if compared to other types of failure mechanisms, cracks are usually localized and located diagonally on the line joining supports and load application point. According to [34], five different types of shear failure modes can be identified in Figure 2.2.

- **Diagonal tension failure:** it starts as a vertical flexural crack, and then it propagates along a diagonal direction, as the load increases. Mainly due to an inadequate amount of shear reinforcement of the reinforced concrete structural member.
- **Shear compression failure:** when dealing with concrete beams having short span or excessive shear reinforcement, this failure mode may be present. Compressive failure of concrete material occurs close to the loading points.
- **Shear tension failure:** also known as splitting, mostly due to inadequate anchorage of longitudinal bars. The diagonal cracks develop along the longitudinal bar itself.
- **Arch rib failure:** Typical failure mode in presence of deep beams with short span and high shear strength. Concrete crushing appears in the web due to buckling or close to the lower supports because of very high compressive stresses.

- **Web crushing failure:** Thickness of the concrete web is not thick enough, consequently the concrete crushes.

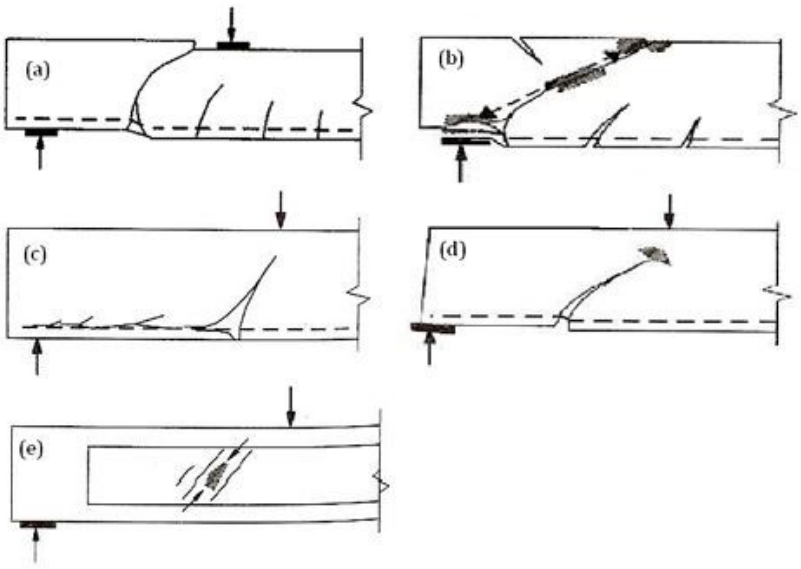

Figure 2.2: Shear failure modes: (a) diagonal tensions failure, (b) shear compression failure, (c) shear tension failure, (e) arch rib failure, (f) web crushing failure [34]

2.2 Shear capacity influencing factors for reinforced concrete beams

Some parameters are typically those that have been demonstrated to significantly influence the shear capacity of RCB. The important factors noted, at least for regular concrete, at flexural shear failure are [4]:

- **Shear span to effective depth ratio (a/d):** the shear slenderness has been proved to be a crucial parameter when dealing with shear failure. Among all tests performed by [27], in which several beams were tested under monotonic load in a four-point bending, only slender beams collapsed due to flexural failure mode. In all cases where $a/d > 3$ a constant shear failure was exhibited by specimens. As a conclusion, by decreasing the shear slenderness, a shear strength at failure increased, mainly due to the arch effect mentioned above.

- **Concrete strength:** more influent for RCB in absence of shear reinforcement.

- **Reinforcement amount:** longitudinal reinforcement is essential not only to fill the gap and resist to transversal displacement of two faces of a flexural crack (dowel effect), but also because the overall shear capacity increases due to the contribution of the shear capacity in the compression zone. Moreover, aggregate interlock is more effective because gaps are not easily widened in presence of longitudinal bars. The flexural tension, ρ_l and compression, $\rho_{l'}$, reinforcement ratio is calculated using Eq. (2.1) and Eq. (2.2) [7]:

$$\rho_l = \frac{A_{sl}}{bd} \tag{2.1}$$

$$\rho_{l'} = \frac{A_{sl'}}{bd} \tag{2.2}$$

- **Size effect:** different studies highlighted that shear capacity of brittle materials like concrete are influenced by their dimensions [36]. Bazant in 1984 [6] states that to effectively investigate only size effects instead of other influential factors, structures of various sizes but uniform shape should be studied. The influence of the sizes of structural members, according to Bazant's theory, is shown in Image 2.3, where the nominal stress σ_n (Y-axis) is related to the ratio between characteristic dimension D and the transitional size, represented by an empirical constant D_0, on a logaritmic scale. A bigger characteristic dimension implies a lower nominal stress at failure.

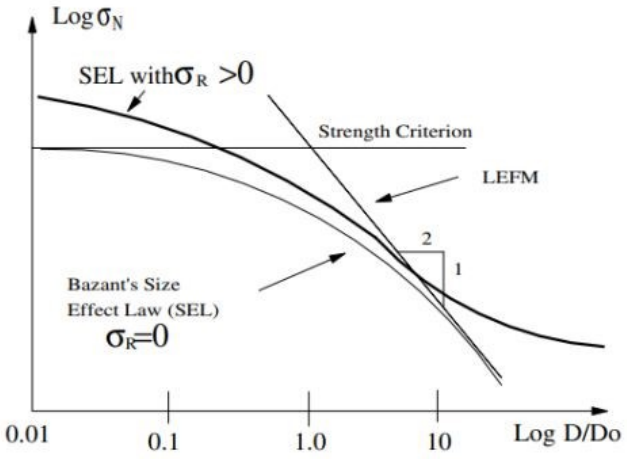

Figure 2.3: Bazant's size effect law [9]

- **Reinforcement bond:** even though it is not always easy to distinguish, two main failure mechanisms occur at the interface between concrete and reinforcement: splitting failure (a) and pull-out failure (b), shown in Figure 2.4. Generally, with splitting failure not only the surface of the specimen is crushed, but at least one crack is initiated from the testing rebar [2]. In this case cracks propagate radially from the reinforcement bar. Pull-out failure occurs due to shear stresses in presence of adequate thickness of concrete cover to prevent from splitting. Cracks are not initiated from rebars.

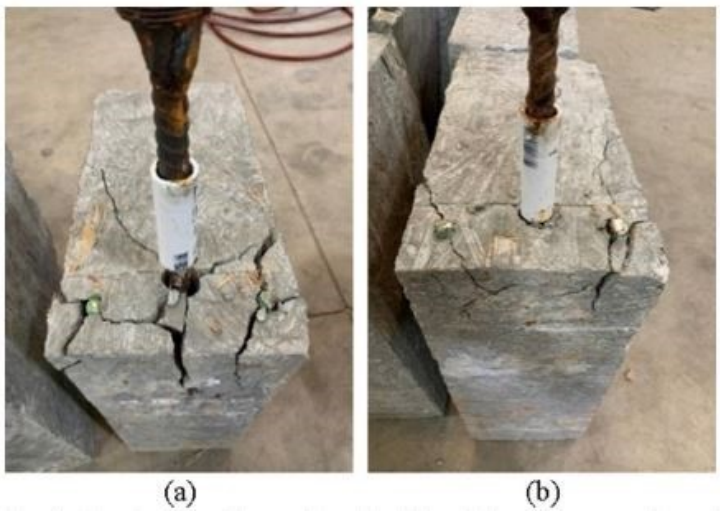

Figure 2.4: Cracking pattern in case of (a) splitting and (b) pull-out [2].

3 | Experimental Program

In this chapter, the experimental benchmark serving as the basis for subsequent modeling through a reverse analysis process will be detailed. The primary geometric and material information, along with the results obtained from the tests, are presented. All selected beams exhibit a shear collapse mechanism (definition in section 2.1) and adhere to the constraints stipulated by [28], as outlined in Appendix 1.2 in the accompanying Tables A1.1 and A1.2.

3.1 Bending test

Bending tests are conducted to gather data, including bending strength/maximum deflection, yielding point or post-peak response on the bending characteristics of materials that are being considered for research.
Generally it is a destructive testing practice applicable to plastics, fiber-reinforced materials, metals, and composite materials like reinforced concrete.
During bending tests not only standardized items like cylindric and cubic specimens can be tested but also large size samples like those RC beams reported in Chapter 3.2. Supports are arranged parallel at a certain distance (span), depending on the size of element to be tested, and should be non-deformable. Then, a testing punch applies an external load at a consistent speed. The test can be load-controlled if external forces are gradually or applied constantly at each step till failure, displacement-controlled when the applied load is function of displacement that increases step after step.
During the test, the values of applied and displacement or strains are recorded in a

stress-strain curve.

If the bending stress applied to the structural element stays below its yield strength, the stress is belonging to elastic field. As the bending stress exceeds it, plastic deformation start to propagate from the edges of the specimen. The yield point, directly determinable from the bending test, represents the maximum bending stress that ductile materials can withstand under bending without undergoing permanent deformation. When materials are extremely ductile they have the ability to undergo significant plastic deformation without breaking, regardless of the magnitude of the applied force.

A different behaviour is expressed by brittle materials that break suddenly without exhibiting warning signs. Most of the RC beams presented in Chapter 3.2 will belong to this category.

Types of bending tests

Based on the number of loading points and supports of the test specimen, bending tests can be categorized as follows:

- 1 point bending test (1PBT)
- 3 point bending test (3PBT)
- 4 point bending test (4PBT)

The 3-point bending test implies the presence of three pressure points in this test setup: a loading testing punch located at midspan on upper surface and two supports. The specimen lies horizontally on the supports and protrudes at the sides. Considering its ease of implementation, the 3-point bending test is most commonly performed rather than other types Although it is very frequent, it has the disadvantage that transverse forces are generated in addition to the compressive and tensile forces.

As regards the 4PBT vertical loads are applied through a double punch. Point of application is no more arranged at mid-span but symmetrical to it on both sides. A constant bending moment in the small area between the two points is generated.

Commonly a 4PBT achieves more accurate results, but the testing set-up is more complex to be operated and more expensive.

3.2 Database

In this section a list of all experimental tests considered and effectively used for further analysis is provided. A few RC beams have been rejected because of doubtful experimental results or unclear failure mechanism. In Appendix 1.1 and 1.2 are provided respectively all Load-Displacement curves of experimental tests and geometrical/material properties of beams.

Number	Specimen ID	Reference
1	ST120	C.G. Karayannis, C.E. Chalioris (2013)
2	ST80	
3	S-0157	L. Jin et al (2023)
4	S-0314	
5	S-0628	
6	S-0942	
7	B44-1.5W	M. Hamrat et al (2018)
8	B44-2W	
9	B86-1.5W	
10	B86-2W	
11	S06	C. Lee et al (2010)
12	S10	
13	S890	M. Tahir et al (2019)
14	F0S0	R. Guo et al (2020)
15	A01	C. Cucchiara et al (2003)
16	A02	
17	B01	
18	B02	
19	B1S06	C. Lee et al (2015)
20	B1S10	
21	B2S06	
22	RCTB-1	H. Ma et al (2023)
23	RCTB-2	
24	RCTB-3	

Table 3.1: Experimental program database

3.2.1 C.G Karayannis, C.E. Chalioris (2013) [7]

In this paper a shear test is conducted on 8 RC beams with continuous rectangular spiral reinforcement as transverse reinforcement. Two beams, used as control specimens, had no transverse reinforcement. To perform an analysis that will be easily achievable and reproducible only specimens ST80 and ST120 have been considered (where ST stands for stirrups), because of their standard geometry, in line with the purpose of this thesis.

Geometry and Materials

All beams, shown in Figure 3.1 have same length of 1840 mm, a shear span a equal to 720 mm, a height of 300 mm and width of 200 mm. Span to depth ratio a/d is 2.67 for all specimens.

Four bars of 18 mm diameter act as tension reinforcement while two bars of 14 mm diameter as compression reinforcement. Longitudinal reinforcement (both tension and compression) was measured to have a yield strength $f_y = 550MPa$ and ultimate strength $f_u = 690MPa$. Diameter of transverse reinforcement is 5.5 mm with spacing equal to 80 mm for ST80 beam and 120 mm for ST120. About stirrups, yield and ultimate tensile strength was respectively $f_y = 310MPa$ and $f_u = 430MPa$.

Reinforcement properties are summarized in Table 3.2 (Elastic Modulus has been imposed equal to 200 GPa).

ϕ (mm)	Elastic Modulus (GPa)	Yield Strength f_y (MPa)	Ultimate Strength f_u (MPa)
5.5	200	310	430
14	200	550	690
18	200	550	690

Table 3.2: Reinforcement mechanical properties of ST-80/120

Compressive and tensile strength have been tested on standard cylinders casted the same day, their values are $f_c = 28.5MPa$ and $f_t = 2.60MPa$. Elastic modulus of con-

crete, missing from this research, is calculated with Eq. (3.1) from [1]:

$$E_c = 22000(\frac{f_c}{10})^{0,3} \tag{3.1}$$

Measurement set-up

Beams are simply supported by rollers (d=1640mm) using a rigid frame. A four-point bending setup was adopted. Load has been imposed by means of a spreader beam in two points 200mm apart. The test is load controlled by a cell with accuracy equal to 0,05kN. Continuous measurement of loads and deflection is recorded at midspan and supports throughout the test.

Results

A pure shear response was demonstrated by both specimens considered. In the shear span of beams, diagonal significant fissures emerged leading to shear failure before the longitudinal tensile reinforcement could even yield. Figure 3.1 displays cracking pattern of beams ST-80 and ST-120 at failure. Initial flexural cracks began to appear on the underside as soon as the applied load reached 35kN. As the load increased, cracks propagated and gradually inclined cracks formed within the shear region at both sides of the beams. At failure both control beams displayed one major diagonal crack.

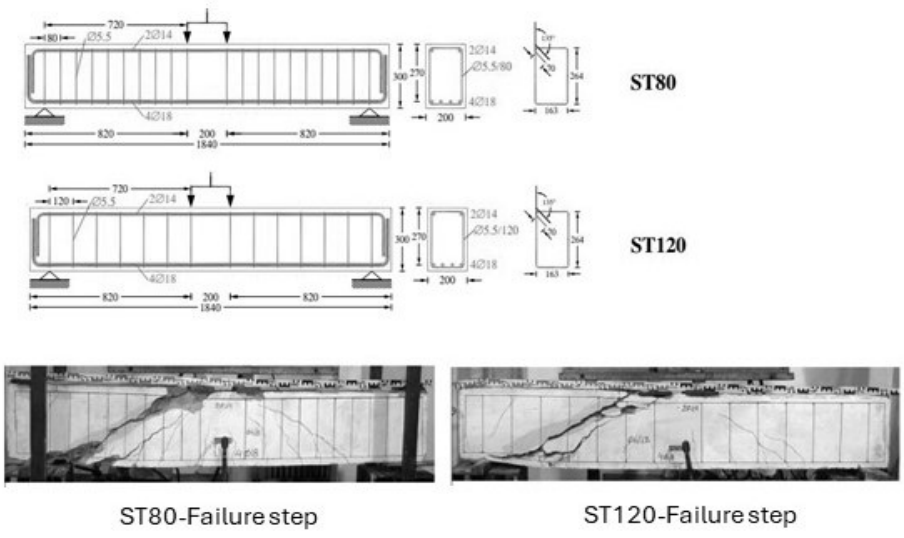

Figure 3.1: Geometry and failure mode of ST80/ST120

3.2.2 L. Jin et al (2023) [18]

The aim of this study is to investigate the impact of the stirrup ratio on the size effect in RC beams. Since shear failure experiments have been performed, S-group beams have been considered. Large-dimension deep beams (M-group and L-group have been excluded). Their varying stirrup ratio is ranging from 0,157% to 0,942%.

Geometry and Materials

S-goup beams are characterized by a beam height h equal to 300mm and distance between two supports (effective length) is equal to 5h for all specimens. All tested beams have same shear-span ratio a/d equal to 1,5 but different stirrups ratio (0,157%, 0,314%, 0,628%, 0,942%). To achieve such ratios a spacing between stirrups was set respectively at 360, 180, 90, 60mm.

All beams are 1800mm long with a base width b of 100mm. Further properties are highlighted in Figure 3.2.

The concrete used in this experiment is a C30 commercial concrete, with aggregate particle sizes ranging from 5 to 25 mm.

Average compressive strength f_{cu}, measured on three cubic samples poured 28 days before, is 41,6MPa; while the average tensile strength f_t is set at 2,60MPa.

Hot-rolled Ribbed steel Bar (HRB400) with mechanical properties shown in Table 3.3 represent lower longitudinal reinforcement (4ϕ18), upper longitudinal reinforcement (2ϕ12) and shear reinforcement (ϕ6).

ϕ**(mm)**	**Elastic Modulus** E_s**(GPa)**	**Yield Strength** f_y**(MPa)**	**Ultimate Strength** f_u**(MPa)**
6	212.4	406	590
12	209.4	408	584
18	210.3	456	593

Table 3.3: Reinforcement mechanical properties of S-series beams

Measurement set-up

All RC beams are simply supported at sides and loaded symmetrically using a two-point central loading system (400-tons electro-hydraulic servo testing machine). For S-serie beams 50mm wide steel gasket are used to prevent localized damages due to compressive stresses.

A force-controlled loading system, capable of a loading rate of 10kN/min has been employed for the tests. To measure beam deflections, strain gauges are localized at mid-span and on each stirrup.

Results

Throughout the experimental tes, bending cracks were initially observed at the mid-span position of the RC beam. As the load increased, these bending cracks propagates vertically, leading to an increase in the number of pure bending cracks. Between 20% to 40% of the peak load, corresponding to 44-50kN for S-serie, oblique cracks suddenly appear. These oblique cracks extended diagonally towards the loading point. Eventually, the oblique cracks extended to the loading point in coincidence with peak load as shown in Figure 3.2. A distinct shear failure mode is highlighted by the development of oblique cracks from the supports to the loading points.

Altought a higher stirrup ratio promoted more extensive internal crack development and increased their quantity, it is evident that he presence of stirrups delayed crack propagation, thereby enhancing the structural integrity and improving the ductility of RC beams.

As regards the stirrup strains, it is clear from the analysis of data that the strain increases approaching the peak load and the higher the stirrup ratio, the smaller the stirrup strain because of a better involvement of reinforcement elements. In this way, shear stress assigned to each stirrup decreases.

Since two specimens of each beam were tested, an average value of load-displacement combination will be considered for further analysis in the next chapters.

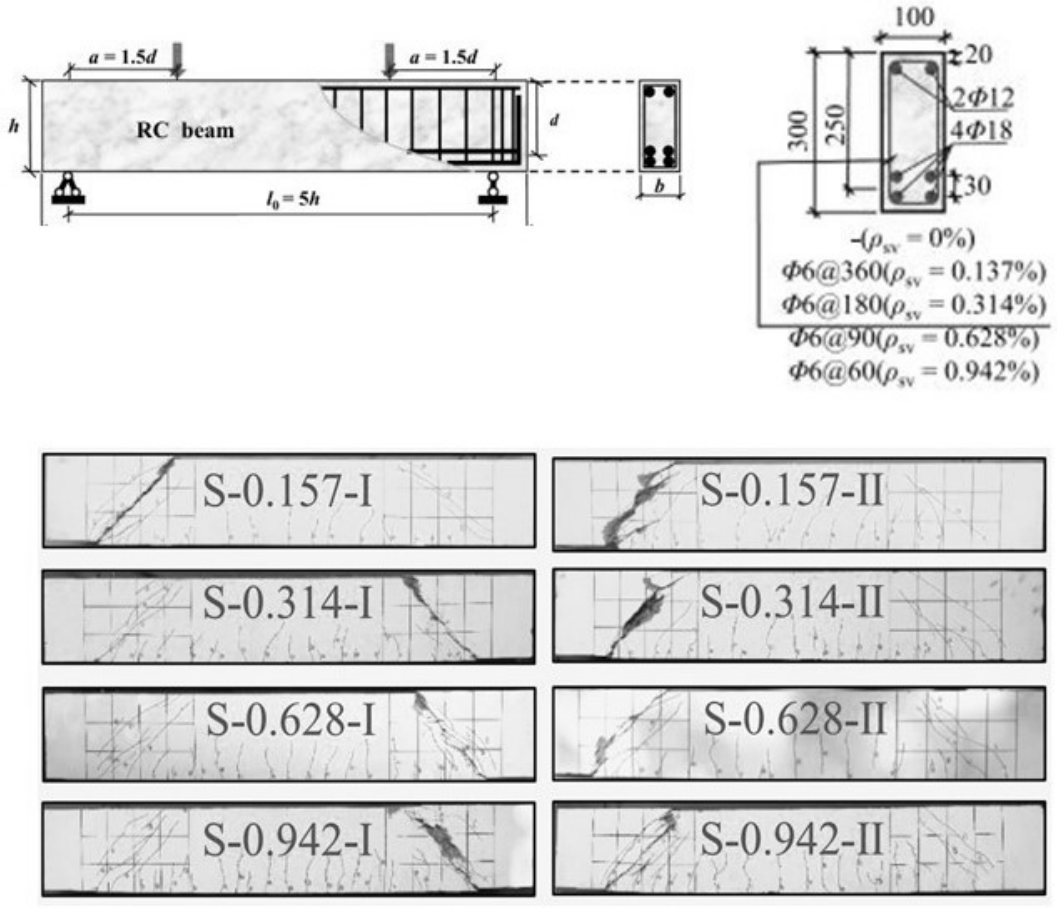

Figure 3.2: Geometry and failure modes of S-series beams

3.2.3 M. Hamrat et al (2018) [20]

This research highlights the impact of shear reinforcement on crack pattern, ultimate load-bearing capacity and ductility of RC beams. Several samples were tested, both made from high-strength concrete and normal-strength concrete, to compare experimental results with ones calculated with major universal codes. Among 26 RC beams tested in this paper, only few specimens (B44-1.5W, B44-2W, B86-1.5W, B86-2W) have been considered for a reverse analysis in Chapter 6, because of the presence of stirrups, shear failure mode and varying geometric properties.

Geometry and Materials

RC beams have been classified in three series according to their concrete strength properties:

- 44 ($f_c = 44,2MPa$; $f_t = 3,37MPa$; $E = 32Gpa$);
- 65 ($f_c = 67,6MPa$; $f_t = 3,74MPa$; $E = 34,5Gpa$);
- 86 ($f_c = 85,5MPa$; $f_t = 4,50MPa$; $E = 37Gpa$).

Only beams with transverse reinforcement, denoted with W, have been considered. Letter A denotes a subgroup whose main longitudinal reinforcement is $2\phi10$, while letter B indicates a $2\phi14$ as main reinforcement (properties in Table 3.4).
Transverse reinforcement is $\phi6$ for all beams with a spacing equal to 90mm.
Elastic modulus of steel is 200 GPa for all reinforcement types.

reinforcement type	ϕ **(mm)**	**Yield Strength** f_y	**Ultimate Strength** f_u	**Yield Strain** $\mu\epsilon$
Transversal	6	508	581	2378
Longitudinal	10	520	635	2397
Longitudinal	14	512	620	2306

Table 3.4: Reinforcement mechanical properties of A/B series beams

Primary testing parameters are reflected in the notation of RC beams. For instance, B44-2W is a beam belonging to B subgroup with $2\phi14$ as main reinforcement, presence of shear reinforcement and a concrete strength of 44,2 MPa.

Measurement set-up

Four-point bending test has been performed using a 250kN servo-controlled hydraulic to apply a monotonic increasing load. Strain gauge placed on the bottom surface was used to measure mid-span displacements. The analysis of the development of diagonal cracks and their width throughout the test was possible thanks to Video Gom-Aramis system.

Results

Specimens with and without shear reinforcement exhibited a similar crack development up to the point of diagonal crack formation.

However RC beams with shorter shear spans (a/d=1,5) showed diagonal cracks covering the full depth of the cross section, it is also true that crack width remained pretty constant during further loading steps.

Most of beams with stirrups failed because of a crushing of concrete in the upper part instead of pure shear as exhibited by beams without transverse reinforcement. By taking a closer look to crack pattern of beams after failure, in Figure 3.3 it is evident that by increasing the concrete strength also number of cracks has increased, maybe because of a better steel-concrete bonding and a redistribution of stresses inside the core.

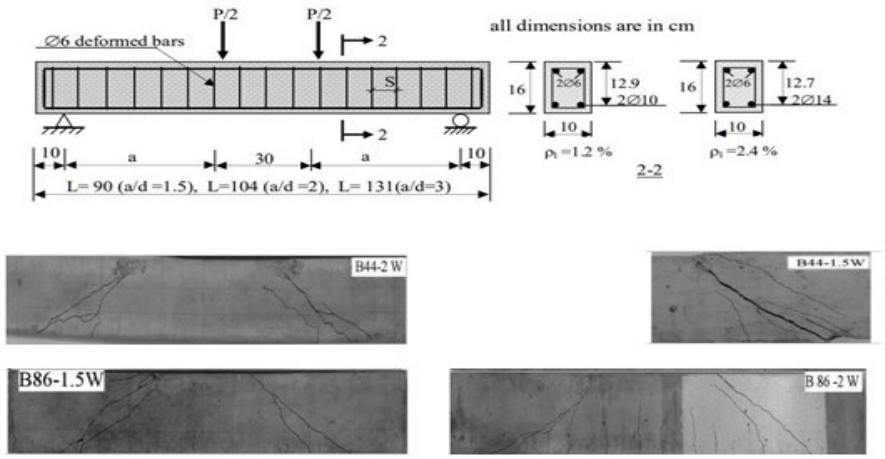

Figure 3.3: Geometry and failure modes of A/B-series beams

3.2.4 C. Lee et al (2010) [12]

This paper analyses the effectiveness of fiber sheet strips (FSS) used instead of steel stirrups. Same beams are then tested using fiber-reinforced polymer rod stirrups and traditional stirrups to compare results.
Although 10 RC beams have been tested, for the purpose of this thesis only control specimens, equipped with basic steel shear reinforcement, S06 and S10 will be considered.

Geometry and Materials

The two selected beams have same geometry and material properties, except from stirrups diameter. S06 has $\phi 6$ stirrups with 100mm spacing, while S10 has $\phi 10$ with 100mm spacing.
Their length is 1400mm and dimensions of cross section is 250mm x 150mm, as illustrated in Figure 3.4. The span between supports is supposed to be 1030mm.
Concrete compressive strength f_c, measured after 28 days on a cylinder specimen, is 32,5 MPa. Elastic Modulus, not given in this research, is calculated according to equation 4.1 and set equal to 31,3 GPa.
Upper longitudinal steel reinforcement is made of $2\phi 6$ bars, while $2\phi 22$ work as lower tensile reinforcement. Yield strength of both longitudinal and transverse reinforcement is $f_y = 400Mpa$. Since E_s and f_u are not provided, they are set respectively equal to 190GPa and 500Mpa to better reflect experimental results while modeling.

Measurement set-up

A three-point loading set up, displacement controlled, has been used to perform bending test. The machine capacity was 1000kN and all specimens have a span-depth ratio of 2.5. Vertical loads are transferred from the testing machine to RC beams by means of a pin-joint steel plate located at mid span on the upper edge. Vertical displacements and tensile strain of longitudinal/shear reinforcement were measured using linear variable differential transducers.
After failure, to better investigate stirrups behaviour, concrete cover has been removed.

Results

In all specimens, flexural cracks, followed by shear diagonal cracks, initially emerged near the midspan.

Under monotonic loading one of these shear cracks eventually expanded into a significant one, resulting in the shear failure of the RCB. The first shear crack appeared under a load of 132.4 kN in S06 beam, close to the maximum moment region during the early loading phase. As the load increased, additional shear cracks formed. A brittle failure is caused by an extended diagonal crack from the support to the loading point (peak load of 241.8 kN).

The S10 specimen, on the other hand, demonstrated not only a higher stiffness (maximum load of 300.7 kN) but also a more significant deflection compared to the other specimens. By increasing the shear reinforcement ratio from 0,004 in S06 to 0,009 in S10, the shear resistance provided by stirrups rose by 71%, explaining the reason behind this behaviour. In both specimens a maximum crack width was recorded near the peak load.

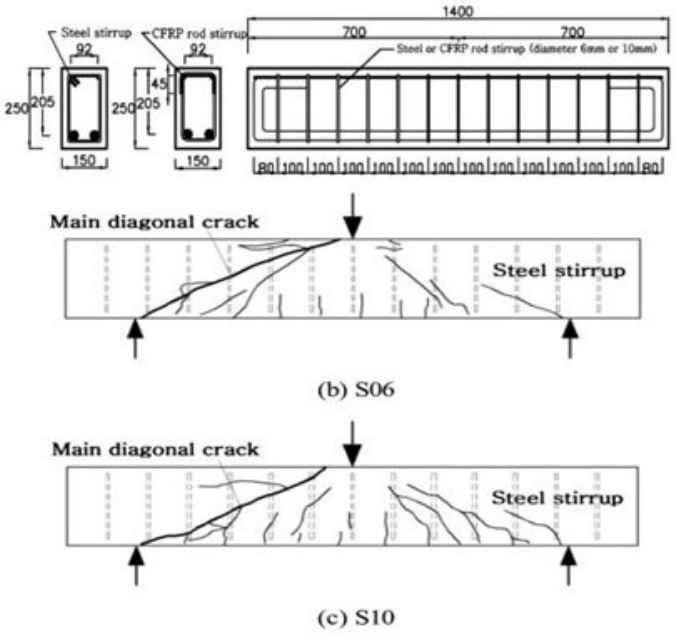

Figure 3.4: Geometry and failure modes of S06/S10

3.2.5 M. Tahir et al (2019) [21]

This paper deals with shear behaviour of RCB reinforced with polymeric carbon fibers (CFRP).

A total amount of seven full-scale specimens were tested. Since this thesis is focusing only on shear failure of RC beams equipped with steel stirrups, only sample S890 has been considered.

Geometry and Materials

S890 is a RCB with rectangular cross-section of 200x500x2650 mm as shown in Figure 3.5. S stands for steel, first number is the diameter of stirrups and last digits represents the inclination of shear reinforcement with respect to horizontal axis. Tensile longitudinal reinforcement consists of $5\phi22$ ($\rho_l = 2,19\%$), and $2\phi22$ as longitudinal reinforcement in compression zone. Shear span-to-depth ratio, designed to lead to a shear failure mode, is 2.3 and stirrups spacing is fixed at 200 mm.

Main properties of steel bars are presented in Table 3.5. Ultimate Strength will be calculated according to [1].

ϕ (mm)	Elastic Modulus (GPa)	Yield Strength f_y (MPa)	Yield Strain $\mu\epsilon$ (%)
8	190	380	0.20
22	200	460	0.25

Table 3.5: Reinforcement mechanical properties of S890

Regarding concrete, an average compressive strength, measured on cylinder samples, was 40MPa. Elastic modulus of concrete is calculated with Eq. (3.1).

Measurement set-up

Electric strain gauges, attached to the longitudinal steel reinforcing bars at their mid-length, measured strain levels. Also stirrups and concrete (compression zone) strains have been monitored using electric strain gauges located above mid-span. To measure the beam's deflection, three LVDTs were employed.

A load-controlled bending test with a rate of 0,1 kN/s has been performed, until the

shear crack width reached 1 mm. At each 30 kN increment, records of the crack patterns were made and the crack width was measured. Then, load was applied continuously until the beam failed.

Results

An inclined diagonal crack from the mid-height, which then expanded and extended toward both the top and bottom of the beam led beam S890 to failure (Figure 3.5).
A diagonal tension failure has been identified once the peak load has been reached. The main crack, suddenly opened wide, causing failure in a brittle manner and leading to a significant drop in load. Taking a look at load-deflection curve in Appendix 1.1 it is clear that initial stiffness of RCB is independent from the type of shear reinforcement. Around 300 kN a reduction of stiffness occurred in beam S890 due to the yielding of steel stirrups. The ultimate load of 470 kN taken by S890 was way lower than other specimens reinforced with CFRP stirrups; it can be addressed to a lower f_y of steel stirrups compared to fiber-reinforced ones.

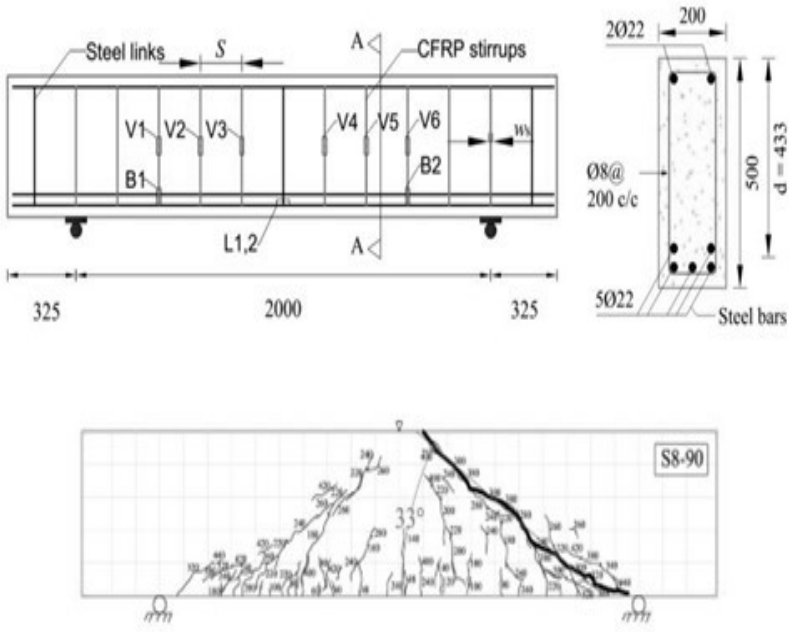

Figure 3.5: Geometry and failure mode of S890

3.2.6 R. Guo et al (2020) [25]

This work explores the shear behaviour of reinforced concrete beams by using alternative reinforcement layers made up of Engineered Cementitious Composite (ECC) and fibre reinforced polymer (FRP) grid.
Out of seven tested beam, only the control specimen F0S0, mixed with ordinary Portland cement, will be investigated for the purpose of this thesis.

Geometry and Materials

F0S0 beam is 1500 mm long, with a 120x200 mm cross-section. Supports span 1300 mm, as depicted in Figure 3.6, while a/d is 3,13.
Mechanical properties of concrete have been measured on cubic samples 28 days after the casting date. Compressive strength of concrete f_c is 31,6 MPa, while tensile strength f_t is 2,19 MPa. Measured elastic modulus E_c is set equal to 28,7 GPa.
Maximum aggregate siza is 10 mm and Water to cement ratio is 52%.
Both longitudinal and transverse reinforcement are made up of HRB400 steel, whose mechanical properties are displayed in Table 3.6.
Compression longitudinal reinforcement is composed of $3\phi18$, while $2\phi18$ reinforce the tension zone. Stirrups have a diameter of 6 mm with a spacing of 250 mm.

ϕ (mm)	Elastic Modulus (GPa)	Yield Strength f_y (MPa)	Ultimate Strength f_u (MPa)
6	200	400	540
18	200	400	540

Table 3.6: Reinforcement mechanical properties of F0S0

Measurement set-up

A 4PBT has been performed, with loads applied to roller bearings and distributed through a girder. A monotonic load was applied under displacement-controlled conditions (rate= 0,01mm/s) by a 1000kN hydraulic loading system.
Among 18 strain gauges placed on the beam, it is important to mention those to measure deflection at mid-span, at roller bars and strain of concrete in compression region and longitudinal tensile reinforcement.

Results

For what concerns the control beam F0S0, flexural cracks occurred within the bending zone at first loading stages. From load-deflection curve in Appendix 1.1, the inflection point shows a change in stiffness when the load approaches 30kN because of the formation of flexural cracking.

By increasing applied load, a diagonal shear crack developed connecting the support to the loading point of RCB (Figure 3.6). A brittle shear-tension failure characterises this beam, whose load carrying capacity suddenly dropped because of the large fracture.

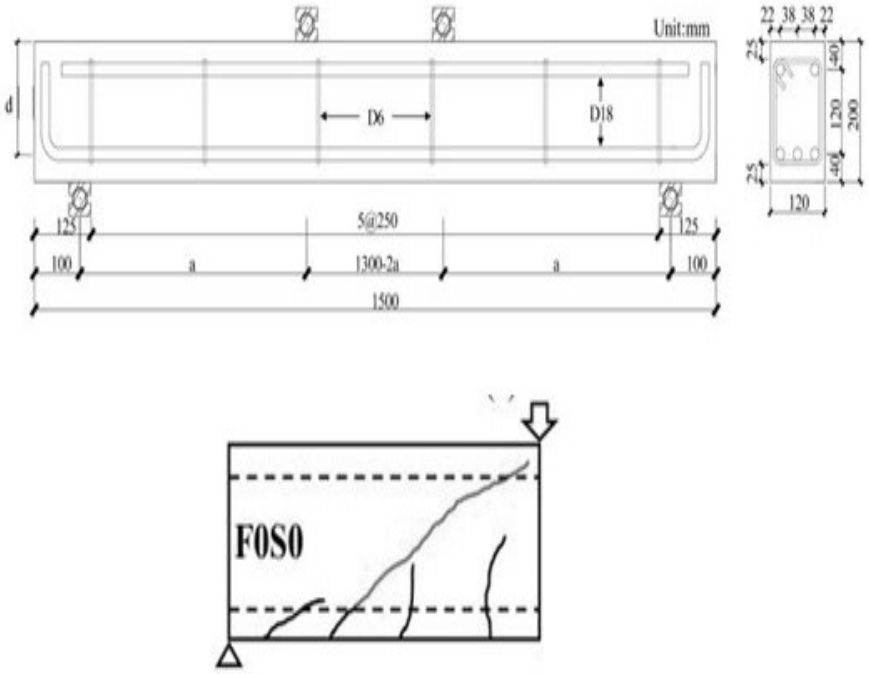

Figure 3.6: Geometry and failure mode of F0S0

3.2.7 C. Cucchiara et al (2003) [11]

A 4PBT has been carried out on rectangular simply supported beams. Both plain concrete and fiber-reinforced concrete have been used to understand the relation between brittle/ductile failure mode and percentage of fibers inside the mix.
Given the presence of stirrups and absence of fibers (denoted by number 0 in the code), beams A01, A02, B02 have been taken in consideration for further analysis. A series has an $a/d = 2,8$, while $a/d = 2,0$ for B series. Last number identifies the spacing of stirrups (1 for s= 200 mm and 2 for s=60mm) as shown in Figure 3.7.
Beam B01 has been discarded because the experimental evidence does not reflect the expected behaviour.

Geometry and Materials

Rectangular cross-section of considered beam is 150x250 mm while overall length is 2500 mm. Concrete cover is 15 mm and supports are located at 100 mm from side edges. A Portland cement type 42,5 was used to prepare the beams and its mechanical properties are listed below:

- $f_c = 41,20$ MPa, measured on three cyclindric specimens;
- $f_t = 2,02$ MPa;
- $\epsilon_0 = 2,513(10^{-3})$;
- $E_c = 26,094$ GPa.

Tension longitudinal reinforcement is made of $2\phi 20$, while 2 bars $\phi 10$ are placed in compression zone to correctly anchor stirrups. Deformed bars $\phi 6$ constitute shear reinforcement. Mechanical properties of A01, A02, and B02 steel reinforcements are highlighted in Table 3.7

ϕ (mm)	Elastic Modulus (GPa)	Yield Strength f_y (MPa)	Ultimate Strength f_u (MPa)
6	232	510	561
10	232	610	671
20	232	610	671

Table 3.7: Reinforcement mechanical properties of A0/B0 series beams

Measurement set-up

A displacement-controlled test (rate of 0,5mm/min) has been performed by means of a testing machine able to apply 600kN through two steel cylinder lying directly on the upper surface. The same steel cylinders were used as supports (spanning 2300 mm) to avoid the occurance of horizontal reactions.

A data acquisition system monitored loads while displacements were registered by three LVDT placed on the bottom part at mid-span and supports.

Results

When spacing s increases, from 60 mm to 200 mm, like in beam A01, a brittle failure mode characterized by the rupture of a stirrup crossed by diagonal crack occurs (right side of Figure 3.7). Shear failure governs the process in beam B02 as well, where a significant crack developed from supports to loading application point.

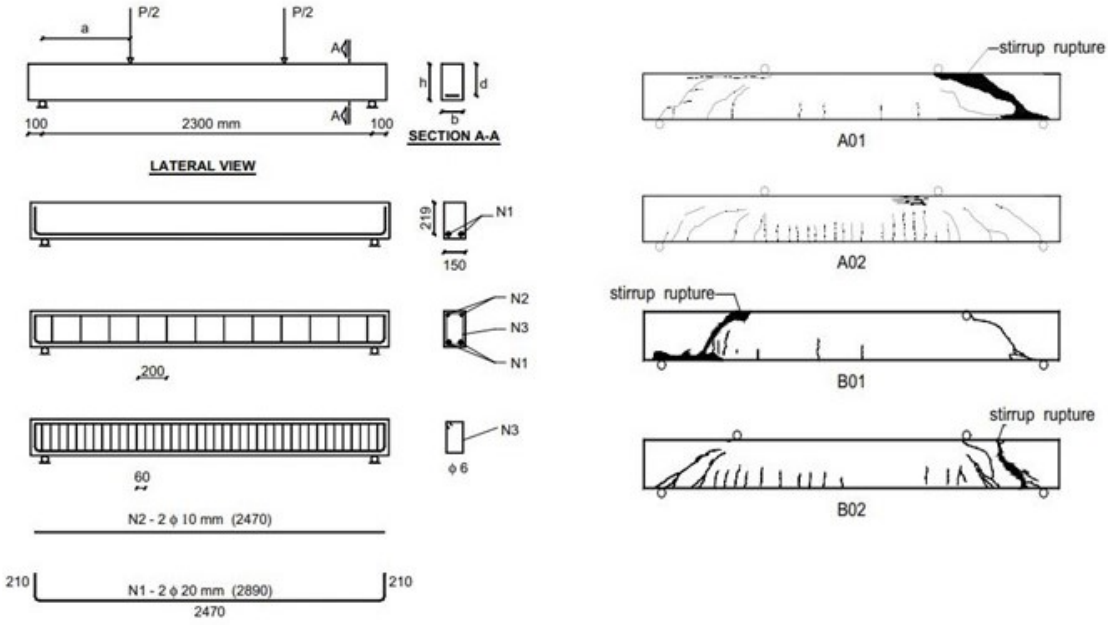

Figure 3.7: Geometry and failure mode of A0/B0 series beams

3.2.8 C. Lee et al (2015) [13]

Shear capacity of RCB embedded with carbon-fyber polymer stirrups has been studied in this research through a 3PBT to compare results with standard specimen.

Geometry and Materials

Two groups of beams specimens (seven in the group 1 and five in group 2) have been prepared to observe shear behaviour and failure modes.

Belonging to each group is highlighted by the first digit in each beam's code.

As already mentioned for previous cases, only steel stirrups will be considered for the purpose of this thesis reducing the analysis to beams B1S06, B2S06, B1S10 and B2S10 only.

Dimensions of cross section are 150x250 mm, and the overall length is 1400 mm (a/d=2.5 for all beams). Stirrups are interspersed each 100 mm, as depicted in Figure 3.8. The cylinder concrete compressive strength is 24 MPa for beams belonging to first group (B1S06 and B1S10) and 30 MPa for beams belonging to the second one (B2S06 and B2S10). The author of the paper provided some further data missing in this article ($E_c = 32Gpa$, $f_t = 2,6MPa$).

Concerning steel reinforcement, $2\phi22$ work in tension zone, $2\phi6$ represent longitudinal reinforcement in compression zone to anchor steel stirrups $\phi6$ and $\phi10$ depending on the group. Its mechanical properties have been resumed in Table 3.8.

ϕ (mm)	Elastic Modulus (GPa)	Yield Strength f_y (MPa)	Ultimate Strength f_u (MPa)
6	190	420	530
10	190	420	530
22	190	420	530

Table 3.8: Reinforcement mechanical properties of B series beams

Measurement set-up

A UTM (Universal loading machine) loaded concrete specimens with a rate of 0,5mm/min under displacement-controlled configuration. Vertical load pass through a pin-joint connected to steel plate, while two cylinders act as supports on both sides. A LVDT

has been used to measure vertical displacement at midspan and two strain gauges acquired data related to longitudinal upper and lower reinforcement. An additional set of 6 electronic strain gauges monitored tensile strain of shear reinforcement.
Crack width and propagation has been measured through a microscope.

Results

It is common for all specimens to initiate flexural cracks when applied loads are low. Then, at a certain point, shear cracks developed diagonally between supports and loading point, activating stirrups against tensile stresses.
Both B1S06 and B2S06, with lower stirrups ratio, have undergone a sudden shear failure at a maximum load of 203 kN and 236 kN.
Beam B1S10 showed a 1,22 times greater resistance than B1S06, and a different failure mode: concrete crushed in compression zone simoultaneous to the development of a diagonal crack (Flexural-shear failure), shown in Figure 3.8.
Specimen B2S10 failed close to 290 kN by flexure (discarded).

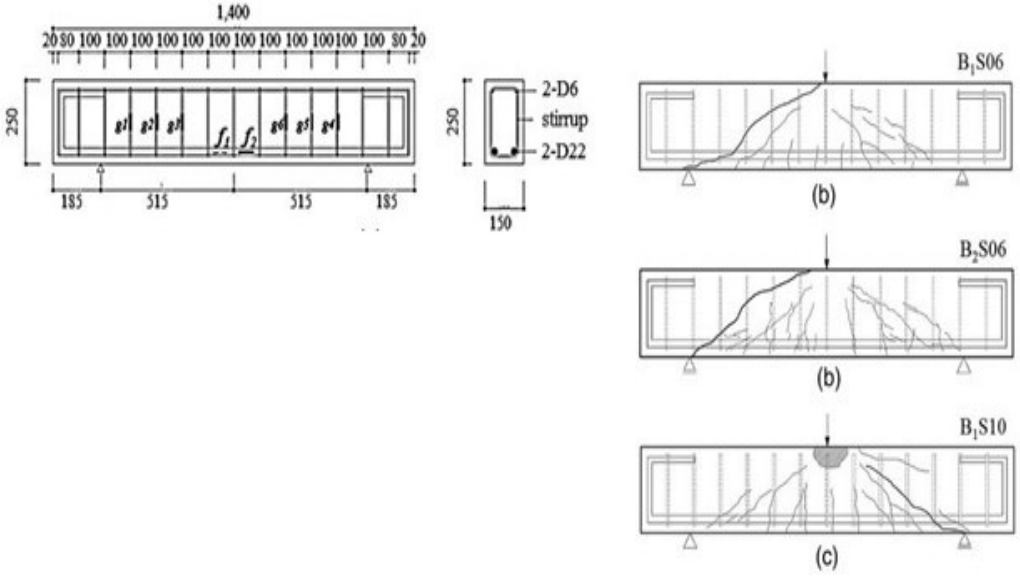

Figure 3.8: Geometry and failure mode of B-series beams

3.2.9 H.Ma et al (2023) [16]

Shear behaviour of double channel steel reinforced concrete (CSRC) transfer beams, double I-shaped steel reinforced concrete (ISRC) transfer beams and RC beams has been analysed in this paper (13 specimens).

Geometry and Materials

Among all beams considered, only RC beams (RCTB-1, RCTB-2, RCTB-3) will be deeper investigated because of their standard steel reinforcement.

Cross-sectional dimensions are 475x400 mm, while effective spans are respectively 800, 1200 and 1600 mm, as highlighted in Figure 3.9. Overall length is 1100, 1500 and 1900 mm with a shear-span ratio λ set to 1.0, 1.5, 2.0.

Thickness of concrete cover is 20 mm. As regards concrete mechanical properties, a class C40 with $f_c = 46,8MPa$ and $f_t = 3,06MPa$ has been employed. Its Elastic Modulus is 35,3 GPa.

Upper longitudinal steel reinforcement is made of 6ϕ16, while longitudinal bars in compression zone are 6ϕ22 (HPB400).

Transverse reinforcement (spacing=100 mm for all beams) is constituted by ϕ8 (HPB300).

Properties of steel reinforcements are given in Table 4.9.

ϕ **(mm)**	**Elastic Modulus** E_s **(GPa)**	**Yield Strength** f_y **(MPa)**	**Ultimate Strength** f_u **(MPa)**
8	210	347	516
16	200	464	662
22	200	458	648

Table 3.9: Reinforcement mechanical properties of RCTB series beams

Measurement set-up

The shear performance tests of these transfer beams were conducted by means of a electro-hydraulic servo press machine. Beams were simply supported.

The loading rate was maintained between 0.5 mm/min and 1 mm/min. To monitor concrete and steel strains, two displacement meters were positioned at the beam's support ends, and one displacement meter at the bottom of the beam (mid-span) to

observe development patterns.

Vertical strain gauges were positioned at the shear span locations, and transverse strain gauges were affixed to the longitudinal reinforcement and stirrups.

Results

Failure mode of considered beams are shown in Figure 3.9.

As soon as the load started to increase, small vertical cracks appeared from the bottom surface. At around 40%-50% of the peak load some diagonal cracks developed from supports upwards.

By increasing vertical load, these cracks turned into main oblique cracks joining lower edge to loading point.

A typical brittle behaviour was not only deductible from load-displacement curve (Appendix 1.1), where after reaching peak load the curve turns downward suddenly, but also because of the noticeable sound of concrete while cracking. During this process, a clear shear failure mode was displayed and the bearing capacity of the reinforced concrete transfer beams significantly decreased.

Strain in the stirrups began to show up when diagonal cracks appeared, because of the concrete no more contributing in the overall bearing capacity of the RCB.

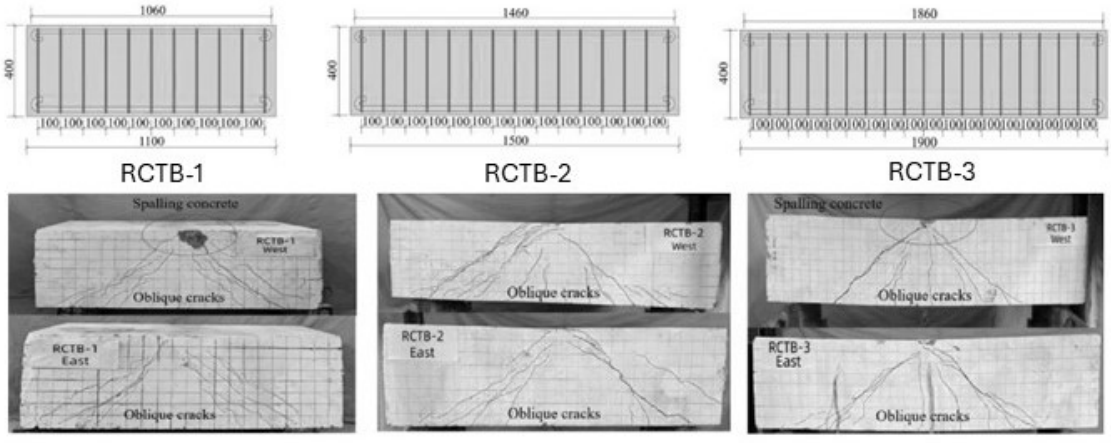

Figure 3.9: Geometry and failure mode of RCTB-series beams

4 | FEA theory and ATENA 2D application

Finite Element Method (FEM) analysis is a computational technique used to solve complex physical problems (governed by differential equations) across various engineering and scientific disciplines. It involves breaking down a large, complex system into smaller, simpler parts called finite elements. These elements are then analyzed individually, and their behaviors are assembled to predict the behavior of the entire system. In structural engineering, dependent variables usually analyzed are stresses, strains or displacements throughout a structural element that can be represented in one-dimension, two or three-dimensions according to the purpose of the analysis. This chapter delves into the theoretical framework of Finite Element Analysis (FEA) and the principles of modeling reinforced concrete beams with stirrups, focusing the attention on the features provided by the software ATENA by Cervenka Consulting. A brief introduction to ATENA 2D will be given, followed by the explanation of how a FEA can be adopted for non-linear problems.

4.1 Theory of Finite Element Analysis

The fundamental concept behind FEM Analysis is to break down a continuous and complex structure into smaller discrete elements. These elements are then interconnected at specific points called nodes. By considering the structure as a combination of single units connected only at nodes, FEM transforms the problem into a system

of linear algebraic equations. Nodal displacements usually represent the unknown variable of the problem. Once solved, these nodal values, along with interpolation functions, can be used to approximate the field variables for each element and the entire structure.

In order to perform a FEA, some common steps, independent from softwares or processors, need to be performed [39]:

- **Discretization**: the first step involves dividing the continuous structure into a mesh of discrete elements. A proper mesh size is essential not only to achieve reliable results, but also to increase computational efficiency.

- **Definition of Displacement function**: once the structure is discretized, appropriate interpolating functions (typically polynomials) are chosen to represent the displacements within each element. These functions must be easy to calculate while accurately representing the element's deformation. Displacement function is generally expressed as:

$$f = [N]\delta_e \tag{4.1}$$

  where f is the displacement vector at any point, $[N]$ the shape function matrix and δ_e the vector of nodal displacements.

- **Element characteristic analysis**: when external forces are applied to a body, a mutual internal force is exchanged between each element; strain and displacement are associated to each point.

  The strain and stresses within each element are calculated using solid mechanics equations:

$$d = [B]\delta_e \tag{4.2}$$

  where d is the strain and $[B]$ the geometric matrix.

  In static analysis, the principle of virtual work relates the nodal displacements to applied loads by introducing virtual displacements, which are small, permis-

sible displacements that satisfy system constraints. The work done by external forces through these virtual displacements defines virtual work, helping derive the relationship between loads and nodal displacements in a static equilibrium system. Based on this the equilibrium equation can be written:

$$P_e = [N]\delta_e \tag{4.3}$$

where P is the load applied to each unit, $[N]$ the element stiffness matrix.

- **Global equilibrium equation**: After analyzing each element, the equations are assembled into a global system that represents the entire structure (Eq.(4.4)). External loads and boundary conditions (e.g., constraints and external forces) are applied in this step.

$$P = [N]\delta \tag{4.4}$$

where P represents the nodal forces, N is the global stiffness matrix, and δ are the global nodal displacements.

- **Numerical Solution**: The system of linear equations is solved to find the nodal displacements. From these nodal displacements, strains and stresses in each element may be calculated.

- **Comparison and visualization**: The final step involves analyzing the results to assess the structure's performance. This includes comparing results with experimental or expected values and visualizing them through graphical representations (e.g. stress and deformation plots).

4.1.1 Non-linear Finite Element Analysis

Concrete is well-known for its non-linear material behaviour, which typically needs a NLFEA to simulate accurate and precise approximations of real-world conditions (e.g. parabola-rectangle mentioned in [1] is an idealization). The FEA method described in previous section becomes more complex in non-linear scenarios because the stiffness

matrix depends on displacement or deformation. As reported in [32] there are three main sources of non-linearity in solid mechanics:

- **Geometric non-linearity:** applied loads and stiffness become dependent on the structure's instantaneous geometry. Second order effects are induced because of large displacements.
- **Material non-linearity:** if strains are large as well, material non linearities may occur. Material properties become dependent on stress or strain current state.
- **Boundary condition non-linearity:** when a contact area between different elements or loads that depend on the deformation of the structure are present, such a condition may occur.

Other cases where NLFEA may be necessary have been introduced by [29], including the estimation of the reliability of reinforced concrete members with complex geometries or reinforcement details, complementing methods like strut-and-tie for more complete equilibrium and compatibility solutions.
It is valuable in assessing existing structures built with outdated standards, allowing for a realistic safety margin evaluation to potentially avoid costly upgrades. NLFEA is also useful for seismic assessment through push-over analysis to estimate structural capacity.
The analysis effectively models "D-regions" with localized stress fields, explains observed crack patterns and local damage origins, and considers second-order effects in slender members where stiffness diminishes with cracking. Additionally, it aids in evaluating robustness under accidental loads, such as explosions or extreme earthquakes, by simulating dynamic effects from the removal of key structural elements. Lastly, NLFEA can assess fire resistance, capturing the impacts of high temperatures on complex structures.

4.2 ATENA 2D

ATENA (Advanced Tool for Engineering Non-Linear Analysis) is a finite element software developed by Červenka Consulting s.r.o., especially designed to perform detailed reinforced concrete analysis. Real behaviour of concrete structures can be simulated, including concrete cracking, crushing and reinforcement yielding. Discrete bars or smeared reinforcement can be modelled, while concrete material properties are automatically calculated using the equations from [28] . Users can trace the propagation of cracks and the distribution of stresses and strains at every stage of the loading process, while the simulation is still going on. Moisture and thermal loads can be also considered before running the analysis. Although ATENA can be used up to three-dimensions interfaces, for the purpose of this thesis only a two-dimensional analysis was performed on concrete beams. Plane-stress and plane strains are involved.

Following the framework given by Červenka Consulting, three macro-phases can be analyzed when using the software:

- **Pre-processing**
- **FE non-linear Analysis**
- **Post-processing**

Detailed information about model generation will be provided in Chapter 5.

4.2.1 Pre-processing

The main goal of the pre-processing phase is to create a geometrical model on which to perform finite element analysis. Starting from an experimental benchmark, as it is this case, geometries should be modelled in the most accurate way by defining joints coordinates and lines to create macroelements. Track of the number of joints, lines, nodes, load cases, etc is available in *General Data* window. Material properties and boundary conditions are essential to properly match with good accuracy model's and real struc-

ture's behaviour. Supports and load cases have to be specified as well. Once mesh is automatically generated and solution parameters has been defined the analysis itself may begin.

4.2.1.1 Materials

A smeared model is used by the software to ensure a uniform distribution of concrete cracks and reinforcement (smeared reinforcement) inside a control volume, associated with an entire finite element. Within smeared approach, a perfect bond between concrete and reinforcement is assumed.

Constitutive model SBeta: the constitutive model is based on the stiffness and is described by the equation of equilibrium in a material point [40]:

$$\mathbf{s=De}, \mathbf{s} = [\sigma_x, \sigma_y, \tau_{x_{y^t}}], \mathbf{e} = [\epsilon_x, \epsilon_y, \gamma_{x_{y^t}}] \tag{4.5}$$

where **s** is the stress vector composed of plane stress state components, shown in 4.1, taking into account both contribution of concrete and reinforcement if present, **D** is the stiffness matrix and **e** the strain vector.

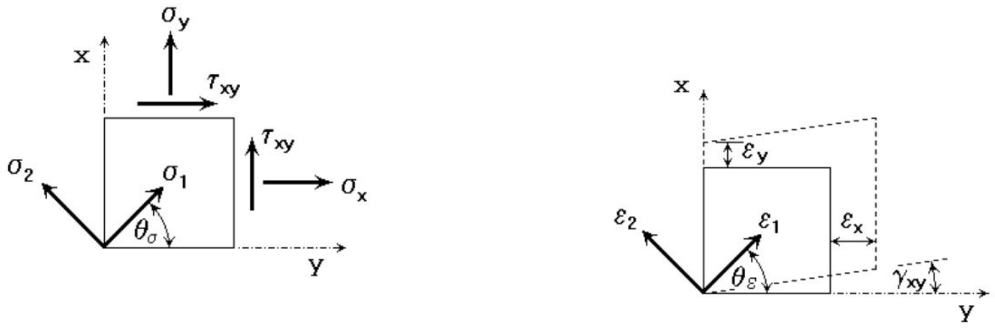

Figure 4.1: Plane stress state components

Basic: the basic tab allows the user to define main parameters that characterize the Sbeta Material. The definition of Elastic modulus E, Poisson's ratio μ , tensile strength

f_t and compressive strength f_c outlines Stress-strain Law and Biaxial Failure Law as shown in 4.2.

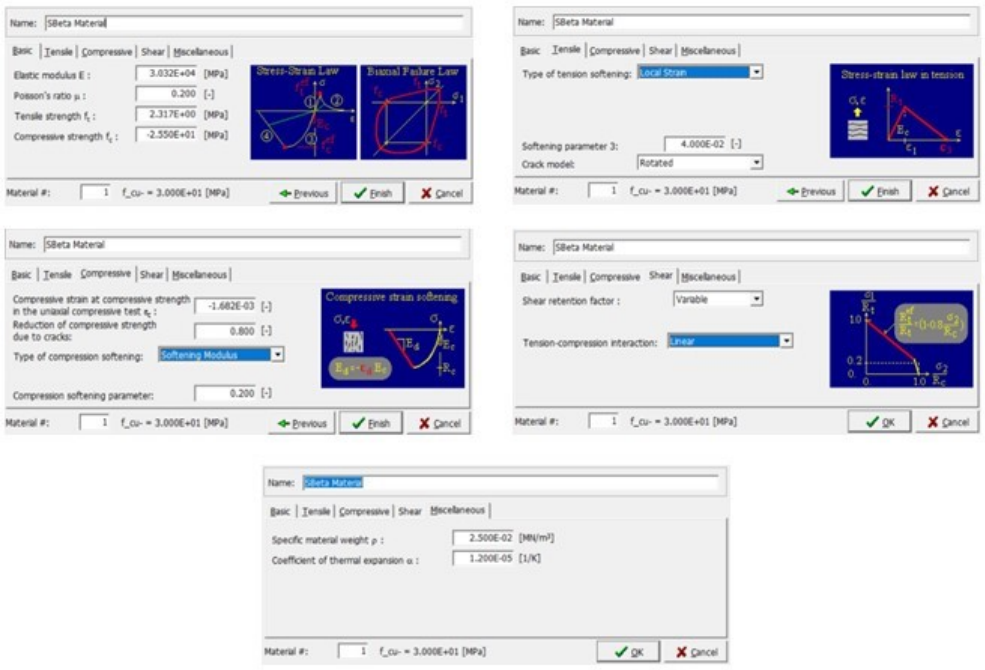

Figure 4.2: Atena tabs to assign concrete properties (*Basic, Tensile, Compressive, Shear, Miscellaneous)*

It's important to note that compressive strength is automatically calculated on the basis of input value of Cube compressive strenght f_{c_u} in Mpa. A factor 0.85 links the mean compressive cylinder strength to the cube strength as follows:

$$f_c = f_{c_u} 0.85 \tag{4.6}$$

Tensile: type of tension softening and crack model can deeply influence the behaviour of the model. Among all softening models included in SBeta material, linear softening based on Local Strain has been used for all considered beams.
The strain parameter c_3, corresponding to the point where stress drops to zero, represents the ultimate point along the descending branch of the stress-strain diagramm for SBeta material.

Correction to the law should be introduced for high-strength concrete, Ultimate capacity is higher but ductility decreases and so does the stiffness that governs the descending branch of stress-strain law in tension.

Two options are available for crack models as highlighted in Figure 4.3:

- **Fixed crack model**: cracks occur when tensile stress exceeds tensile strenght of concrete. The direction of crack is perpendicular to principal stress direction and also in case of further loading crack direction remains constant and fixed. After cracking, the concrete displays anisotropic properties because stress and strain direction are no more coincident.
- **Rotated crack model**: rotated crack model assumes that direction of cracks rotates continuously on the changes in the axes of principal strains when cracks are initiated [26]. Only normal stress components are considered.

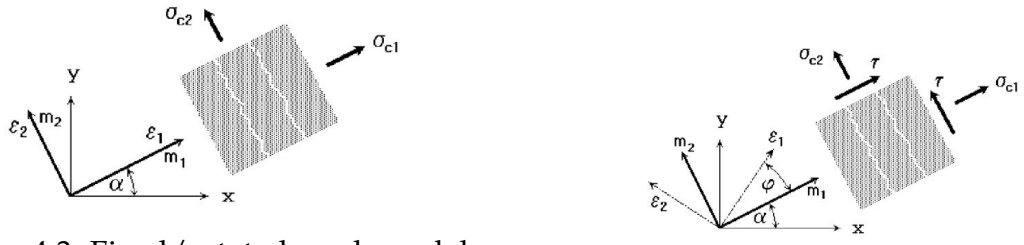

Figure 4.3: Fixed/rotated crack model

Compressive: experimental values for compressive strain at compressive strenght ϵ_c have been used. If not provided, they have been calcuated according to [1]. Reduction of compressive strenght coefficient due to cracks varies in a range 0.45-0.80 in accordance to experimental results found by [17] and [31] . It mostly depend on reinforcement type and mesh sizing.

Instead of performing the analysis by assuming a fictitious crush band model working with compressive displacements and energy dissipation, a simpler softening law based on strain has been adopted. This formulation, mesh dependent, is defined by means of plain concrete elastic modulus E and a compression softening parameter C_d.

Shear: the amount of shear stress transferred accross a crack is characterized by a Shear retention factor. This parameter ranges between 0 and 1. A shear retention factor of 0 refers to no aggregate interlock, while 1 represents full aggregate interlock [35]. However it has been fixed at 0.2 with linear tension-compression interaction, its influence is crucial only to the post-peak response, which is something not really covered by this thesis.

Miscellaneous: in this tab the user is asked to insert specific material weight γ and the coefficient of thermal expansion α. Unless specific data are provided by experimental benchmark, a specific weight of $2.5E^{-2}MN/m^3$ is considered (higher than default value of $2.3E^{-2}MN/m^3$ because the weight of rebars is already taken into account at this step and it will not be accounted again under reinforcement properties), while α is set to the default value $1.2E^{-5}1/K$.

Reinforcement: Depending on the scope and type of structural element to be analysed in ATENA, reinforcement can be modeled as either smeared or discrete.
On one side the smeared reinforcement is represented by layers of elements (mesh generated) that enhance the concrete stiffness at the nodes they connect to. A specific volume ratio of reinforcement is taken into account by modeling these elements with composite material properties. On the other side, discrete reinforcement is modeled using one-dimensional truss elements that extend across the concrete macro-element, ensuring compatible displacements between the two materials. Both approaches assume a uniaxial stress state.

Basic: constitutive models of reinforcement are available in this tab. Linear and bilinear characterise strenght and ductility of reinforcement. The first specifies only the Elastic modulus E, while the latter introduces a yielding limit σ_y.
To perform accurate analysis, a bilinear stress-strain law with hardening, shown in Figure 4.4 has been taken into account since data about ultimate strenght are usually provided. Reinforcement is able to carry increased load after yielding up to a specified ultimate strenght [3].

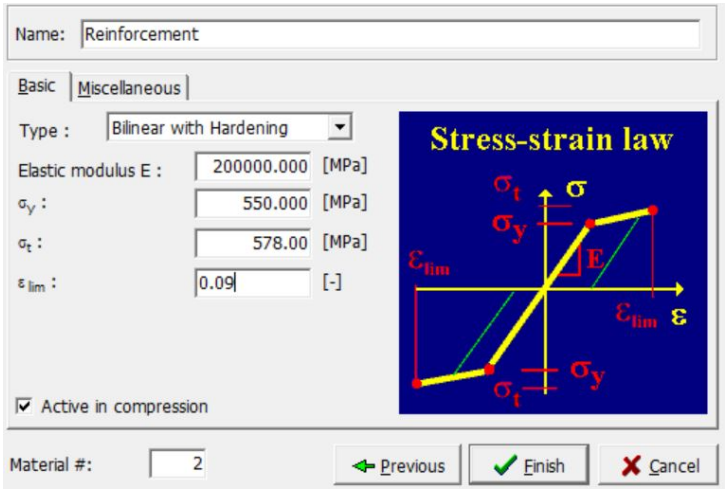

Figure 4.4: ATENA reinforcement constitutive model

Miscellaneous: As mentioned when analysing properties of SBeta material, specific weight γ of reinforcement is set to 0 because already accounted. Since thermal expansion coefficient α of plain concrete and steel is similar, a default value of $1.2E^{-5}1/K$ has been taken into account.

Plane stress Elastic Isotropic: A plane stress elastic isotropic constitutive model has been considered for steel plates used as supports of RC beams. Same material has been taken into account at the top of RC elements to model plates on which load is applied. Their presence is essential to reproduce boundary conditions of experimental tests but their geometrical and material properties should be hyphothised because data are lacking.

Basic and Miscellaneous: Parameters, as they appear, are set by default values and weight is neglected not to influence self-weight of RC beam during loading steps.

Spring: Spring element has been used to define support conditions for some RC beams, where forces acting on boundaries of structural elements are linearly proportional to associated displacements. The boundary force at a node i of the spring element is calculated through Eq. (4.7) [40]:

$$R = \frac{u_i k A}{n \, |dir|} \tag{4.7}$$

where:

u_i	Displacement at spring element node i
k	Spring material stiffness
A	Area of spring element
n	number of element nodes (1 for CCspring)
$\|dir\|$	Euclidean norm of direction value

Due to a stiffness discrepancy between ATENA analysis and experimental results, it was found out that high-stiffness springs (calibrated according to tests) better represent boundary condition at a point for some of the beams highlighted in Tables A1.3 and A1.4. Area and direction value of springs will be associated when defining macro-elements.

4.2.1.2 Topology

Although materials have been properly specified with reference to experimental data, the geometry and mesh elements of RC beams is still missing.

Joints and lines

Joints (set of bidimensional coordinates in ATENA 2D) and lines that connect joints define the geometrical boundaries of the RC beam. No refinement has been selected.
A beam may be constituted by different geometrical entities like main core, support plates and load plates; in case of I-shape beam also the flanges should be modelled. ATENA allows the user to choose among three types of connection between those elements:

- ***Rigid connection*** is used to define the interface between elements made up of different materials like steel plates and concrete beam.
- ***Interface*** is useful in case there is an interface between element of the same material.

- ***No connection*** should be used in all cases where there is no interface between elements.

Since beams are characterized by straight lines, arc or circle functions have not been adopted.

Macro-elements

Macro-elements can be created only after having properly defined lines and joints. Macro-elements let the user to fill the space inside a boundary list of lines. To perform a correct analysis, some properties need to be set when creating a macro-element.

- ***Mesh type and Mesh size:*** triangles, quadrilaterals or both can be used when defining the mesh type. As highlighted by [40], mesh sensitivity problems may arise when a smeared crack model is adopted. In real concrete spacing of micro-cracks is dictated by the size of aggregates, while ATENA distributes a crack over the element defined by the mesh size. As mentioned by [3], if a mesh is extremely fine, more than necessary, there is the possibility that too many micro-cracks are generated before a macro-crack appears. This behaviour, due to software limitations, may cause stiffer structural response than real case and underestimation of cracks width. A proportional relation with maximum aggregate size is useful to associate a value to lower limit of a mesh:

$$L_t = 1.5 d_a \tag{4.8}$$

  where:

  L_t Lower limit

  d_a Maximum aggregate size

  The upper limit is represented by the maximum crack spacing, if known, or reinforcement spacing (typical range of 80-300mm).

- ***Material and thickness:*** materials can be chosen among those defined in Section 4.2.1.1, while thickness is essential to characterize RC beams. Steel plates have

been modelled with same thickness as concrete core.

- ***Type of quadrilateral elements:*** simple CCISOquad have been used for steel plates, while CCQ10SBeta elements have been selected for SBeta macro-elements because specifically designed for that material.

Reinforcement

At this point concrete core and steel plates of RC beams are complete while reinforcement still need to be modelled with discrete elements. A polyline of straight segment is used and begin/end coordinates of the segment are specified in a tab. In this way both longitudinal reinforcement and stirrups take shape. Material and area, automatically calculated by the software by specifying number and diameter of bars, are associated to each element.

4.2.1.3 Loads and supports

The location and dimensions of support and loading plates were assumed starting from CAD transpositions of provided figures and adjusted in height and length to better match with experimental results. Data are available in Tables A1.3 and A1.4

Load cases

Among all load cases provided by ATENA only some of them were effectively adopted during our analysis.

- ***1-Body force:*** to account for self-weight of concrete beam a body force load case has been employed. A LC coefficient equal to 1 is assumed along the negative Y-Direction.

- ***2-Supports:*** forces reaction at the base of RC beams are taken into account by Supports LC. Once the load case is defined, support conditions need to be assigned to specified joints or lines.

  Since all RC beams have been considered simply supported, only right side sup-

port allows displacements along X direction. To avoid early rupture of concrete in tension along support's side, this load case should be applied only to the central joint of steel plate.

For those beams mentioned in Appendix 1.3 springs are introduced to reduce stiffness of supports in case it is overestimated by the software.

- ***3-Loads:*** external loads are taken into account within this load case. During three-points and four-points bending tests, loads are distributed over steel plates to avoid localized failure at contact points with the concrete beam. To better account for these conditions, the load is assumed to be applied vertically from top to bottom (negative Y-axis) with a continuous full-length configuration on the upper surface of plates.

  Magnitude of applied loads should be specified by the user in MN/m, when dealing with a load-controlled simulation.

4.2.1.4 Run

Data check is automatically done by the software; if something is missing the analysis can not start. At this point analysis steps, monitoring points and solver features should be defined.

Analysis steps

Experimental tests are all characterized by a loading history (displacement history if the test is displacement-controlled) that mainly depends on the equipment used to perform them.

Loading history consists of several load steps that should be defined through this tool in ATENA. At each step, a configuration of load cases is defined as well as the definition of a solution method.

Self-weight of RC beam, corresponding to load case 1 (body force), combined with load case 2 is taken into account during the first load step. Loading history is represented by all following steps that consider load cases 2 and 3. For all steps multiplier

is fixed to 1 to make computation easier during post-processing.

Solution parameters

In non-linear FEA, a series of gradual steps is needed to generate the load-displacement curve without knowing its shape in advance.

Two solution methods are provided by [40] to solve non-linear problems.

- ***Newton-Raphson:*** is a common method to solve non-linear problems. It is useful to solve equilibrium equations where the stiffness matrix [K] depends on the value assumed by displacement vector [U]. The following Eq. (4.9) governs the procedure:

$$k(u)u = P \tag{4.9}$$

  where stiffness k is displacement-dependent (u) while load P is not. At first step no load is applied so that P_0=0, and no displacement is present (u_0=0).
  Based on uniform load steps, the load-displacement curve is generated and k(u) and u are updated through iterations. At each iteration, a load imbalance e_p is calculated according to Eq. (4.10):

$$e_{p_i} = P_i - k_t(u_j)u_{j+1} \tag{4.10}$$

  where:
  i current load step
  j current iteration within load step
  Iterative procedure skips to the next step only when the load imbalance e_p is sufficiently close to a pre-defined tolerance level specified by the user.

- ***Arc-length:*** another method to solve problems characterized by non-linear phenomena is Arc-length. Due to its robustness and computational efficiency it can be a useful tool even in case where Netwon-Raphson fails (material non-linearity with discontinuous stress-strain diagrams or stability issues related to

snap-back/snap through phenomena). In all these cases, convergence may be reached by introducing an additional degree of freedom associated to load.
Within an iteration not only loading is observed but the complete load-displacement relationship.

Detailed modeling assumptions will be provided in Chapter 5.1.

Monitoring points

To be able to generate a load-displacement curve during the analysis monitoring points should be added to the model. Displacements, loads and reactions, stress or strains can be monitored in correspondence of monitoring points. In our model, governed by load-controlled cycle, a displacement (along Y-axis) monitoring point is always placed at mid-span close to the bottom edge of the beam to measure mid-span deflections. If additional data are provided, some monitoring points may be placed where maximum crack width is registered.

4.2.2 Analysis

Once pre-processing tabs have been properly compiled, the analysis itself can begin. Before running it, data that generate the load-displacement curve should be specified, also if they could be changed later through the interactive window. A check of the beam deformation and the distribution of stresses and displacements is constantly visible throughout the analysis, thanks to the visualization options.

4.2.3 Post-processing

At the completion of analysis a new graphical interface will appear. It may happen that analysis ends prematurely because of numerical errors or limited load steps.
In post-processing window results belonging to each load step are available and could be highlighted through rendering and coloured legends. Among all the functions provided by Athena 2D, only those useful for the work carried out will be mentioned.

Deformed shape

Deformed and underformed configuration are both available. Deformed shape with magnified displacement can be useful to generally understand the behaviour of RC beam subjected to imposed loads.

Engineering strain

Maximum (tension) and minimum (compression) principal strain can be displayed during post-processing.

Principal strains not only provide insight into material behavior, allowing for a better understanding of how different regions of the beams are deforming, but helps in identifying potential failure modes and localized deformation where strains exceed material's capacity.

Stress

Principal stress analysis provides a detailed understanding of the stress distribution within a beam. This information is important for identifying regions that are highly stressed or at risk of failure. Furthermore, if principal stresses are similar to experimental tests (when data are available), the confidence in the accuracy of the analysis is increased.

Cracks

Cracks are widely used to identify their location both at elements and integration points. Their labelled width is crucial to better recognize failure modes and compare models' behaviour to the one from the Experimental program.

Bar reinforcement

It may happen, although it is rare, that a beam modelled in ATENA and same beam from experimental benchmark collapse under different failure modes. Principal strain of bar reinforcement can be confirmation tools when results are doubtful. Plastic strain may be useful to identify which bars have actually experienced yielding.

When results have been saved, they can be exported. Load-displacement curve can be automatically downloaded.

To better manage numerical data a text output called CCO-file should be downloaded. When running a new analysis instead, another text file (CCT-file) can be mentioned

due to its powerful features.

CCO file

Text output containing all data related to monitoring points when the analysis is complete. In correspondence of each load steps, displacement and number of iterations required by solution method is displayed. These data have been exported into Excel to generated load-displacement curve cleansed of self-weight associated displacement. Moreover, if number of iterations approaches the upper limit it may imply a lower accuracy of the solution.

CCT file A direct association to an Indentity card is not reductive. It contains all data related to geometrical characteristics, materials, loads, monitoring points, etc of a beam available during the pre-processing. This file will be extremely useful when performing a probabilistic analysis. Each beam will be modelled thirty times by changing input parameters like material properties directly from CCT file.

5 | RC Beams modeling based on inverse analysis of experimental data

Conducting physical experiments and observing the resulting data of interest is a widely used method to study the structural behaviour of any type of Reinforced concrete structure.
In this thesis the experimental benchmark introduced in Chapter 3.2 has been numerically replicated through validated NLN modeling assumption, following the guidance introduced by [14].

5.1 Inverse analysis procedure

This report uses an Inverse analysis methodology derived from a manual iterative process introduced by the software developer Červenka Consulting for NLFEM. This approach, based on a smeared crack modeling (rotated crack model), focuses on fine adjustment of the load-displacement curve to match experimental data by adjusting parameters, in an iterative way, within the CCQ10SBeta Material model in Atena 2D. Main parameters that have been modified within this method are the ones that govern the tensile, compressive and shear behaviour of RC structures:

- Compressive and tensile strength
- Tension law and softening parameter c_3
- Crack model

- Compression law and compression softening parameter
- tension-compression interaction

The finite element mesh size has determined through a calibration process for each structural element, with values ranging between 3,5 cm and 10 cm. This range provides a good compromise in terms of predictions accuracy and computational effort. The nonlinear system of equations was solved using a modified Newton-Raphson iterative method, whose settings are provided in Table 5.1

Parameter	**Value**
Iteration number limit	500-1500
Solution method with iteration	-
Unbalanced energy limit	0.8
Limit of line search iterations	3
Displacement error multiple (break after step)	10
Residual error multiple (break after step)	10
Absolute residual error multiple (break after step)	10
Energy error multiple (break after step)	1000

Table 5.1: Newton Raphson solver modeling assumptions

For what concerns concrete behavior, the *SBeta material* accounts for a curvilinear response under compression, transitioning to linear compression softening (LCS) after the peak, governed by the softening modulus. The LCS calibration is designed to ensure that once the peak load is reached, the compressive strength decreases by 50% (60-70% when f_c overcomes 45-50 Mpa) at the ultimate compressive strain of the concrete.

For tensile behavior, the concrete remains elastic up to its tensile strength, beyond which it follows a linear tension softening (LTS) pattern, governed by softening parameter c_3.

To consider the fracture energy after cracks formation, the ultimate strain in tension has been set between 2-14 times the tensile strain corresponding to tensile strength of concrete [22].

As regards steel reinforcement, a bilinear constitutive law with hardening has been

adopted to simulate the behavior of steel in both compression and tension.
Since longitudinal reinforcement and stirrups play a vital role within a reinforced concrete beam a discrete approach has been used to model steel elements.
Experimetally measured Young's modulus of steel has been employed when available, if missing it has been assumed equal to 200 GPa. The ultimate strain of steel is taken equal to 9% [24].
Steel and concrete properties have been assigned according to experimental database and when data are lacking, the corresponding parameters have been calculated following [1].
After having defined main modeling assumption the numerical simulation may begin. Main steps to be performed to complete an inverse analysis and their sequential order are displayed in Figure 5.1.

- **Step 1**: Define input parameters of mechanical properties of RCB that match with experimental tests if available. If not, calculate missing parameters according to [1].
  Assign parameters, obtained through validated modeling assumptions, that better describe compression, tension and shear behaviour of concrete.
  Solution parameters should be defined to solve non-linear system of equations.

- **Step 2**: Assign the Sbeta material model to the regions of macro-elements that are supposed to represent concrete in the FE-model.
  Assign Reinforcement material model to longitudinal and transversal reinforcement matching their properties with experimental data.
  Assign a plane stress Elastic Isotropic material model to steel plates used as supports or loading-spreaders. Their ρ is set to zero to avoid an over weight contribution.

- **Step 3**: Run the analysis. Sometimes the analysis may be forced to a premature end due to convergence issues. In this case Step 2 and 1 should be redone in this order.

- **Step 4**: Result data can be exported. A comparison of the load-displacement curves (experimental-numerical) represents a good indicator of successful analysis. If the error is too large; update the input parameters and redo all steps. On the other side, if the results are satisfactory they can be used for further application (Probabilistic Analysis) and the NLFEA is complete.

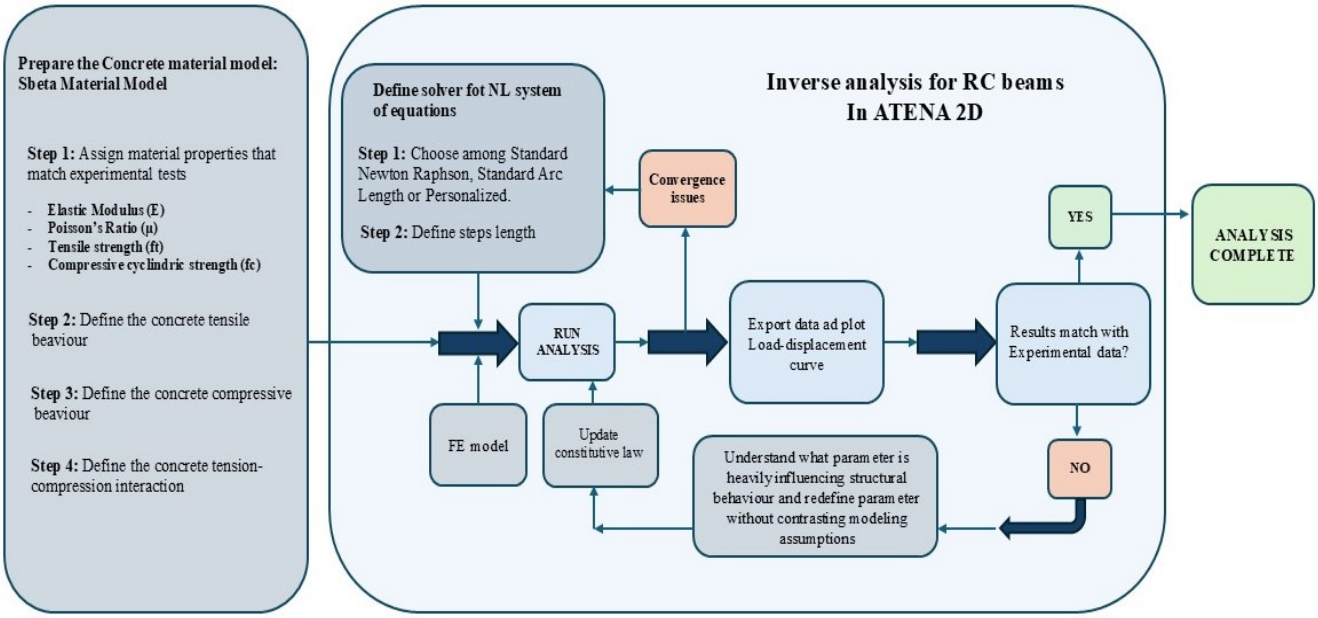

Figure 5.1: Inverse Analysis flowchart, adapted from [3]

5.2 Geometry, boundary conditions and loads

The tested beams have been analyzed in 2D plane stress conditions. When given, dimensions of supports and loading plates or loading cylinders have been taken into account.

If not available, steel plates have been modeled with simplified geometries in order to achieve a good fit with the mesh quadrilateral elements. The width is the same as the beam.

Their thickness has also been chosen to reduce as much as possible the risk of local crushing due to concentration of forces directly applied on the concrete.

Although some hyphotesis have been done, their influence can be considered as negligible on final results.

A rigid contact surface has been selected when an interface between two different materials occurred.

Loads are simmetrically applied in both 3PBT and 4PBT configurations. Loads are linearly applied on the upper edges of steel loading plates to avoid force concentration.

To simulate as much as possible the simply supported conditions, a pinned constraints (both x and y-axis) has been assigned to bottom left support, while a roller supports the beam on the right side.

Only load-controlled analysis have been performed since this thesis purpose is to find peak bearing capacity of RCB and better reflecting experimental results.

A summary of modeling assumption and geometrical properties of constraints are reported in Appendix 1.3.

5.3 NLNAs results

Figures 5.2-5.5 highlight the results from the NLNAs performed in Atena considering experimental values of both materials (f_{exp}) and geometrical (a_{exp}) properties compared to those coming from experimental tests (R_{exp}).
Failure modes, consistent with experimental results, are reported with experimental mechanical properties of concrete and both longitudinal and shear reinforcement.
A monitoring point that measure displacement along Y-axis is located at midspan for all beams and peak strains of both reinforcement is also recorded and shown in the exact position.
Reinforcement yield point, when present, is denoted by a blue dot in the load-displacement curve of NLNAs. It represents the beginning of plastic field associated to further deformations.
Generally, the failure of each simulation during inverse analysis process occurs in the last load step, confirming the validity of the convergence assumptions. Particular attention was paid to avoiding premature numerical failures that could diverge from experimental reality.
Considering the type of brittle collapse, the simulations were able to fairly accurately replicate the actual behavior of the structures observed during the experimental tests [7, 11, 12, 13, 16, 18, 20, 21, 25] .

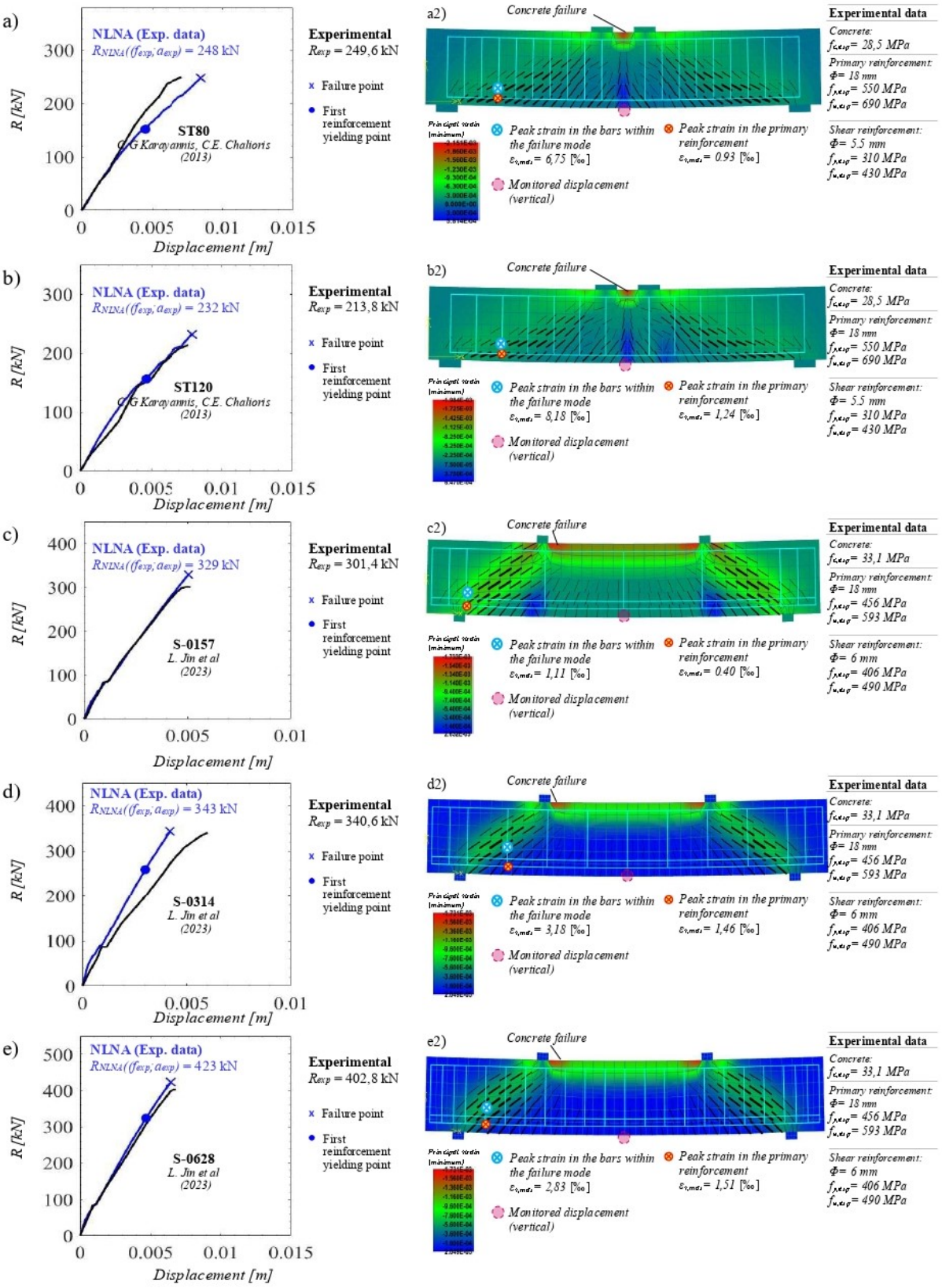

Figure 5.2: RC members belonging to database (Chapter 3.2): comparison between experimental results Rexp and NLNAs outcomes RNLNA(f_{exp}; a_{exp}) (a, b, c, d, e); representation of the failure mechanism in concomitance of failure (a2, b2, c2, d2, e2).

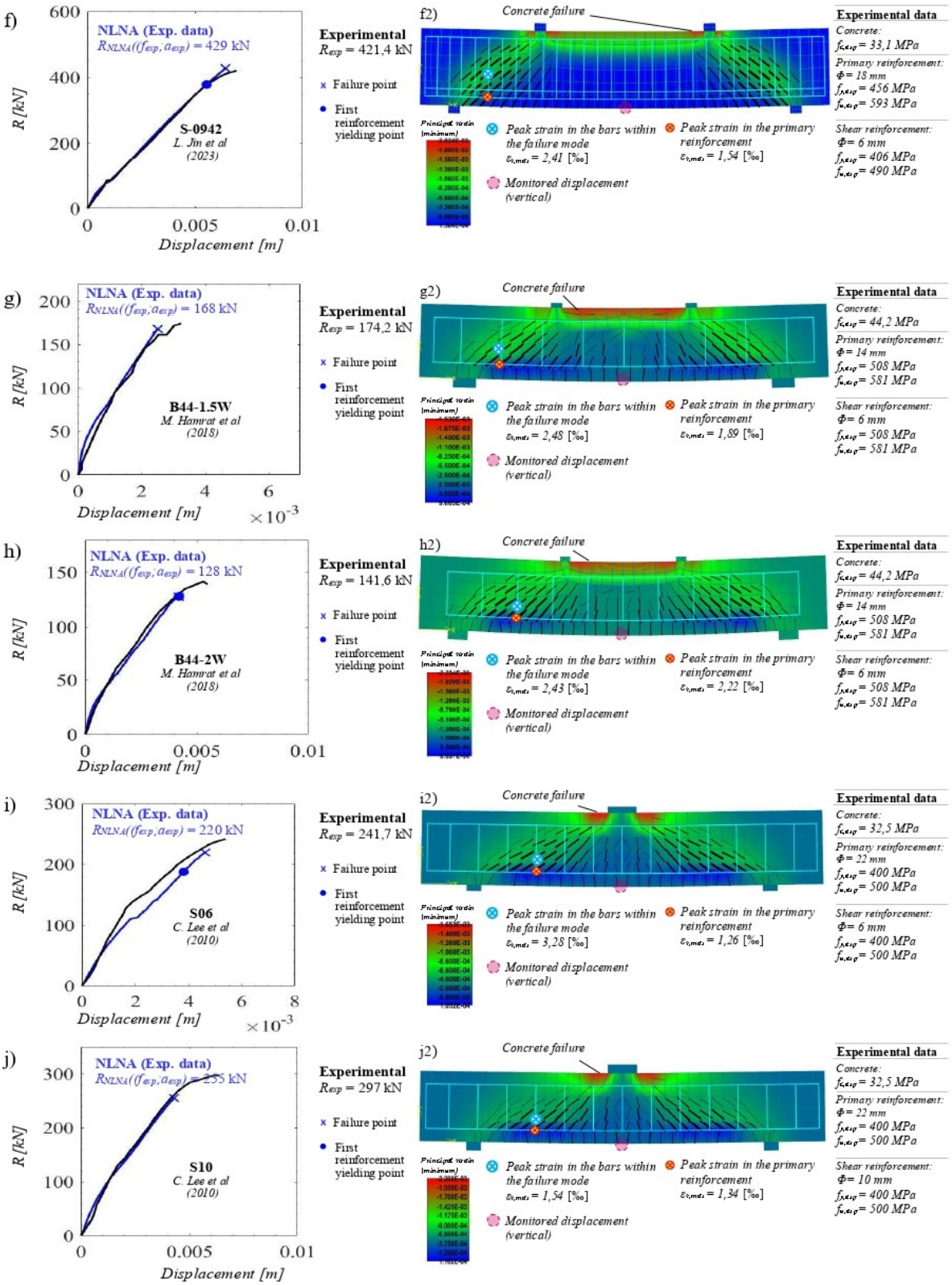

Figure 5.3: RC members belonging to database (Chapter 3.2): comparison between experimental results Rexp and NLNAs outcomes RNLNA($f_{exp}; a_{exp}$) (f, g, h, i, j); representation of the failure mechanism in concomitance of failure (f2, g2, h2, i2, j2).

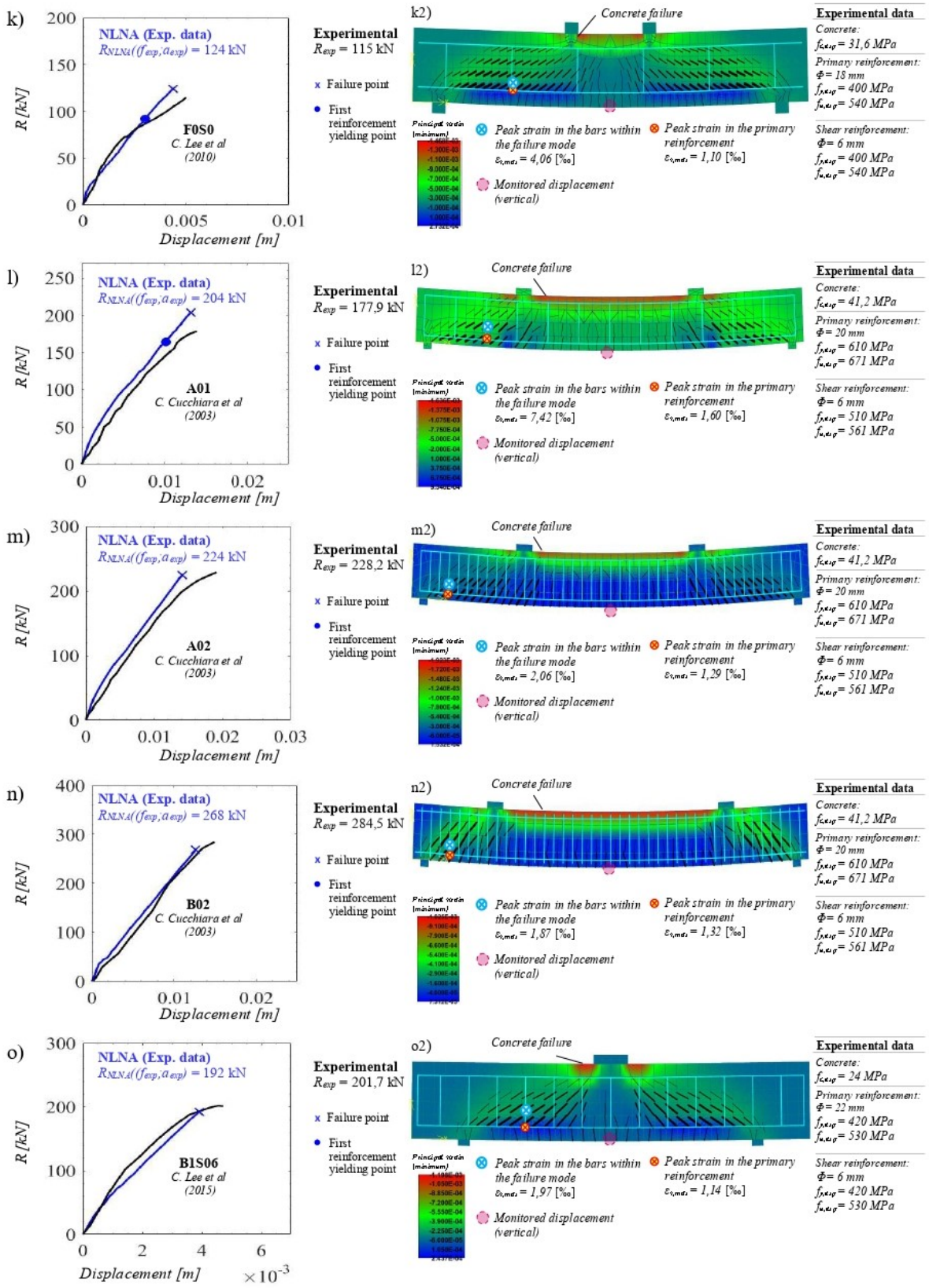

Figure 5.4: RC members belonging to database (Chapter 3.2): comparison between experimental results Rexp and NLNAs outcomes RNLNA(f_{exp}; a_{exp}) (k, l, m, n, o); representation of the failure mechanism in concomitance with failure (k2, l2, m2, n2, o2).

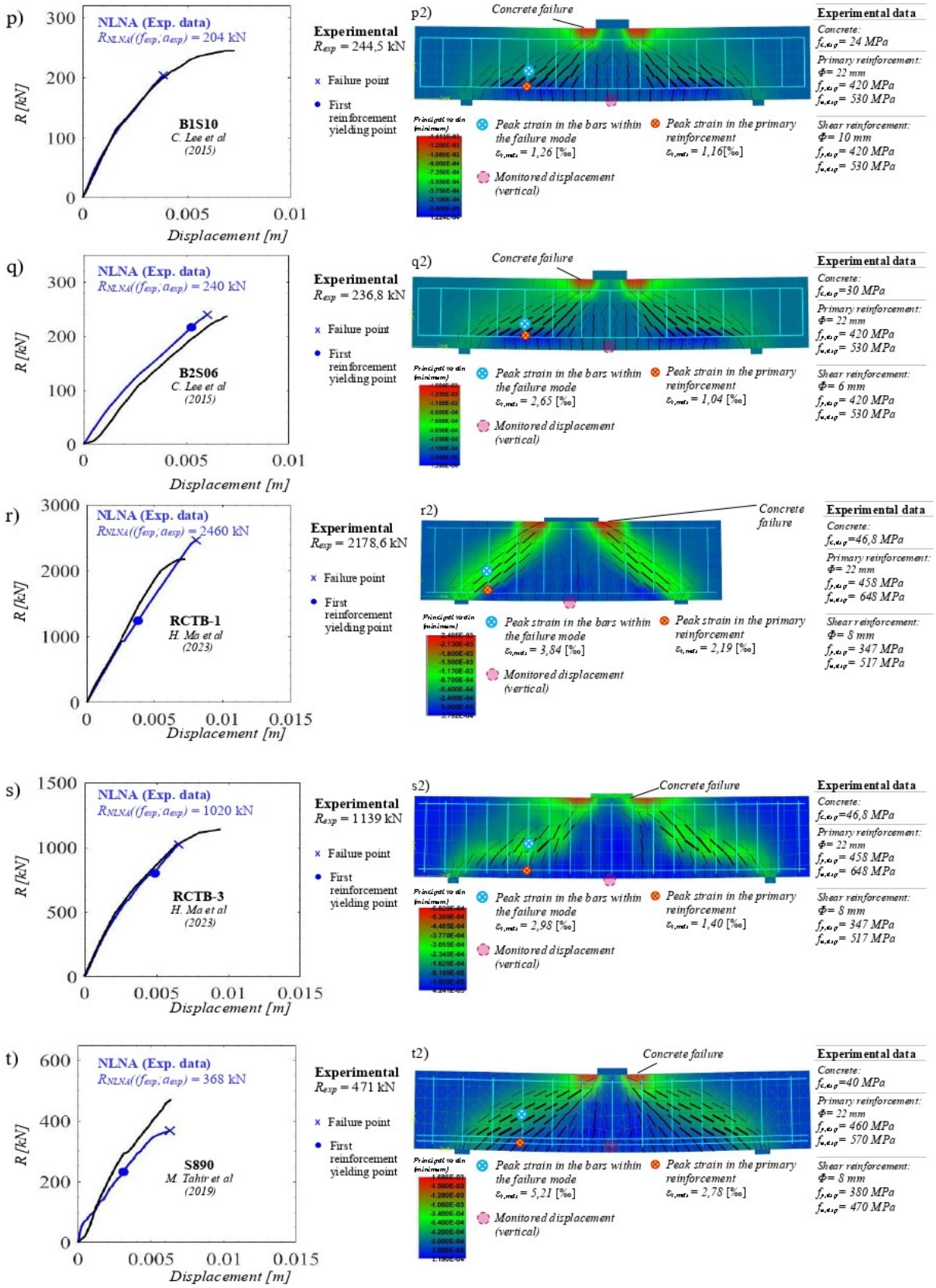

Figure 5.5: RC members belonging to database (Chapter 3.2): comparison between experimental results Rexp and NLNAs outcomes RNLNA(f_{exp}; a_{exp}) (p, q, r, s, t); representation of the failure mechanism in concomitance with failure (p2, q2, r2, s2, t2).

Before conducting a probabilistic analysis of the structural behavior of beams collapsing in shear, it is important to examine the value assumed by θ (R_{exp}/R_{NLNA}). According to [24], the random variable θ partly represents the epistemic uncertainty associated with a non-linear model (derived from the ML method and assuming a log-normal distribution).

Figure 5.6 shows, for each beam, the value of θ relative to the ratio $\epsilon_{s,max}/\epsilon_y$ (strain ratio between the peak strain $\epsilon_{s,max}$ of the primary reinforcement in correspondance of mostly strained stirrup, derived from a NLNA with experimental values for geometric and material properties, and the yielding strain ϵ_y computed according to mechanical properties provided in Chapter 3.2.). It is easy to observe that, as brittle failure mechanisms are approached ($\epsilon_{s,max}/\epsilon_y$ <1), the dispersion of θ is greater compared to ductile-type collapses presented by [14]. In this case, it confirms the hyphotesis of brittle behavior as a consequence of a shear collapse, adding further evidence to the findings of [14].

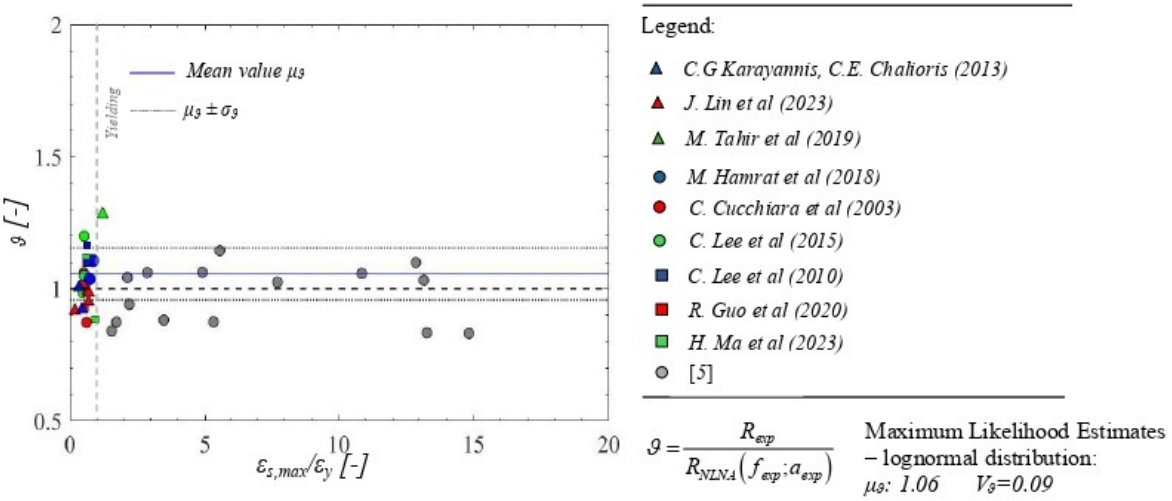

Figure 5.6: Representation of the realization of the model uncertainty random variable for the considered solution strategy and RC members belonging to experimental benchmark

6 | Probabilistic analysis

In this chapter we introduce the foundational assumptions and methodologies employed in the probabilistic analysis of the structural response, focusing particularly on the uncertainties in mechanical properties (geometrical and material properties).
The analysis leverages the Latin Hypercube Sampling (LHS) method to effectively capture the variability inherent in these uncertainties. The combination of this sampling technique with the chosen probabilistic framework ensures a comprehensive exploration of the structural behavior under uncertain conditions.

6.1 Probabilistic Analysis Framework

To initiate the probabilistic analysis, the relevant random variables are first defined (Section 6.2), allowing for the subsequent application of the Latin Hypercube Sampling (LHS) method. This approach enables, starting from mean values (sample 31), the determination of material properties for 30 NLN models.
A MATLAB script facilitates the creation of CCT files for each model, streamlining the process before running the analysis in ATENA 2D.
For each model, key outputs are recorded, including mid-span vertical displacements, longitudinal and transverse steel strains, peak and yield loads (adjusted to exclude the initial self-weight load step). These outputs will be crucial for completing the analysis in subsequent stages and evaluate the global resistance safety factors by means of the strain-based method.
A summary matrix of these results, as the one shown in Table 6.1, will serve as the

starting point for further analysis.

LHS	Max_{Step}	$Load_{max}$	$Disp_{max}$	Eps_{max}	$Yield_{def}$	$Yield_{Step}$	$Load_{yield}$	$Disp_{yield}$
1	...	...	...	...	...	...	...	...
2	...	...	...	...	...	...	...	...
...	...	...	...	...	...	...	...	...
30	...	...	...	...	...	...	...	...
Mean	...	...	...	...	...	...	...	...
Char.	...	...	...	...	...	...	...	...
Des.	...	...	...	...	...	...	...	...

Table 6.1: Outputs obtained for all 30 LHS samples after running the analysis in ATENA 2D.

where:

LHS	Latin Hypercube Sample (1 to 30)
Max_{Step}	Maximum loading step
$Load_{max}$	Maximum load associated to ultimate step
$Disp_{max}$	Maximum vertical displacement associated to ultimate step
Eps_{max}	Maximum reinforcement strain associated to ultimate step
$Yield_{def}$	Reinforcement strain associated to yielding step
$Yield_{Step}$	Yielding step
$Load_{yield}$	Load associated to yielding step
$Disp_{yield}$	Vertical displacement associated to yielding step
Mean	Mean value (Sample 31), mean properties from experimental database
Char	Characteristic value [1]
Des	Design value [1]

6.2 Relevant random variables

In alignment with previous studies [14], the sampling size in this analysis is deemed sufficient, as long as the overall coefficient of variation (CoV) for the variables and the global structural response remains below 0.3.

The probabilistic models for the relevant random variables are developed following

the guidelines set forth in [33].

The study specifically examines the impact of aleatory uncertainties related to material properties on the global structural response, focusing on the CoV of the material properties (Vr).

The random variables considered are detailed in Table 6.2, with their corresponding material properties and CoV values derived according to [33]. The mean values for these variables are based on experimental data from reinforced concrete members documented in the literature.

For each RC member, 30 Latin Hypercube samples of each random variable were generated, ensuring a robust analysis of the material uncertainty effects. The CoV of the concrete cylinder compressive strength Vc has been assumed fixed and equal to 0.15.

Random Variable	**Prob. Distribution**	**Mean Value**	**CoV**	**Correlation**
Concrete cylinder compressive strength f_c [MPa]	Lognormal	F_c, exp	0.15	-
Reinforcement tensile yielding f_y [MPa]	Lognormal	F_y, exp	0.05	f_u(0.85) e_u(-0.50)
Reinforcement ultimate tensile strength f_u [MPa]	Lognormal	F_u, exp	0.05	f_u(0.85) e_u(-0.50)
Reinforcement Young Modulus E_s [MPa]	Lognormal	E_s, exp	0.03	-
Reinforcement ultimate strain ϵ_u [-]	Lognormal	0.09	0.09	f_y(-0.50) f_u(-0.55)

Table 6.2: Characterization of the probabilistic models related to the aleatory uncertainties associated to material properties with reference to the Experimental benchmark.

6.3 LHS

Latin Hypercube Sampling (LHS), introduced by W. J. Conover in 1975, is a method designed to improve the efficiency of Monte Carlo simulations by reducing computational cost.

Instead of relying on purely random sampling, LHS divides the cumulative probabil-

ity distribution of each variable into equal probability intervals on the Y-axis (Figure 6.1(a)). From each of these intervals, a value is randomly selected, ensuring that the entire range of the distribution is adequately represented. This approach significantly improves the distribution of the sampled values, ensuring a uniform coverage across all intervals. Fig. 6.1 (b) highlights the difference between a pure random sampling (red line) and a stratified sampling of a log-normal distribution (blue line).

Sampling

First, the probability interval (0,1) for each random variable $X_1, ..., X_k$ is divided into n equal non overlapping sub-intervals, so that the area belonging to each interval is equal to the probability value of:

$$P(X) = \frac{1}{n} \tag{6.1}$$

A random value is then drawn from each sub-interval, and these values are combined through a random permutation process. This mixing process permits to simulate the pairing of observations in a simple Monte Carlo process [30].

This is particularly advantageous in reliability analysis using non-linear finite element methods (FEM) [29], as it reduces the number of simulations needed to assess the statistical characteristics of structural resistance. It is demonstrated that, LHS requires a limited number of samples to reliably estimate statistical parameters (for CoV<0.3).

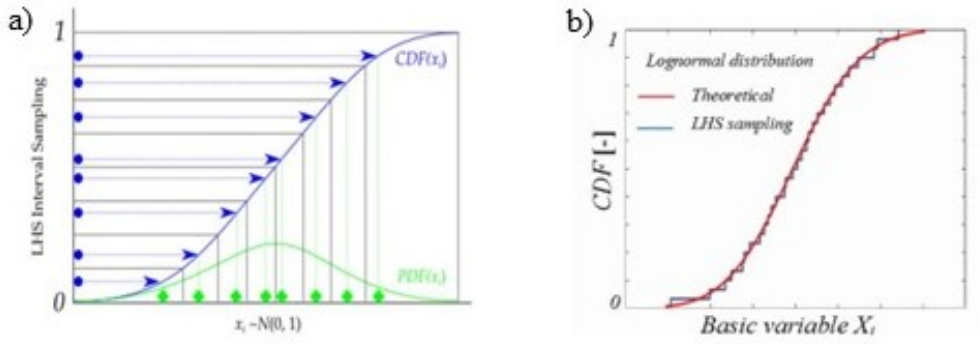

Figure 6.1: (a) LHS interval sampling and (b) Cumulative frequency distribution.

6.4 Statistical test

This work of thesis features a statistical test (Anderson-Darling) to understand whether the hyphotesis of log-normal distribution of the random variables is respected by comparing the observed distribution with a theoretical one.

Anderson-Darling test

This test evaluates the area between F(X) and P(X), which represent respectively the data's cumulative distribution function and the theoretical cumulative distribution. The area A^2, calculated through Eq. 6.2 [38] is then compared to a critical value in accordance with a specified tolerance level (set at 5% for this work):

$$A^2 = n \int_{ALLX} \frac{(P(X) - F(X)^2}{P(X)(1 - P(X))} dP(X) \tag{6.2}$$

The Anderson-Darling test has been implemented through a MATLAB script whose output, the P-value, corresponds to the confidence level.

6.5 Probabilistic analysis of the global structural resistance

This section presents the main findings of the probabilistic analysis, using the random variables introduced in Section 6.2. The Latin Hypercube Sampling approach was applied to generate 600 NLN models (30 LHS samples for every 20 RC beams), using the strategy established in Chapter 5 based on Inverse Analysis methodology.
In Figures 6.2-6.3 not only the load-displacement curves for each set of the probabilistic investigation have been reported, but also the failure point and first reinforcement yielding point if present. Each image features 30 curves, representative of 30 LHS models associated to each beam.
Figures 6.4-6.6 highlight both empirical and best-fitted CDFs related to the Global structural Resistance (R), defined as the load in correspondance of the last conver-

gent step.

To understand whether the random variable may be conform to a log-normal distribution, Anderson-Darling test has been performed on outcomes of the global resistance for each of the RC structural members.

The test confirmed the log-normal distribution hypothesis at a 5% significance level, supported by high P-values as illustrated in Figures 6.4-6.6.

At this point it is possible to state that R can be described by a log-normal distribution, with its parameters estimated through the Maximum Likelihood (ML) method. The ML estimates of statistical parameters provides the mean value $\mu_{R,m}$, the standard deviation of log-normal distribution $\sigma_{R,m}$ and the Coefficient of Variation $V_{R,m}$, all noted in Pictures 6.4-6.6.

To differentiate between experimental values and the log-normal fit obtained through statistical analysis, the subscript m has been introduced. Specifically, $\delta_{R,m}$ denotes the mean-to-mean deviation, which is calculated as the ratio of the Global Resistance obtained from probabilistic analysis $\mu_{R,m}$ to the Global Resistance derived using the mean experimental values of geometrical and material properties (nominal values) $R_{NLNA}(f_{exp}, a_{exp})$ as follows:

$$\delta_{R,m} = \frac{\mu_{R,m}}{R_{NLNA}(f_{exp}, a_{exp})} = \frac{\mu_{R,m}}{R_{NLNA}(f_m, a_n)} \tag{6.3}$$

Although the probabilistic analysis provides insights into the overall structural response and highlights variations in failure modes across different combinations of material properties for few beams, the failure mechanism observed in simulations using experimental material and geometric property values proves to be by far the most probable scenario.

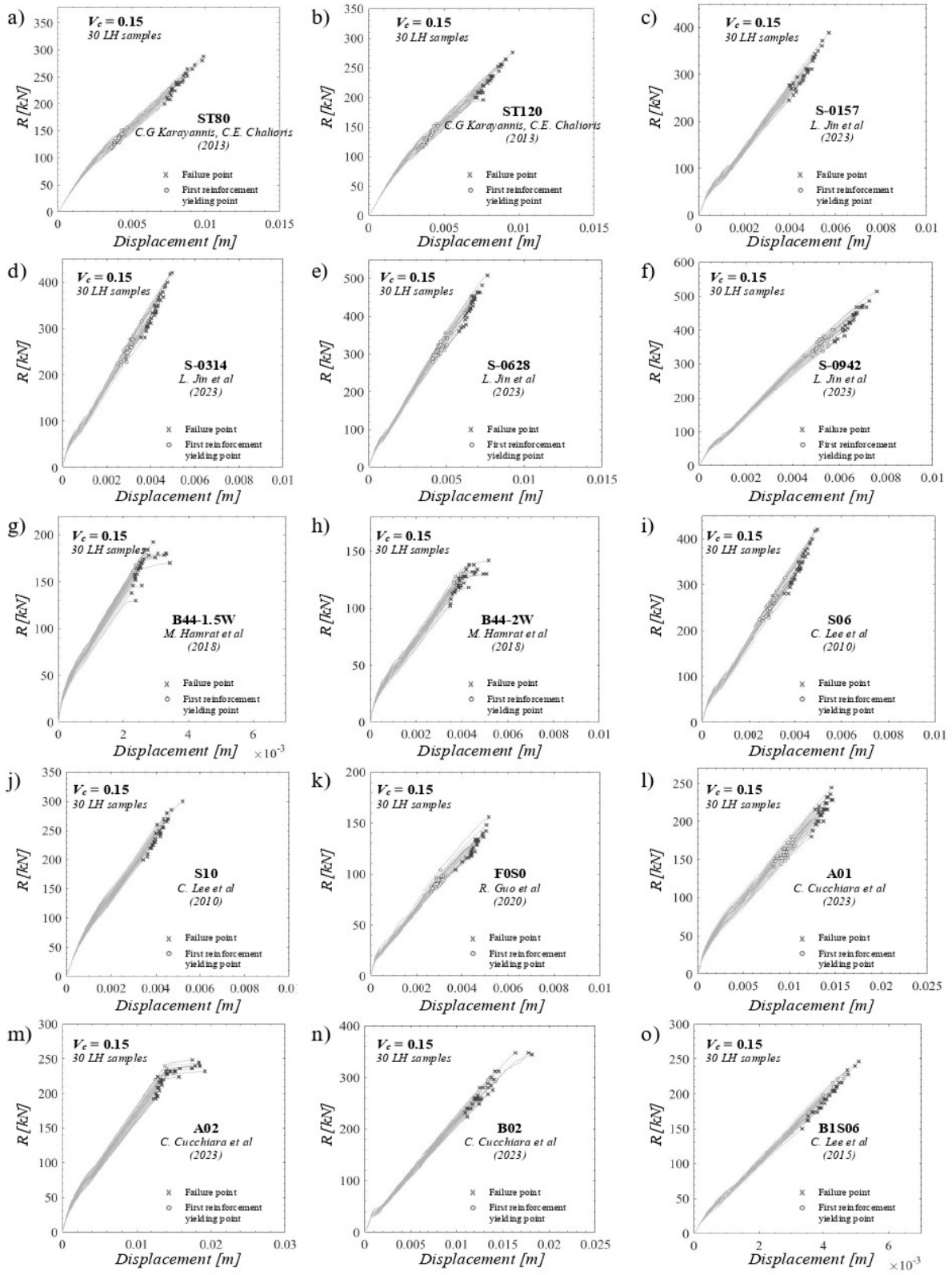

Figure 6.2: Load-displacement curves from the probabilistic analysis of RC specimens (a-o) from database

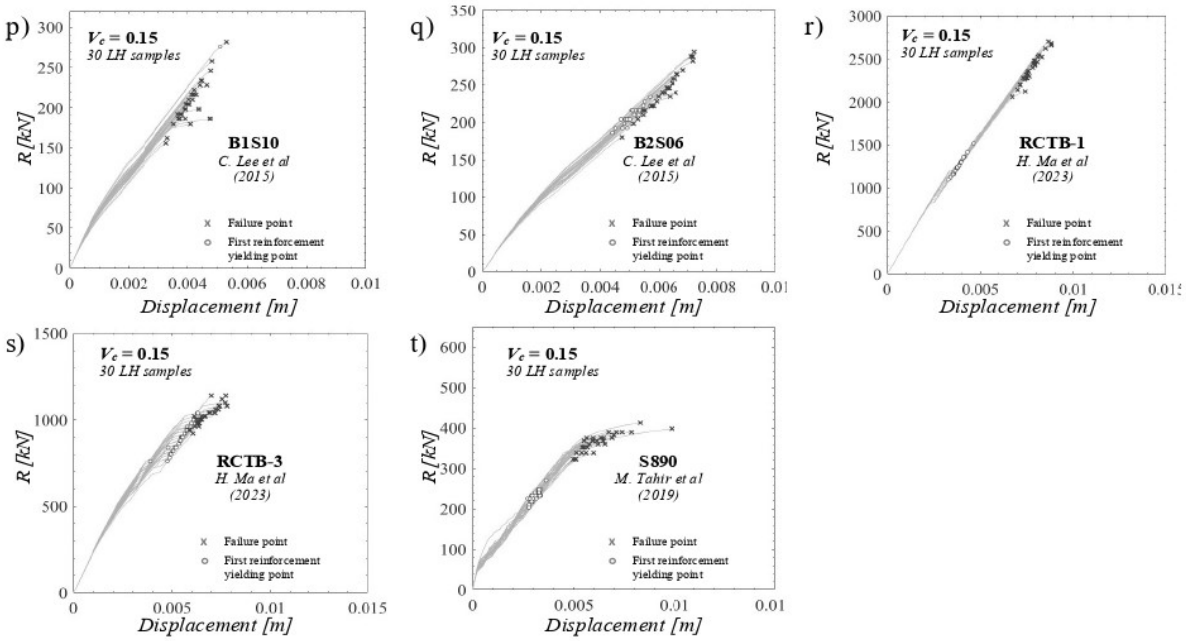

Figure 6.3: Load-displacement curves from the probabilistic analysis of RC specimens (p-t) from database

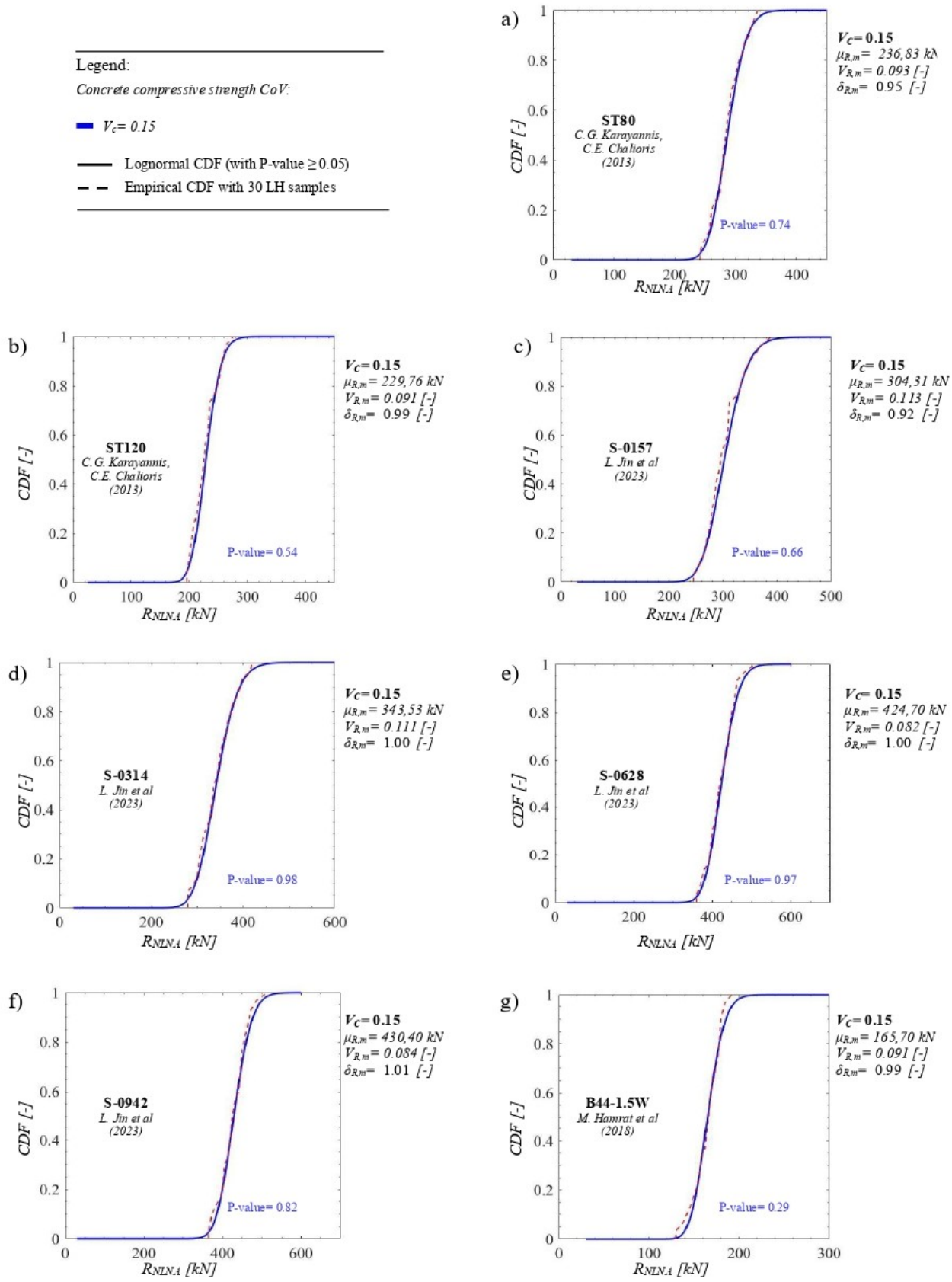

Figure 6.4: Empirical and lognormal CDFs of tests of RC members (a-g) from database

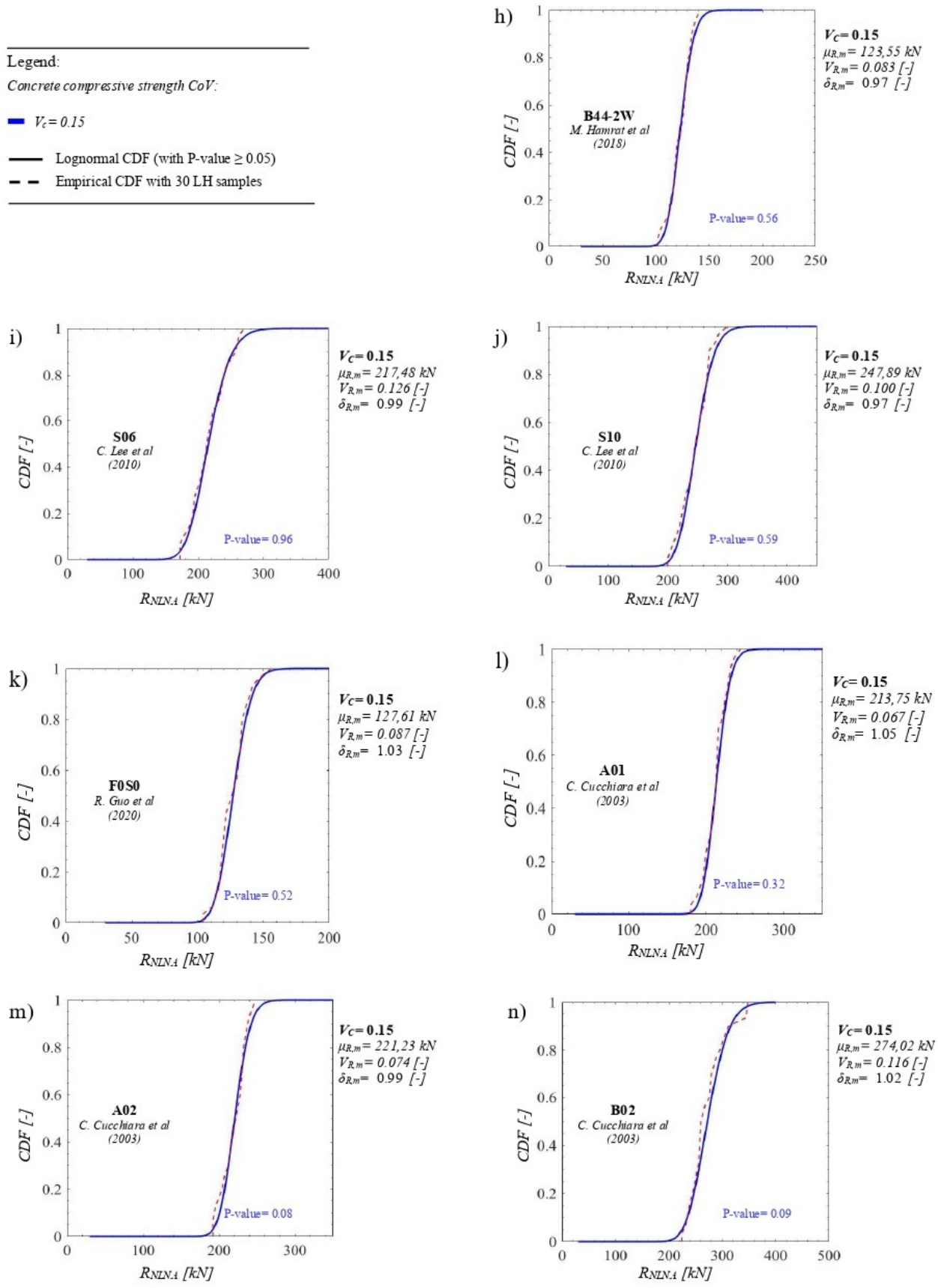

Figure 6.5: Empirical and lognormal CDFs of tests of RC members (h-n) from database

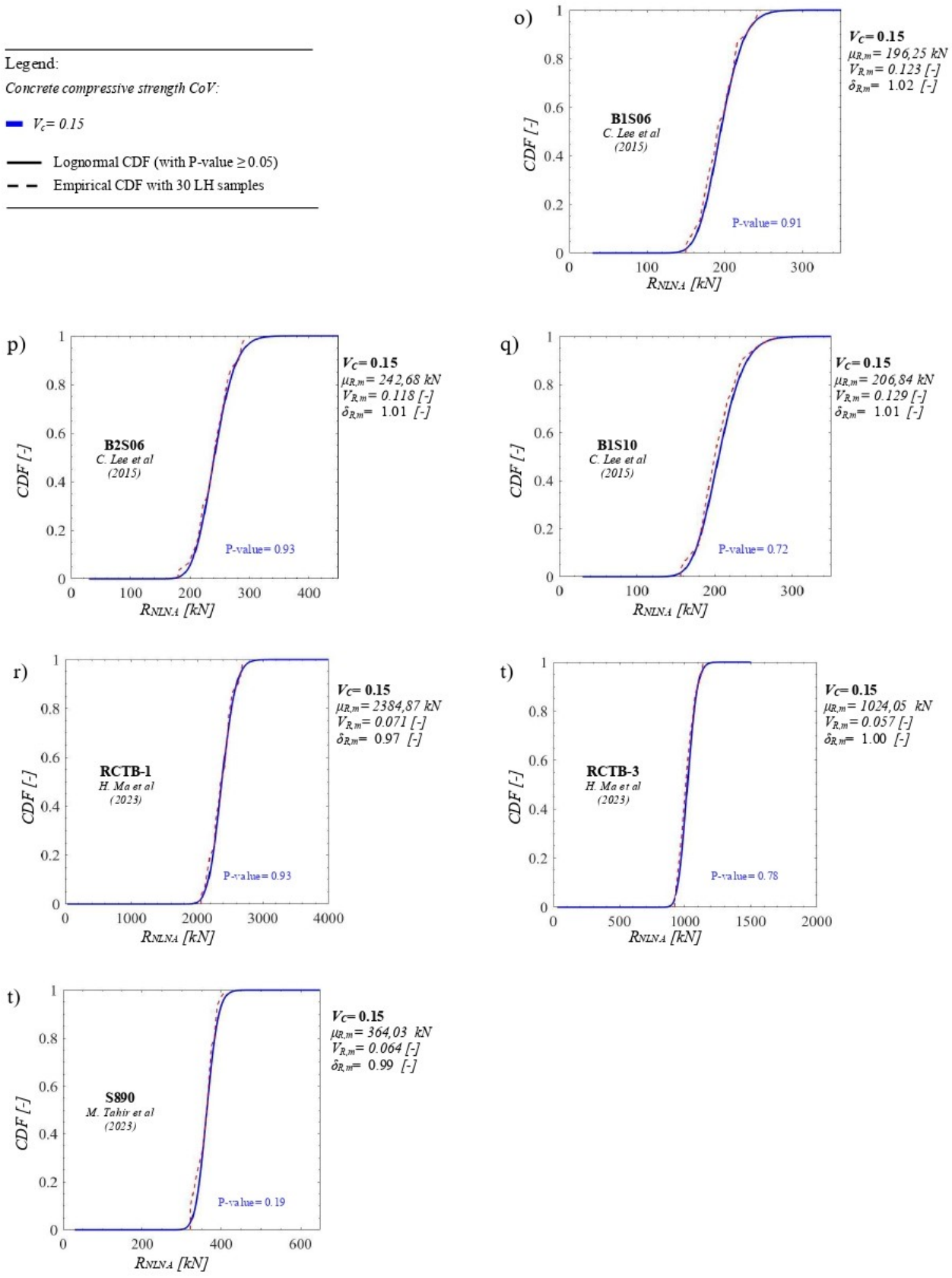

Figure 6.6: Empirical and lognormal CDFs of tests of RC members (o-t) from database

7 | Application of the Strain-based method to RC beams failing in shear

At this point, the results of the probabilistic analysis will be examined and compared with the outcomes obtained from [5, 14]. This chapter expands the Strain-based Method to reinforced concrete beams prone to shear failure, confirming the consistency of statistical parameters $\delta_{R,m}$ and $V_{R,m}$ in relation to the strain ratio $\epsilon_{s,max}/\epsilon_y$, without significant changes in their analytical correlation.
These results will be used to refine the Strain-based Method for determining the global resistance safety factor γ_R within the safety framework of the Global Resistance Method (GRM).

7.1 Results of the Probabilistic Analysis

Figure 7.1 highlights the interdependence between $\delta_{R,m}$, introduced with Eq. (6.3), and the strain ratio $\epsilon_{s,max}/\epsilon_y$.
Since the plot confirms the trend tested by [5, 14], Eq. (7.1) and Eq. (7.2) can be derived and used to determine $\delta_{R,m}$ and $V_{R,m}$ in practical applications [14].

$$\delta_{R,m} = a\left(\frac{\epsilon_{s,max}}{\epsilon_y}\right) + b \tag{7.1}$$

$$V_{R,m} = V_c\left(\frac{\epsilon_{s,max}}{\epsilon_y} + 1\right)^{\eta} \tag{7.2}$$

where:

- a Lower bound of the 95% confidence level ($V_c = 0.15$)
- b Upper bound of the 95% confidence level ($V_c = 0.15$)
- V_c CoV for the compressive cylinder concrete strenght
- η Best fit expression

The mean value of the probabilistic distribution of global structural resistance, $\mu_{R,m}$, leads to a very similar result if compared to the value of a single non-linear analysis performed using mean values of material properties and nominal values for geometry $R_{NLNA}(f_m, a_n)$. Due to this reason, in practical engineering applications, the mean-to-mean deviation $\delta_{R,m}$ can be assumed equal to 1.

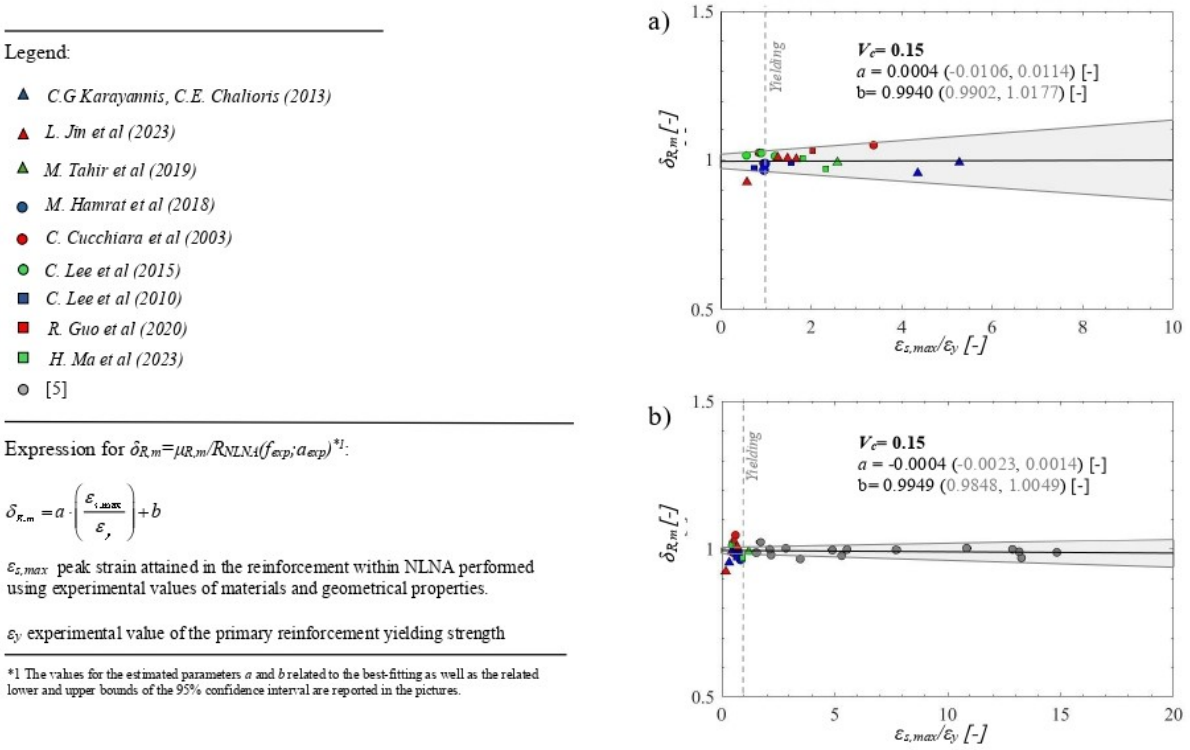

Figure 7.1: Trend of variation of the mean-to-mean deviation $\delta_{R,m}$ with respect to the strain ratio $\epsilon_{s,max}/\epsilon_y$ (reinforcement involved in the failure mechanism) for V_c equal to 0.15 (a). The values of a and b corresponding to the lower and upper bounds of the 95% confidence interval as well as the best-fit expression are, respectively, also reported. In figure (b) the trend encompasses both RC beams failing due to shear and flexure [5] and $\epsilon_{s,max}$ refers to primary reinforcement for both datasets.

The correlation between$V_{R,m}$ and $\epsilon_{s,max}/\epsilon_y$ of transverse reinforcement is shown in Figure 7.2 (a) together with the value of η from Eq. (7.2), considering $V_c = 0.15$.

As a consequence of the modeling assumption from Table 6.2, the function that represents The CoV of the global resistance $V_{R,m}$ is ranging between V_c and V_y.
When the ratio $(\epsilon_{s,max}/\epsilon_y)$ is lower than 1,$V_{R,m}$ approaches V_c because RC beams are failing due to very brittle mechanisms governed by concrete without yielding of the transverse reinforcement.

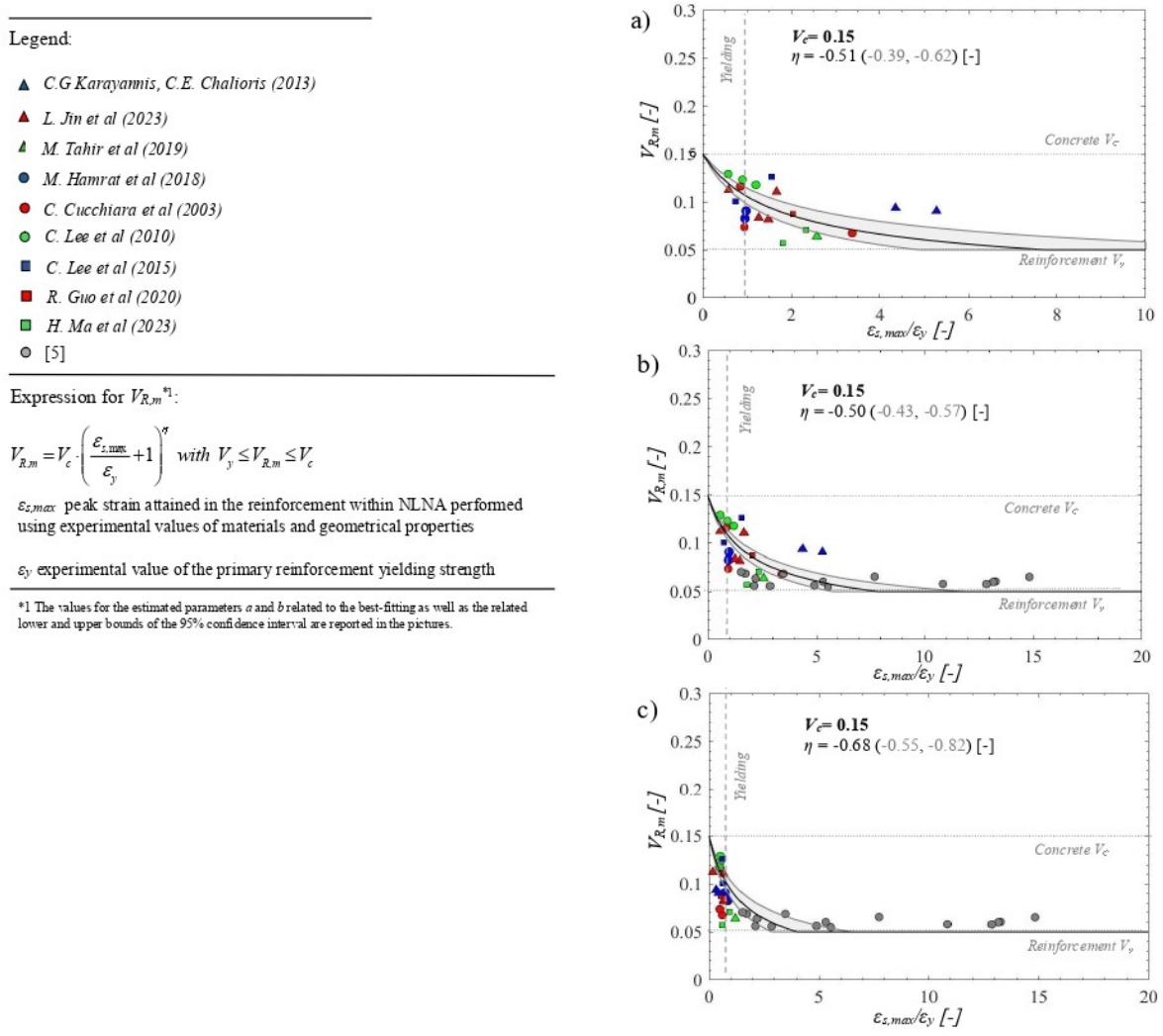

Figure 7.2: Trend of variation of the CoV of the global resistance $V_{R,m}$ with respect to the strain ratio $\epsilon_{s,max}/\epsilon_y$ for V_c equal to 0.15 considering stirrups (a). In figure (b) the strain ratio $\epsilon_{s,max}/\epsilon_y$ referred to transverse reinforcement by including experimental tests studied by [5]. Figure (c) addresses the same pattern considering longitudinal reinforcement for both RC beams failing in shear and flexure. The values of η corresponding to the lower and upper bounds of the 95% confidence interval as well as of the best-fit expression are, respectively, also reported.

To better asses the validity of the non-linear trend introduced by Eq. (7.2) both results from Database and [5] have been depicted in Figure 7.2 (b). This ensure a comprehensive analysis of a wide sample of reinforced concrete beams covering all potential failure modes (shear and flexural).

As $\epsilon_{s,max}/\epsilon_y$ grows, there is a noticeable reduction in the value of $V_{R,m}$ because the longitudinal reinforcement yields starts governing the process before reaching the ultimate bearing capacity.

Moreover, it is easy to observe that the values of η corresponding to the lower bound of the 95% confidence interval and the best-fit curve turn out to be pretty the same found by [14], leading to the conclusion that it is almost independent of the type of structure.

In Figure 7.2 (c), the same type of relationship is shown, but it refers to the longitudinal reinforcement, which does not participate in the failure mechanism for all beams failing in shear and therefore is not yielded in most cases. As expected, the points cluster on the left side of the graph, highlighting a brittle or semi-brittle behaviour typical of shear failure.

7.2 Assessment of the Global Safety Factors

Calculating the design resistance of a structure stands as one of the fundamental objectives of a structural engineer. Following the framework introduced by the GRM, the design value of the Global Structural Resistance (R_d) can be calculated relatively simply using Eq. (1.1) once the results from a single non-linear analysis (NLNA), calculated assuming mean material properties f_m and nominal geometric values a_n, are known.

In the same equation the concept of structural reliability is taken into account by the safety factor γ_R, which considers aleatory uncertainties, and by γ_{R_d} that encompasses epistemic uncertainties arising from numerical modeling.

As mentioned at the beginning of this Chapter, the purpose of this thesis is to provide an expression for the immediate calculation of γ_R for reinforced concrete members, while an in-depth study on the same experimental benchmark was conducted by [37] to find a range of adoptable values for γ_{R_d}.

Eq.(1.3) features the calculation of γ_R given the CoV of the global resistance V_R , its bias factor δ_R, the target reliability index β_t and the FORM factor α_R, as long as V_R stays below 0.3.

The flowchart in Figure 7.3 shows the logical steps to be performed to calculate γ_R and R_d as a consequence.

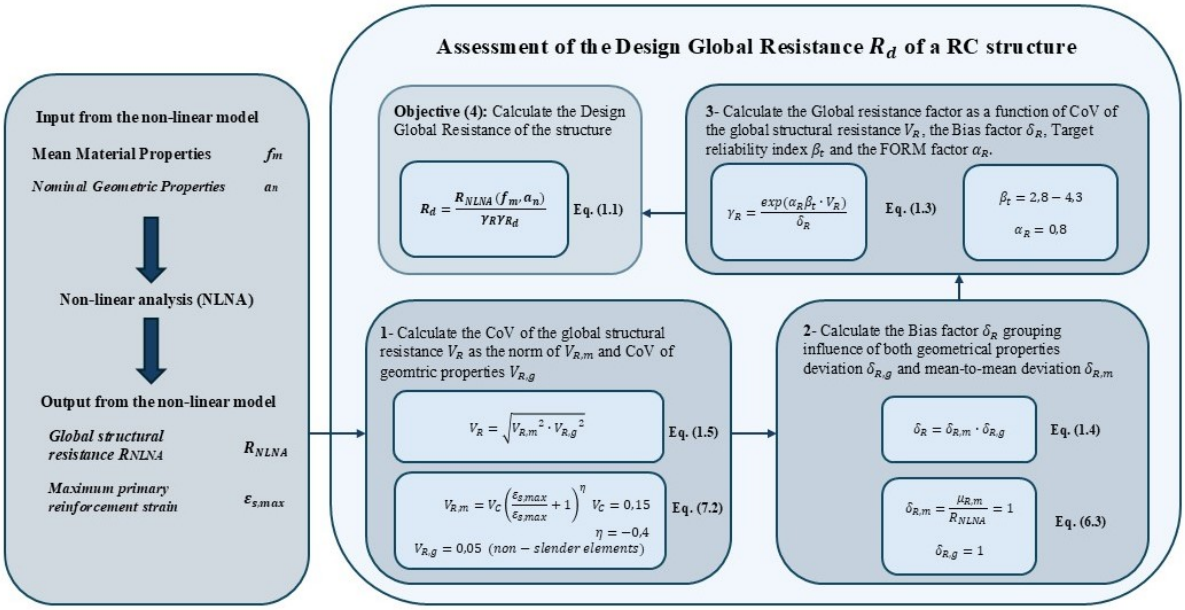

Figure 7.3: Flowchart of steps to be performed to assess the Design global structural resistance within the GRM.

Specifically, Eq. (1.5) computes the CoV of global structural resistance (V_R) as the euclidean norm of CoV of structural resistance related to material aleatory uncertainties (V_{R_m}) and the one of global geometry (V_{R_g}).

In accordance with results from Chapter 7.1 and those from [5, 14], V_{R_g} is limited to 0.05 for non-slender elements while V_{R_m} is calculated through Eq. (V_{R_m}) by entering the peak strain of the reinforcement involved in the failure mechanism $\epsilon_{s,max}$ from a NLNA with mean and nominal values of materials and geometry, and $\eta = -0.4$.

A graphical representation of Eq. (7.2) is visible in Figure 7.4 (a), where V_{R_m} is calculated for reinforced concrete members ranging from brittle to ductile behaviour and $V_c = 0.15$.

The last parameter to be found before calculating γ_R is δ_R (Eq. (1.4)). The results of the probabilistic analysis from Chapter 7.1 make it possible to set its value equal to 1.

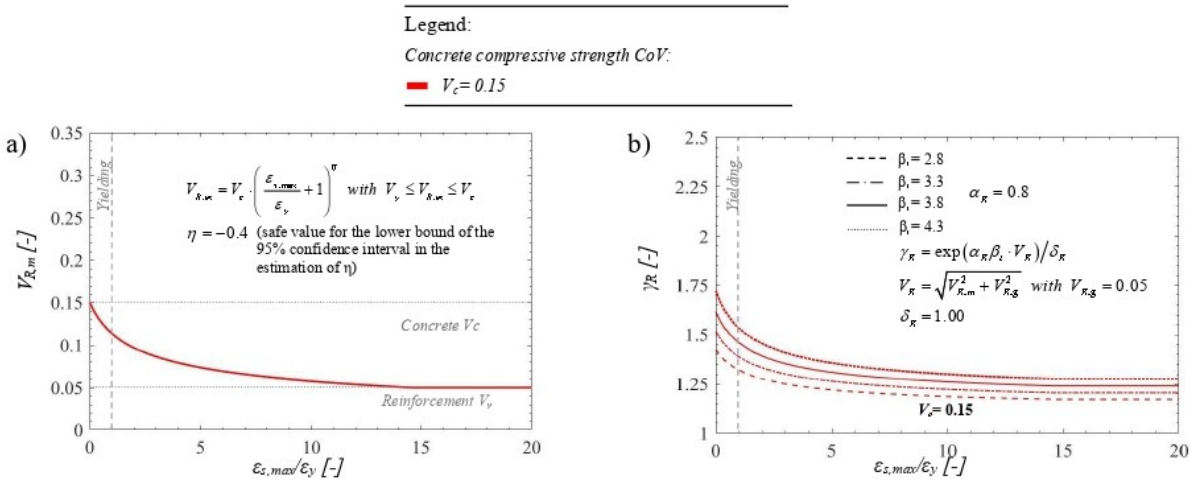

Figure 7.4: Graphical representation of Eq.(7.2) evaluated adopting $\eta = -0.4$ (a); global resistance safety factors assuming different target reliability indices β_t and $V_c = 0.15$ (b).

A plot of the global resistance safety factors assuming different common target reliability indices is shown in Figure 7.4 (b), assuming aleatory uncertainties dominant in respect to epistemic ones.

To resume, by knowing the mean values of the material properties and the nominal values of the geometric ones obtained from a single non-linear analysis of the structure or in-situ tests (existing structures), it is possible to determine the appropriate value of the global resistance factor γ_R to be applied.

This, in turn, allows for the calculation of the design strength as a function of the maximum deformation of the primary reinforcement for both new and existing structures (with 50-year or 100-year reference working life depending on the reliability index).

7.3 Sensitivity analysis of the global structural response

This study aims to quantify and analyze the influence of modeling uncertainties, stemming from the resistance model uncertainty safety factor γ_{R_d} in Eq. (1.1), for both 20 reinforced concrete beams that fail in shear (brittle behavior) and 16 beams that fail in bending (ductile behavior).

To achieve this, a sensitivity analysis of the global structural resistance is introduced, considering both aleatory and epistemic uncertainties. The study is limited to the analysis of non-slender specimens, while further information on slender elements can be found in [15]. In table 7.1 the actual statistical parameters for resistance model uncertainty are provided by the work [37] considering the same experimental benchmark, while CoV introduced in Figure 7.2 will be used to effectively consider aleatory uncertainties.

Failure mechanism	V_θ	μ_θ
Shear	**0.150**	**1.05**
Flexure	**0.098**	**1.04**

Table 7.1: Coefficient of Variation accounting epistemic uncertainties [37]

The results shown in Figure 7.5 are consistent with expectations and align with the findings of [15]. Specifically, it is observed that epistemic uncertainty dominates over aleatory uncertainty in all cases for the considered CoV of concrete ($V_c = 0.15$).

For the 35 RC beams, the ratio V_R/V_θ is less than one in all scenarios.

It is highly probable that for higher values of V_c, aleatory uncertainties will dominate for flexural-failing beams.

Given these results, the curves defining γ_R as a function of $\epsilon_{s,max}/\epsilon_y$ highlighted in Figure 7.4 must be calibrated with a new value for the first order reliability sensitivity factor α_R, considering that the random variables are non-dominant compared to the epistemic uncertainties. Figure 7.6 displays the curves when $\alpha_R = 0.32$

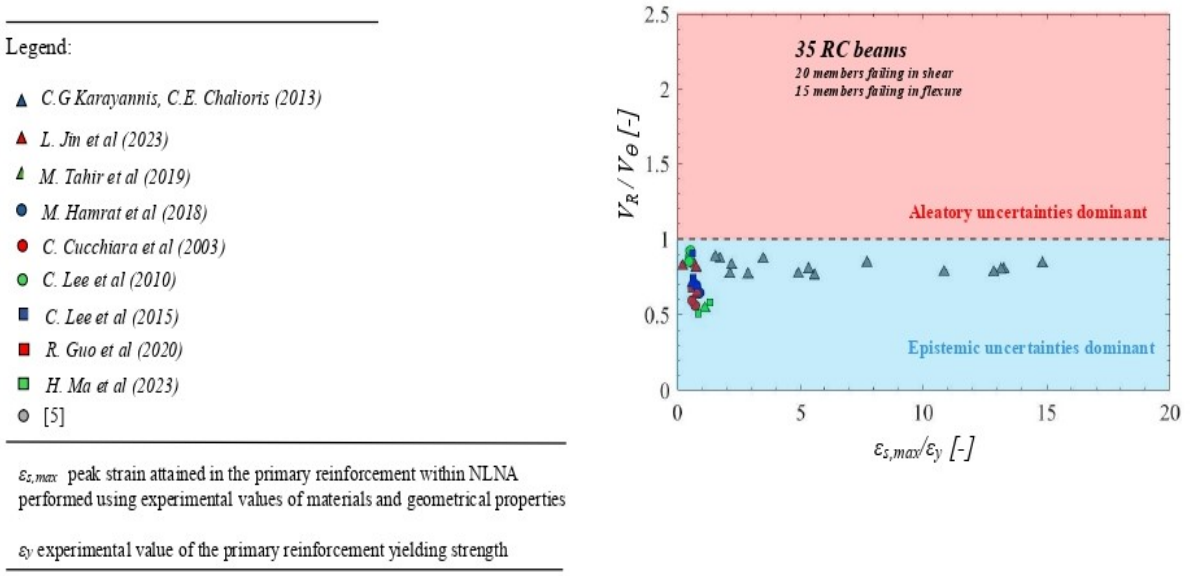

Figure 7.5: Comparison of Coefficient of Variation for what concerns aleatory and epistemic uncertainties.

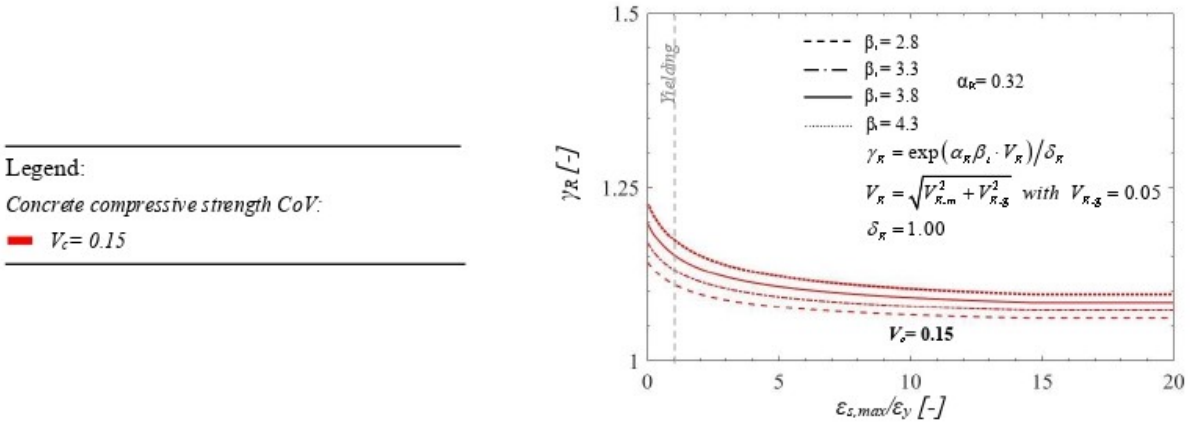

Figure 7.6: global resistance safety factors assuming different target reliability indices β_t, $\alpha_R = 0.32$ and $V_c = 0.15$.

7.4 Proposal for a more accurate estimation of the global safety factor considering different failure modes on its own

Due to different failure mechanism in RC beams, a better fit of data representing the interdependence between V_R and $\epsilon_{s,max}/\epsilon_y$ could be obtained by separately interpolating data belonging to brittle failure and ductile collapse. The yielding border ($\epsilon_{s,max}/\epsilon_y$=1) separates the two fit regions as shown in Figure 7.7.

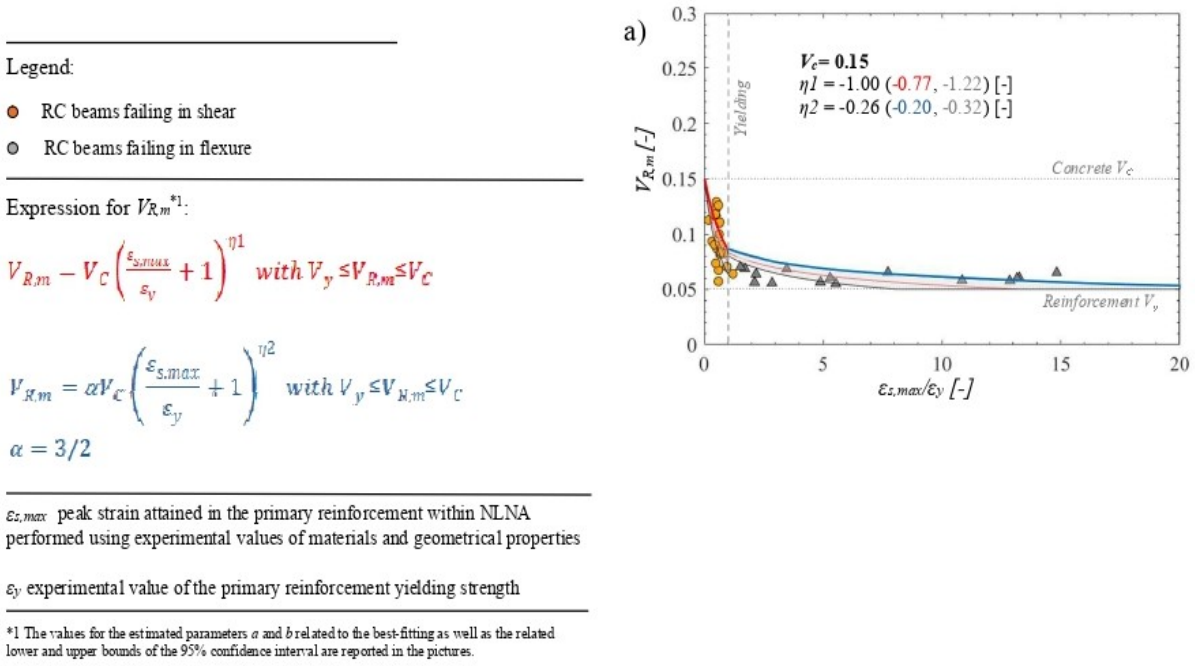

Figure 7.7: Trend of variation of the CoV of the global resistance $V_{R,m}$ with respect to the strain ratio $\epsilon_{s,max}/\epsilon_y$ for V_c equal to 0.15 considering both RC beams failing in shear and flexure. In figure (a) the strain ratio $\epsilon_{s,max}/\epsilon_y$ is referred to longitudinal reinforcement for both. The values of η_1 and η_2 corresponding to the lower and upper bounds of the 95% confidence interval as well as of the best-fits expression are, respectively, also reported. The equation useful for practical application remains nearly unchanged, only a coefficient α should be introduced to represent the second fit.

The change in slope occurs when $\epsilon_{s,max}/\epsilon_y$ is equal to 1 and lower bounds have been considered for practical applications.

The equation for practical applications remains unchanged for the first fit (red line),

while a coefficient α needs to be introduced for the second fit (blue line). This new coefficient is set equal to 3/2 to reflect experimental evidence of this dataset. It has been proven that ductile collapses never exploited a Vr higher than 0.10.

As done in Chapter 7.2 and 7.3 a new graphical representation of Eq. (7.2) and corresponding global resistance safety factors have been provided in Figure 7.8, taking in consideration the change in slope of the best fit.

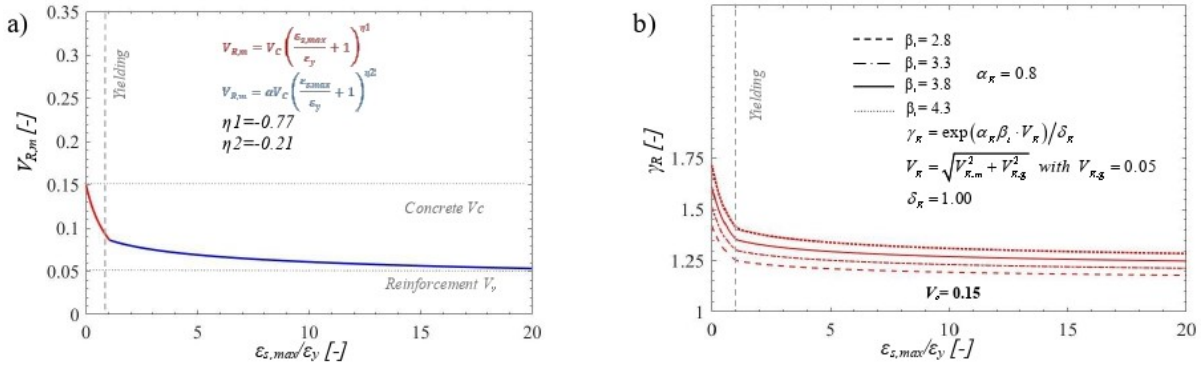

Figure 7.8: Graphical representation of Eq.(7.2) evaluated adopting $\eta_1 = -0.77$ and $\eta_2 = -0.21$ (a); global resistance safety factors assuming different target reliability indices β_t and $V_c = 0.15$ (b).

In light of the new results, the influence of aleatory and epistemic uncertainties can be re-evaluated analysing the dependence between V_R (accounting both geometrical and material uncertainties) and $\epsilon_{s,max}/\epsilon_y$, as shown in figure 7.9. It is clear that when CoV of concrete increases, the influence of aleatory uncertainties beacomes greater.
When $V_c = 0.15$ epistemic domain covers all ranges of $\epsilon_{s,max}/\epsilon_y$, while for a $V_c = 0.20$ and $V_c = 0.25$ the aleatory domain increases.

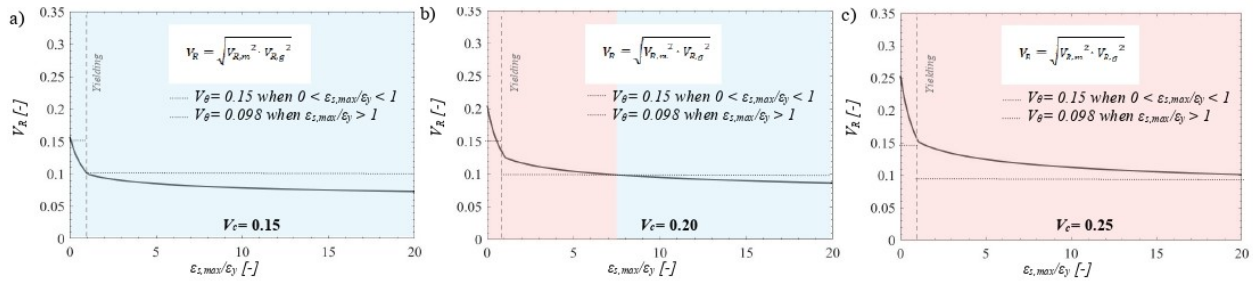

Figure 7.9: Comparison of Coefficient of Variation for what concerns aleatory and epistemic uncertainties. Different values of V_c (0.15, 0.20, 0.25), that simulate concrete conditions, have been accounted in Figure (a), (b) and (c). By increasing the CoV of concrete, the influence of aleatory uncertainties becomes greater.

7.5 Different approaches to assess the global safety factors

In this section two distinct approaches for estimating global safety factors are introduced. Data from Chapter 7.1 have been considered.

- ***Approach I***: The first approach, that has been used till now, involves using separate safety factors to account for aleatory γ_R and epistemic uncertainties γ_{Rd}. The global safety factor following this approach can be computed as follows:

$$\gamma_{GL(I)} = \gamma_R \gamma_{Rd} \geq 1 \tag{7.3}$$

where γ_R is estimated through Eq. (1.3) with a FORM factor $\alpha_R = 0.8$ in case of dominant aleatory uncertainties, and γ_{Rd} computed with Eq. (7.4).

$$\gamma_{Rd} = \frac{exp(\alpha'_R \beta_t V_\theta)}{\delta_\theta} \geq 1 \tag{7.4}$$

where the CoV V_θ and bias factor δ_θ are referred to epistemic uncertainties. The FORM factor set at $\alpha'_R = 0.32$ in the hypothesis of non dominant random variable θ.

Another approach, denominated *Approach I/b* may be introduced by considering

dominant epistemic uncertainties ($\alpha_R = 0.32$, $\alpha'_R = 0.8$).

- ***Approach II***: The second approach combines both types of uncertainties into a single global safety factor γ_{GL}, calculated directly using Eq. (7.5).

$$\gamma_{GL(II)} = \frac{exp(\alpha_R \beta_t V_{GL(II)})}{\delta_{GL(II)}} \geq 1 \tag{7.5}$$

In this approach, the sensitivity factor α_R, set at 0.80, reflects the assumption that resistance is the dominant variable, accounting for both aleatory and epistemic uncertainties. The terms $V_{GL(II)}$ and $\delta_{GL(II)}$ represent the coefficient of variation (CoV) and bias factor for global structural resistance R_{GL} (Eq.(7.7), considering contributions from both types of uncertainties. These values can be approximated using simplified formulas [15], where the total variability is expressed as the combination of V_R and V_θ as shown in Eq. (7.6).

$$V_{GL(II)} = \sqrt{V_R^2 + V_\theta^2} \tag{7.6}$$

$$\delta_{GL(II)} = \delta_R \delta_\theta = \delta_R \mu_\theta \tag{7.7}$$

Here, the parameters V_R, V_θ, δ_R, δ_θ, μ_θ hold the same interpretations defined in Chapter 7.3. It is necessary to distinguish among failure modes as anticipated in Table 7.5

The goal is to determine the effectiveness of each method in evaluating the reliability of RC members in the GRM, while also addressing the relevance of both aleatory and epistemic uncertainties.

The results in terms of $\gamma_{GL(II)}$ over strain ratio $\epsilon_{s,max}/\epsilon_y$ are presented in Figure 7.10 for both shear and flexure-critical beams, and are valid under the assumptions introduced in Sections 7.3 and 7.4.

As expected, the safety factors for RC beams failing due to flexure are lower at the same same strain ratio if compared to shear-collapsing specimens, because of smaller

values of V_R and V_θ.

It is also evident that Approach I/b leads to more conservative results, favoring safety as reported by [15]. Approach II tends to be an intermediate solution between Approaches I and I/b as the strain ratio increases.

In correspondence with the yielding strain, all three approaches provide nearly identical results for the calculation of $\gamma_{GL(II)}$ for this specific sample.

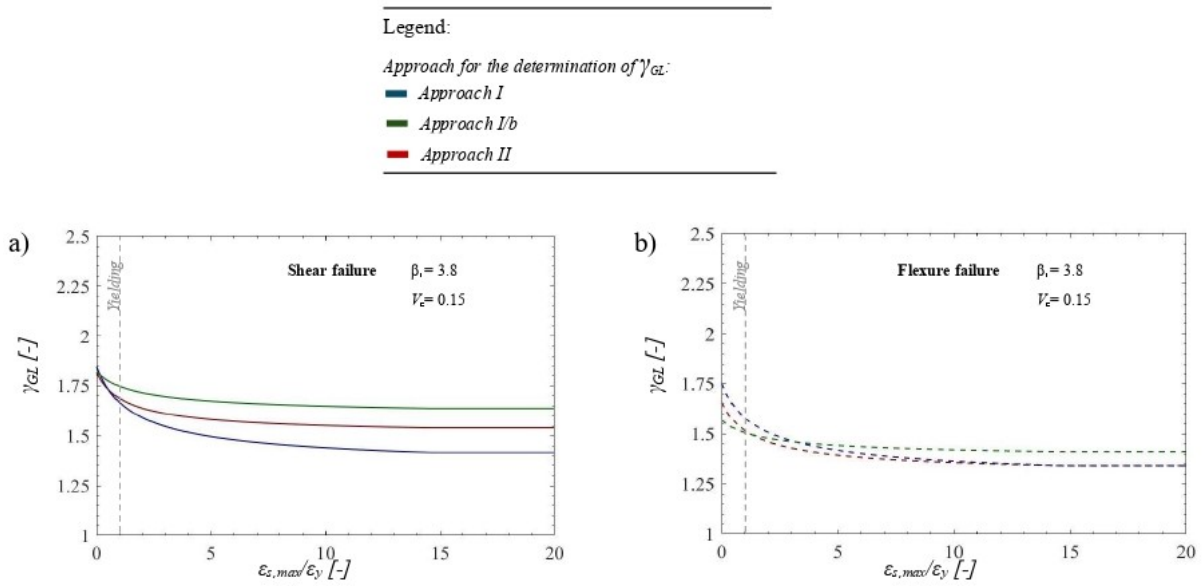

Figure 7.10: Different approaches (I,I/b,II) to estimate global safety factor γ_{GL}. A distinction should be made depending on the failure mode:(a) shear failure, (b) flexure failure

While the first method typically considers aleatory uncertainties as dominant [28], even if it may not happen as stated in Chapter 7.3, the second approach is often more advantageous as demonstrated by [15].

By integrating both uncertainties in a unified factor, it simplifies the process and avoids assumptions regarding which type of uncertainty is more significant when determining the global structural resistance.

7.6 Comparison with other safety formats within GRF

In this section, a comparison is made between the novel strain-based approach and other commonly used safety formats within the GRF, specifically considering a target reliability index β_t of 3.8, relevant to newly realized structures with a reference working life of 50 years [28].

This analysis features only beams from Chapter 3.2 failing in shear, because the results related to flexure failure are already available in [5].

The two safety formats compared to the strain-based approach are the Estimation of Coefficient of Variation (ECoV) method and the Partial Factor Method (PFM). The comparison focuses on the design value of the global structural resistance R_d for each safety format, alongside the design value derived from probabilistic analysis $R_{d,Prob}$, which assumes a lognormal distribution of random variables.

All types of uncertainties, including aleatory and epistemic, are considered in line with earlier discussions. The results are presented in terms of the ratio $R_d/R_{d,Prob}$, where a ratio below 1 indicates that the safety format is on the safe side.

As shown in Figure 7.11, all methods meet the safety criterion for most of the considered samples, but the strain-based approach shows less variability in the $R_d/R_{d,Prob}$ ratio compared to the ECoV and PFM methods, proving its effectiveness for broader applications.

Moreover, it allows for efficient non-linear analysis (NLNA) using average material properties and nominal geometric values, providing a more streamlined and robust alternative to the traditional safety formats.

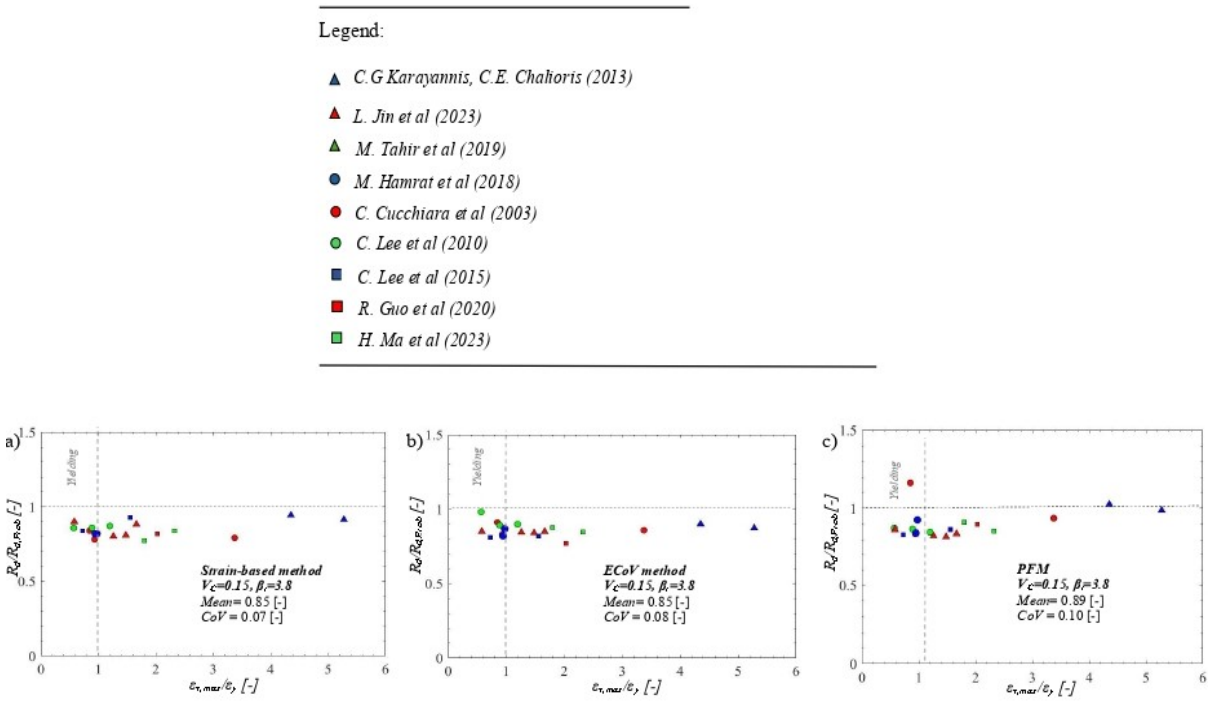

Figure 7.11: Comparison between (a) the strain-based method, (b) ECoV method [28] and (c) PFM [28], as regards the ratio between the estimated design value of the structural resistance R_d and the actual design global resistance from the probabilistic analysis $R_{d,Prob}$

8 | Conclusions

This thesis explores and extends a novel strain-based approach to estimate the design value of global structural resistance R_d, specifically for reinforced concrete beams subject to shear failure.

Working within the framework of the Global Resistance Format (GRF), this method relies on Non-Linear Numerical Analyses (NLNAs) to assess the global resistance while accounting for material uncertainties.

The study began by developing non-linear models for 20 reinforced concrete beams, found in literature, that failed due to both pure shear and shear-compression failure mechanisms. These models were carefully calibrated to reflect real-world conditions, while accounting for model uncertainties.

The NLNAs were then used to perform a probabilistic analysis of the global resistance, considering the variability in material properties through the definition of relevant random variables.

The primary outcome of this analysis was the calculation of the mean value $\mu_{R,m}$ and the Coefficient of Variation of resistance $V_{R,m}$ for each beam with a fixed value of the concrete CoV ($V_C = 0,15$). A crucial aspect of this research was establishing a link between the $V_{R,m}$ and certain structural characteristics, notably the strain ratio $\epsilon_{S,max}/\epsilon_y$, which compares the maximum strain in the primary reinforcement to its yielding strain. This ratio, calculated using average material properties and nominal geometrical values, provided valuable insight into the beams' structural performance and was instrumental in adapting the strain-based method for beam behavior.

By employing a least squares fitting method, a useful correlation between the strain

ratio and $V_{R,m}$ was derived, including the upper and lower limits within a 95% confidence interval. This allowed to calculate the global resistance safety factor γ_R through practical expressions, based on target reliability levels.
One of the key benefits of this approach is its ability to significantly streamline the design process, as it only requires a single NLNA to evaluate the strain ratio and determine the safety factor, reducing both computational time and mistakes by designers.
Moreover, a sensitivity analysis performed integrating data from [37] made it possible to obtain an optimized expression to evaluate the global safety factor accounting for both aleatory and epistemic uncertainties.
In comparison with other GRF safety formats, such as the ECoV method and the Partial Factor Method (PFM), this novel method showed strong efficiency and reliability in predicting global resistance.

In conclusion, this work provides an innovative and efficient approach to structural design through the use of NLNAs for evaluating global resistance. The strain-based method, initially developed for flexural collapse, has now proven capable of accurately estimating the global resistance in shear-dominated failure cases as well.
By simplifying the calculation process and maintaining accuracy, this method has the potential to reduce computational effort for both new designs and existing structures, while opening doors for further integration with structural health monitoring.

Bibliography

[1] CEN. EN 1992–1-1. Eurocode 2 – design of concrete structures. part 1–1: general rules and rules for buildings. 2014.

[2] Q. Huang A. Soraghi. Probabilistic prediction model for rc bond failure mode. *Civil and Environmental Engineering Faculty Research and Publications, 284*, 2021.

[3] D. Andersson. Shear failure of steel fiber and bar reinforced concrete beams without stirrups. Master's thesis, Royal Institute of Technology (KTH) - Department of Civil and Architectural Engineering, 2023.

[4] A. Ansell. *Concrete structures EDITION 2014*, 2014.

[5] S. Bargetto. Determination of global resistance safety factors for rc beams failing in bending according to strain-based method using nlnas. Master's thesis, Politecnico di Torino - DISEG, 2024.

[6] Z. P. Bazant. Size effect in blunt fracture: Concrete, rock, metal. *Journal of engineering mechanics 110*, 1984.

[7] C. Chalioris C. Karayannis. Shear tests of reinforced concrete beams with continuous rectangular spiral reinforcement. *Construction and Building Materials 46*, 2013.

[8] Hai. Dinh. Shear behavior of steel fiber reinforced concrete beams without stirrup reinforcement. Master's thesis, University of Michigan, USA, 2009.

[9] R. Ince E. Airici. Size effect in bearing strength of concrete cubes. *Construction and Building Materials 18*, 2004.

[10] A. Slobbe et al. On the value of a reliability-based non linear finite element analysis approach in the assessment of concrete structures. *fib, Structural concrete*, 2019.

[11] C. Cucchiara et al. Effectiveness of stirrups and steel fibres as shear reinforcement. *Cement Concrete Composites 26*, 2003.

[12] C. Lee et al. Experimental observation on the effectiveness of fiber sheet strip stirrups in concrete beams. *Journal of composite for construction*, 2010.

[13] C. Lee et al. Shear capacity of rc beams with carbon fiber-reinforced polymer stirrups with rectangular section. *Journal of composite for construction*, 2015.

[14] D. Gino et al. Strain-based method for assessment of global resistance safety factors for nlnas of reinforced concrete structures. *Engineering structures 304*, 2024.

[15] E. Miceli et al. Approaches to estimate global safety factors for reliability assessment of rc structures using non-linear numerical analyses. *Engineering Structures 311*, 2024.

[16] H. Ma et al. Shear performance test and nominal bearing capacity on the transfer beams of steel reinforced concrete in subway station structure. *Structures 56*, 2023.

[17] H. Nakamura et al. Experimental investigation of compressive strength and compressive fracture energy of longitudinally cracked concrete. *Cement and Concrete Composites*, 2018.

[18] L. Jin et al. Effect of stirrups on shear performance of geometrically-similar reinforced concrete deep beams: An experimental study. *Engineering structures 295*, 2023.

[19] M. Corrado et al. Experimental evidences of flexural to shear to crushing failure mode transition in reinforced concrete beams without stirrups. *Engineering structures 271*, 2022.

[20] M. Hamrat et al. Effects of the transverse reinforcement on the shear behaviour of high strength concrete beams. *Advances in structural engineering*, 2018.

[21] M. Tahir et al. Shear behavior of concrete beams reinforced with cfrp sheet strip stirrups using wet-layup technique. *Structures 22*, 2019.

[22] P. Castaldo et al. Partial safety factor for resistance model uncertainties in 2d non-linear analysis of reinforced concrete structures. *Engineering structures 176*, 2018.

[23] P. Castaldo et al. Safety formats for non-linear finite element analysis of reinforced concrete structures: discussion, comparison and proposals. *Engineering structures 193*, 2019.

[24] P. Castaldo et al. Aleatory uncertainties with global resistance safety factors for non-linear analyses of slender reinforced concrete columns. *Engineering structures 255*, 2022.

[25] R. Guo et al. Experimental study on flexural shear strengthening effect on low-strength rc beams by using frp grid and ecc. *Structures 227*, 2021.

[26] V.A. Georgewill et al. Punching shear failure of reinforced concrete flat slab system- a review. *European Journal of Advances in Engineering and Technology 6(2)*, 2019.

[27] R. Walter F. Leonhardt. Beiträge zur behandlung der schubprobleme im stahlbetonbau. *Beton und Stahlbetonbau 57*, 1962.

[28] Fib. Model code for concrete structures. *Fib 2013, Lousanne*, 2010.

[29] D. Gino. *Advances in reliability methods for reinforced concrete structures*. PhD thesis, Politecnico di Torino - DISEG, 2019.

[30] R. L. Iman. Latin hypercube sampling. 1999.

[31] G. Mehlhorn J. Kollegger. *Material model for the analysis of reinforced concrete surface structures*. Comp. Mech. Vol 6, 1990.

[32] G. Mehlhorn J. Kollegger. *Guidance on Nonlinear Finite Element Analysis of marine and offshore structures*. American Bureau of Shipping, 2021.

[33] JCSS. Jcss probabilistic model code. 2001.

[34] E. Mondo. Shear capacity of steel fibre reinforced concrete beams without conventional shear reinforcement. Master's thesis, Royal Institute of Technology (KTH) Department of Civil and Architectural Engineering, 2009.

[35] L. Lowes N. Mitra. Factors influencing analytical continuum simulation of three point bend test of a concrete notched beam. 2008.

[36] M. Slowik. Shear failure mechanism in concrete beams. *Procedia material sience 3*, 2014.

[37] F. Trombetta. Calibration of model uncertainty safety factors for nlfeas of reinforced concrete beams with shear and flexural failure modes. Master's thesis, Politecnico di Torino - DISEG, 2024.

[38] M. Virdis. Assessment of aleatory and model uncertainties for non-linear analysis of slender reinforced concrete members. Master's thesis, Politecnico di Torino - DISEG, 2018.

[39] Z. Zhang. Application of finite element analysis in structural analysis and computer simulation. *Applied Mathematics and Nonlinear Sciences*, 2023.

[40] V. Červenka et al. *ATENA Program Documentation*. Červenka Consulting, 2021.

A1 | Appendix

Here below will be provided further information related to database. It is important to consider that few beams (B86-1.5W, B86-2W, RCTB-2, B01) have been modelled with data provided in Table A2.1 and A2.2 but not further analysed during probabilistic analysis. They can not be considered as reliable samples due to a mismatch in experimental results and numerical failure.

Appendix 1.1 presents the load-displacement curves of all the beams included in the database referenced in Chapter 3.2.
These curves were used to compare the NLNA curve with average values to the experimental results.

Appendix 1.2 lists the geometric and mechanical properties of the individual beams (Table A1.1 and A1.2) and illustrates the distribution of these properties across the entire sample in Figures A1.3 and A1.4.

Appendix 1.3 provides the modeling parameters considered to perform NLNAs in ATENA 2D (tables A1.3 and A1.4).

A1.1 Load-deformation curves

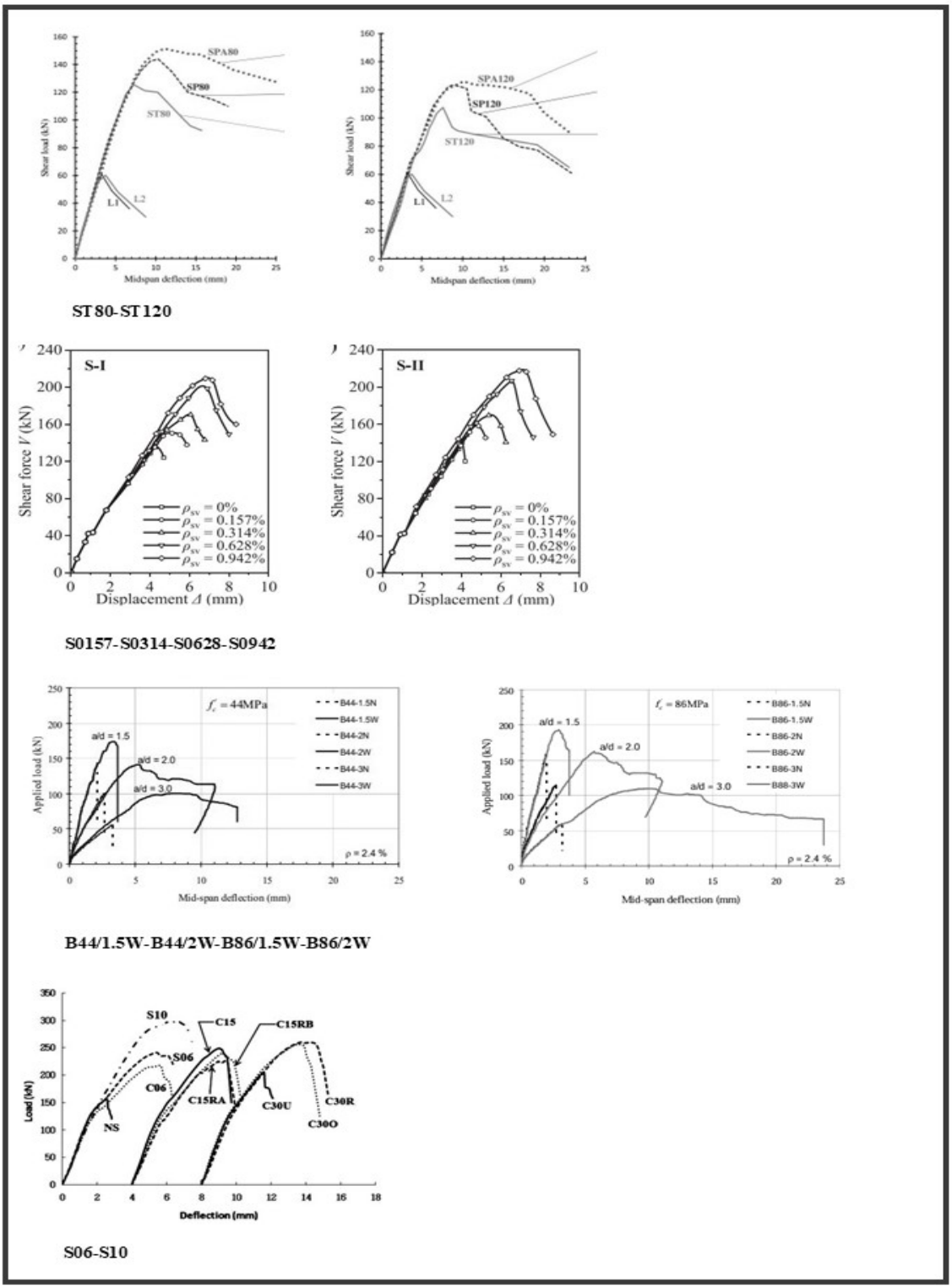

Figure A1.1: Load-deformation curves of beams considered for an inverse analysis introduced at Chapter 6.

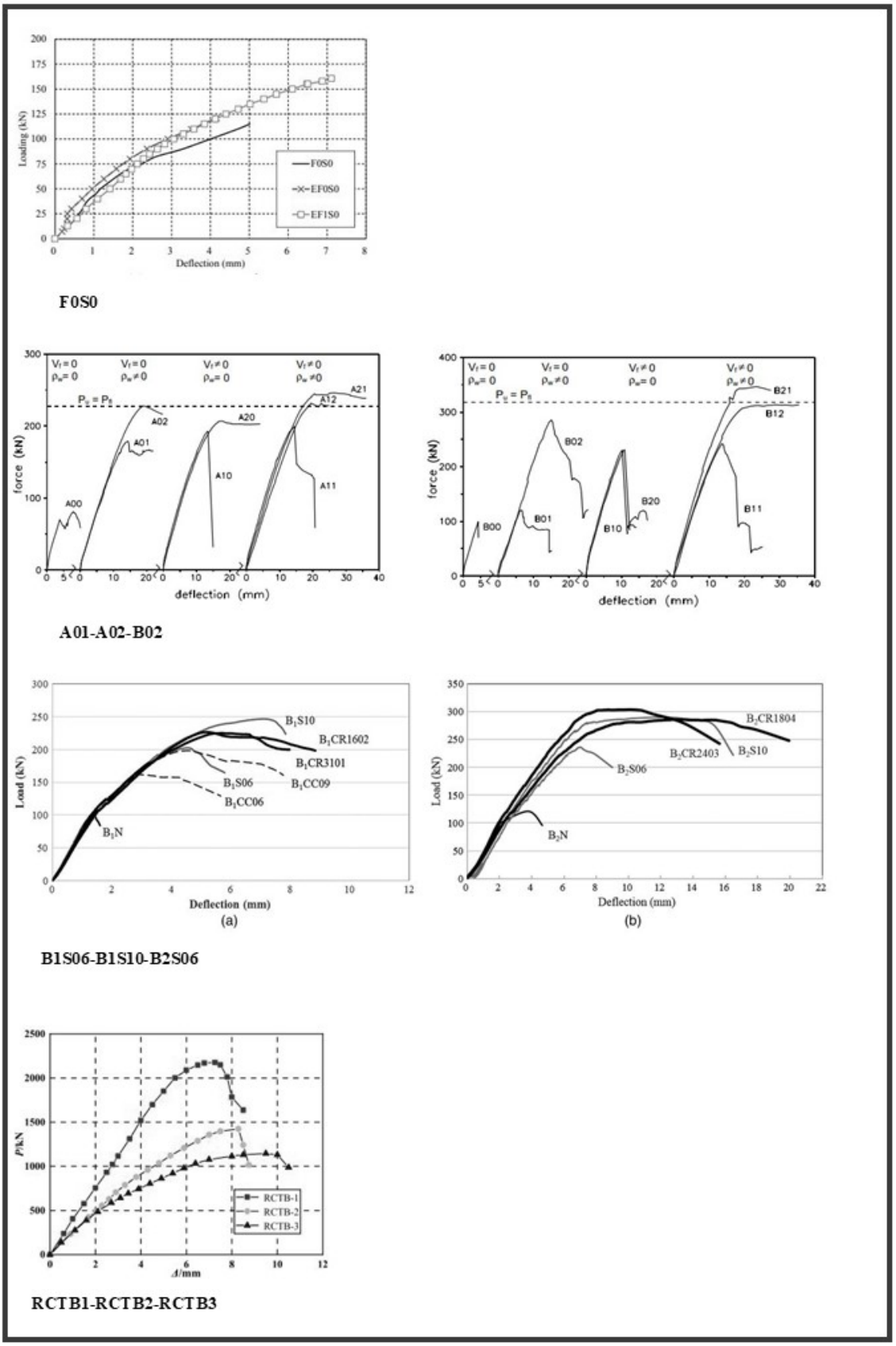

Figure A1.2: Load-deformation curves of beams considered for an inverse analysis

A1.2 Mechanical and geometrical properties

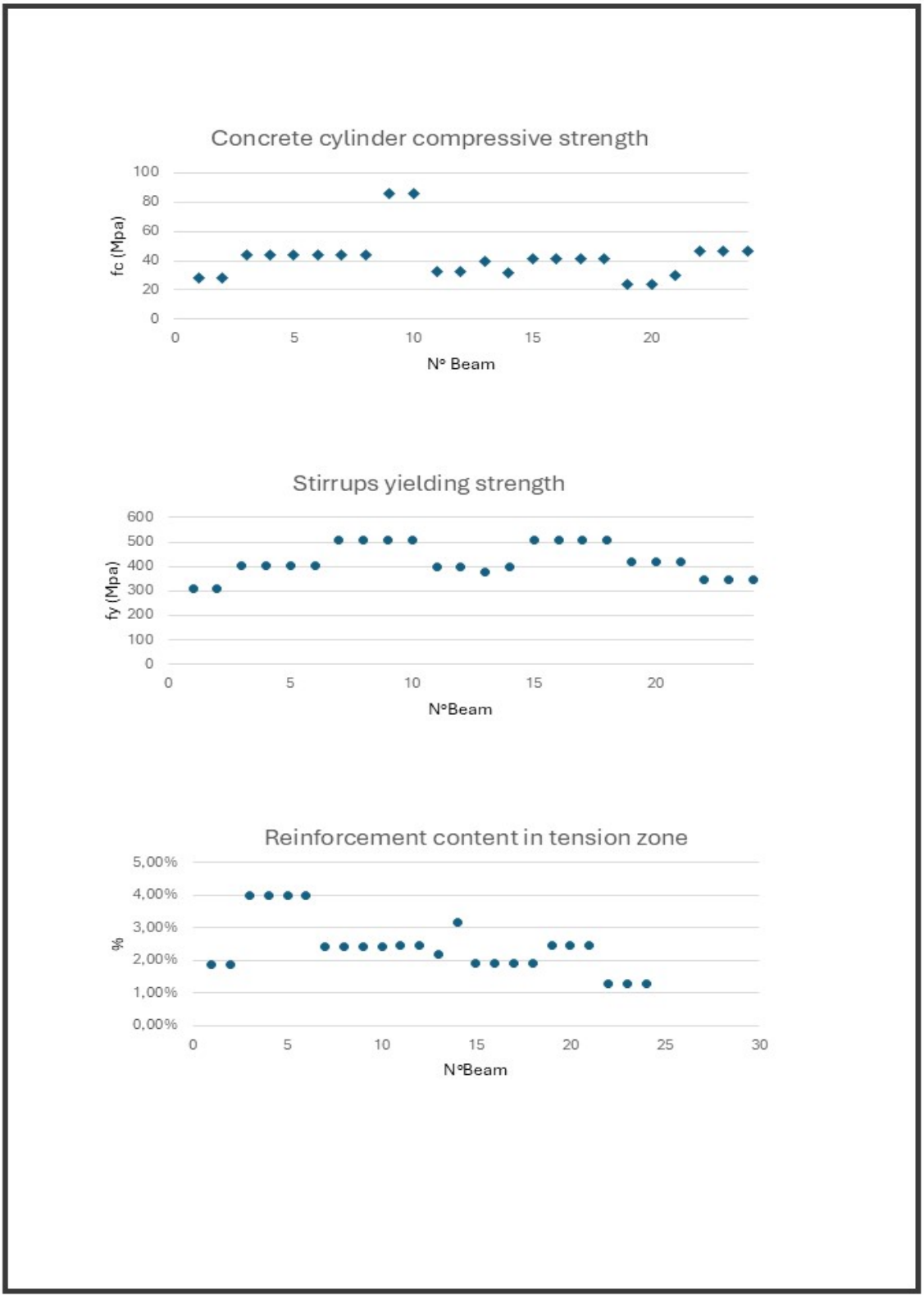

Figure A1.3: Mechanical and geometrical properties distribution (1)

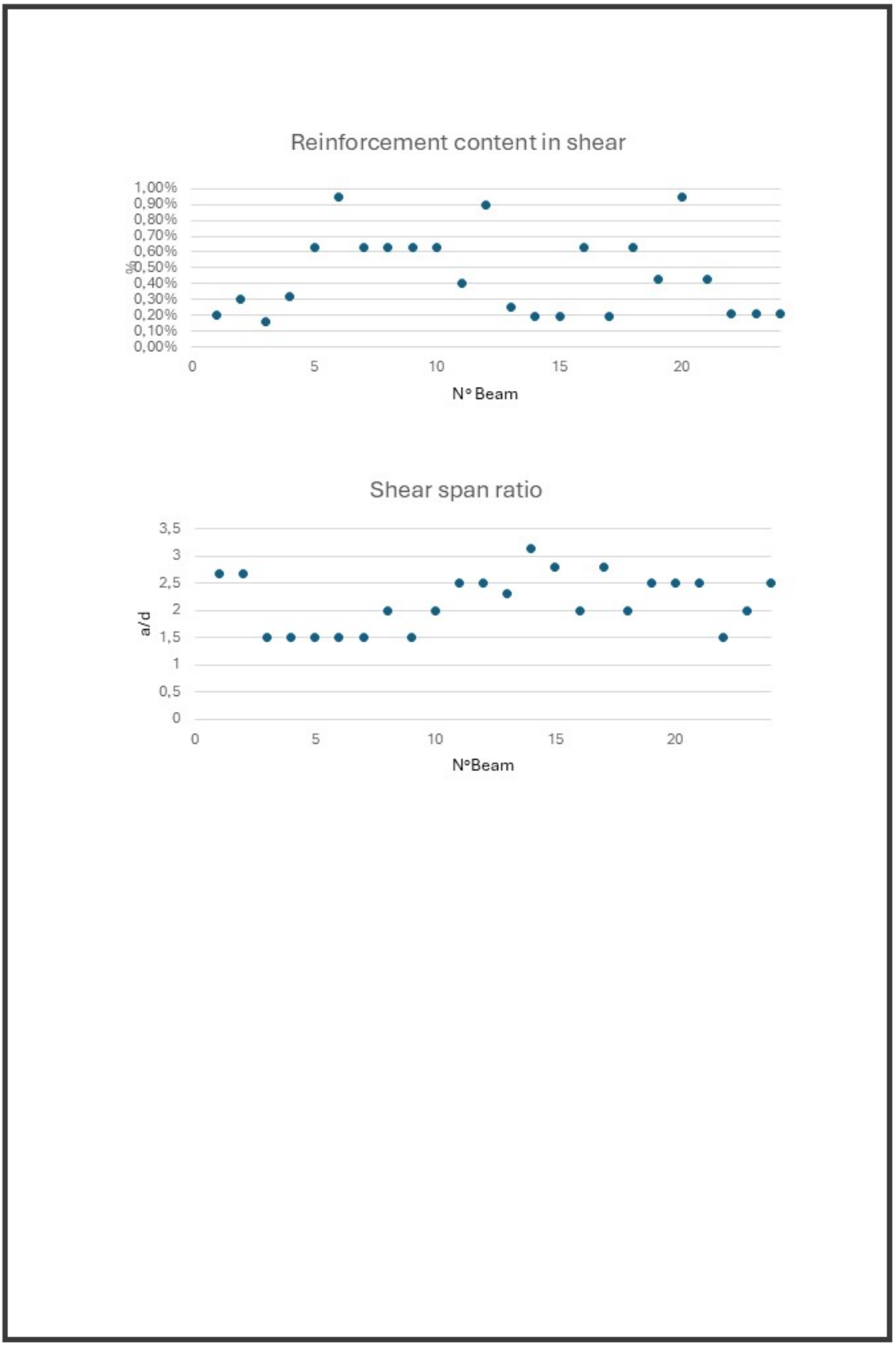

Figure A1.4: Mechanical and geometrical properties distribution (2)

N°	Name	f_c	f_y (stir)	f_u	B	H	A_c	A'_s	A_s	d	ρ
		[MPa]	[MPa]	[MPa]	[mm]	[mm]	[mm^2]	[mm^2]	[mm^2]	[mm^2]	[%]
1	ST120	28,5	310	430	200	300	60000	2ϕ14	4ϕ18	270	1,88%
2	ST80	28,5	310	430	200	300	60000	2ϕ14	4ϕ18	270	1,88%
3	S-0.157	33,1	406	590	100	300	30000	2ϕ12	4ϕ18	250	4,07%
4	S-0.314	33,1	406	590	100	300	30000	2ϕ12	4ϕ18	250	4,07%
5	S-0.628	33,1	406	590	100	300	30000	2ϕ12	4ϕ18	250	4,07%
6	S-0.942	33,1	406	590	100	300	30000	2ϕ12	4ϕ18	250	4,07%
7	B44-1.5W	44,2	508	581	100	160	16000	2ϕ6	2ϕ14	127	2,43%
8	B44-2W	44,2	508	581	100	160	16000	2ϕ6	2ϕ14	127	2,43%
9	B86-1.5W	85,5	508	581	100	160	16000	2ϕ6	2ϕ14	127	2,43%
10	B86-2W	85,5	508	581	100	160	16000	2ϕ6	2ϕ14	127	2,43%
11	S06	32,5	400	500	150	250	37500	2ϕ6	2ϕ22	205	2,47%
12	S10	32,5	400	500	150	250	37500	2ϕ6	2ϕ22	205	2,47%
13	S8-90	40	380	470	200	500	100000	2ϕ22	5ϕ22	433	2,19%
14	F0S0	31,6	400	540	120	200	24000	2ϕ18	3ϕ18	160	3,18%
15	A01	41,2	510	561	150	219	32850	2ϕ10	2ϕ20	219	1,91%
16	B01	41,2	510	561	150	219	32850	2ϕ10	2ϕ20	219	1,91%
17	A02	41,2	510	561	150	219	32850	2ϕ10	2ϕ20	219	1,91%
18	B02	41,2	510	561	150	219	32850	2ϕ10	2ϕ20	219	1,91%
19	B1S06	24	420	530	150	250	37500	2ϕ6	2ϕ22	206	2,46%
20	B1S10	24	420	530	150	250	37500	2ϕ6	2ϕ22	206	2,46%
21	B2S06	30	420	530	150	250	37500	2ϕ6	2ϕ22	206	2,46%
22	RCTB-1	46,8	347	516	475	400	190000	6ϕ16	6ϕ22	380	1,26%
23	RCTB-2	46,8	347	516	475	400	190000	6ϕ16	6ϕ22	380	1,26%
24	RCTB-3	46,8	347	516	475	400	190000	6ϕ16	6ϕ22	380	1,26%

Table A1.1: Database geometrical and mechanical properties - Part 1

N°	Name	A_{sw}	s	ρ_{sw}	L	a	Type of test	Failure Mode	Source
		$[mm^2]$	[mm]	[%]	[mm]	[mm]			
1	ST120	ϕ5.5	120	0,20%	1840	720,9	4 p. b.	pure shear	C.G Karayannis, C.E. Chalioris (2013)
2	ST80	ϕ5.5	80	0,30%	1840	720,9	4 p. b.	pure shear	
3	S-0.157	ϕ6	360	0,16%	1800	375	4 p. b.	pure shear	L. Jin et al (2023)
4	S-0.314	ϕ6	180	0,32%	1800	375	4 p. b.	pure shear	
5	S-0.628	ϕ6	90	0,63%	1800	375	4 p. b.	pure shear	
6	S-0.942	ϕ6	60	0,95%	1800	375	4 p. b.	pure shear	
7	B44-1.5W	ϕ6	90	0,63%	900	190,5	4 p. b.	shear comp	M. Hamrat et al (2018)
8	B44-2W	ϕ6	90	0,63%	1040	254	4 p. b.	shear comp	
9	B86-1.5W	ϕ6	90	0,63%	900	190,5	4 p. b.	shear comp	
10	B86-2W	ϕ6	90	0,63%	1040	254	4 p. b.	shear comp	
11	S06	ϕ6	100	0,40%	1400	512,5	3 p. b.	pure shear	C. Lee et al (2010)
12	S10	ϕ10	100	0,90%	1400	512,5	3 p. b.	pure shear	
13	S8-90	ϕ10	200	0,25%	2650	1000	3 p. b.	pure shear	M. Tahir et al (2019)
14	F0S0	ϕ6	250	0,19%	1500	500,8	4 p. b.	pure shear	R. Guo et al (2020)
15	A01	ϕ6	200	0,19%	2500	613,2	4 p. b.	pure shear	C. Cucchiara et al (2003)
16	B01	ϕ6	200	0,19%	2500	438	4 p. b.	pure shear	
17	A02	ϕ6	60	0,63%	2500	613,2	4 p. b.	shear comp	
18	B02	ϕ6	60	0,63%	2500	438	4 p. b.	pure shear	
19	B1S06	ϕ6	100	0,43%	1400	515	3 p. b.	pure shear	C. Lee et al (2015)
20	B1S10	ϕ10	100	0,95%	1400	515	3 p. b.	shear comp	
21	B2S06	ϕ6	100	0,43%	1400	515	3 p. b.	pure shear	
22	RCTB-1	ϕ8	100	0,21%	1100	570	3 p. b.	pure shear	H. Ma et al (2023)
23	RCTB-2	ϕ8	100	0,21%	1500	760	3 p. b.	pure shear	
24	RCTB-3	ϕ8	100	0,21%	1900	950	3 p. b.	shear comp	

Table A1.2: Database geometrical and mechanical properties - Part 2

ID	ST-80	ST-120	S-0157	S-0314	S-0628	S-0942	B44-1.5W	B44-2W	S06	S10
Softening parameter c3	0,00146	0,00146	0,00009	0,00025	0,00025	0,00025	0,00143	0,00117	0,00113	0,00113
Reduction of compressive strength	0,45	0,45	0,8	0,8	0,8	0,8	0,8	0,45	0,8	0,8
Compression softening parameter	0,37	0,37	0,368	0,368	0,368	0,368	0,52	0,52	0,36	0,36
Shear retention factor	0,2	0,2	0,2	0,2	0,2	0,2	0,2	0,2	0,2	0,2
Mesh size (m)	0,042	0,042	0,069	0,069	0,075	0,075	0,028	0,027	0,050	0,060
Support type (MPa)	spring 200	spring 200	spring 2000	spring 2000	spring 2000	spring 2000	steel plate	spring 1000	spring 600	spring 900
Support height (m)	0,03	0,03	0,03	0,03	0,03	0,02	0,02	0,02	0,02	0,03
Support length (m)	0,05	0,05	0,05	0,05	0,05	0,05	0,05	0,05	0,05	0,05
Upper plate height (m)	0,02	0,02	0,03	0,03	0,03	0,03	0,01	0,01	0,02	0,03
Upper plate length (m)	0,05	0,05	0,05	0,05	0,05	0,05	0,025	0,025	0,10	0,10

Table A1.3: Database: modeling parameters (1)

ID	F0S0	A01	A02	B02	B1S06	B1S10	B2S06	RCTB-1	RCTB-3	S890
Softening parameter c3	0,00016	0,00166	0,000356	0,00166	0,00016	0,00014	0,00014	0,00121	0,00121	0,00018
Reduction of compressive strength	0,8	0,8	0,8	0,8	0,8	0,8	0,8	0,45	0,8	0,8
Compression softening parameter	0,349	0,8	0,8	0,8	0,231	0,231	0,231	0,55	0,55	0,46
Shear retention factor	0,2	0,2	0,2	0,2	0,2	0,2	0,2	0,2	0,2	0,2
Mesh size (m)	0,050	0,055	0,045	0,060	0,050	0,051	0,050	0,052	0,092	0,074
Support type (MPa)	steel plate	steel plate	steel plate	spring 800	spring 600	spring 400	spring 400	spring 1300	spring 1000	steel plate
Support height (m)	0,03	0,03	0,03	0,03	0,02	0,02	0,02	0,02	0,03	0,03
Support length (m)	0,05	0,05	0,05	0,05	0,04	0,04	0,04	0,05	0,05	0,10
Upper plate height (m)	0,03	0,03	0,01	0,03	0,03	0,03	0,03	0,02	0,02	0,04
Upper plate length (m)	0,05	0,10	0,10	0,10	0,12	0,12	0,12	0,20	0,20	0,20

Table A1.4: Database: modeling parameters (2)